University of Évora

ARCHMAT
(ERASMUS MUNDUS MASTER IN ARCHaeological MATerials Science)

Mestrado em Arqueologia e Ambiente (Erasmus Mundus – ARCHMAT)

In-Situ Analysis of Roman Mosaics at Cástulo, Linares (Jaén, Spain): a Comparative and Non-Destructive Study

Delphine Saelens, m38412

Prof. José Antonio Paulo Mirão
(Supervisor - Universidade de Évora)

Prof. Peter Vandenabeele
(Co-Supervisor- Ghent University)

Évora, September 2018

University of Évora

ARCHMAT
(ERASMUS MUNDUS MASTER IN ARCHaeological MATerials Science)

Mestrado em Arqueologia e Ambiente (Erasmus Mundus – ARCHMAT)

Análise In-Situ de Mosaicos Romanos em Cástulo, Linares (Jaén, Espanha): um estudo comparativo e não destrutivo

Delphine Saelens, m38412

Prof. José Antonio Paulo Mirão

(Supervisor - Universidade de Évora)

Prof. Peter Vandenabeele

(Co-Supervisor- Ghent University)

Évora, September 2018

Abstract

The *Mosaico de los Amores* is an outstandingly well-preserved roman mosaic dating back to the end of the 1st and beginning of the 2nd century CE. Due to the remarkable preservation state and the technical quality, the mosaic forms an important part of cultural heritage. Handheld X-ray Fluorescence (hXRF) and Raman spectroscopy were employed to analyse the material composition of the mosaic tesserae to get insight in the production technology and raw materials used. These techniques can also determine the conservation state of the mosaic as weathering products can be detected. The thesis contributes to the preventive conservation of the *Mosaico de los Amores.* Additionally, this thesis aims to compare different Raman instruments and their lasers and their suitability in the field for analysing cultural heritage. A total of 144 tesserae originating from two scenes of the mosaic are discussed in this thesis. The elemental and mineralogical compositions are discussed revealing two major groups, glass and stone tesserae. The stone tesserae with a high Ca content are made from carbonaceous stones, which were abundant in the their locality of the site. The colorants and opacifiers used to produce the different glass colours were identified with the hXRF results since the Raman results on the glasses were limited. The results gave insights in the production technology of Roman glasses. Furthermore, the comparison of the different Raman instruments yielded interesting results.

Keywords: Archaeometry, mosaics, Cástulo, handheld X-ray Fluorecence, Raman spectroscopy.

Resumo

Análise in-situ de mosaicos romanos em Cástulo, Linares (Jaén, Espanha): um estudo comparativo e não destrutivo

O *Mosaico de los Amores* é um mosaico Romano excepcionalmente bem preservado que remonta ao fim do primeiro e início do Segundo século DC. O notável estado de conservação e a qualidade técnica fazem deste mosaico uma parte importante do patrimônio cultural. Espectroscopia de Fluorescência de Raios-X (hXRF) e espectroscopia Raman foram empregadas para analisar a composição material das tesselas do mosaico e obter uma percepção na tecnologia de produção e as materiais utilizados. Essas análises também podem determinar o estado de conservação do mosaico e os produtos de intemperismo podem ser detectados. A tese contribui para a conservação preventiva do *Mosaico de los Amores.* Além disso, esta tese tem como objectivo comparar diferentes instrumentos Raman e seus lasers no campo de análise do património cultural. Um total de 144 tesselas provenientes de duas cenas do mosaico são discutidas nesta tese. As composições elementares e mineralógicas são discutidas revelando dois grupos principais: tesselas de vidro e de pedra. As tesselas de pedra apresentam um alto teor de Ca, sendo feitas a partir de pedras carbonosas, que eram abundantes na localidade. Os corantes e opacificantes utilizados para produziras diferentes cores de vidro forma identificados com os resultados de hXRF já que os resultados obtidos por Raman foram limitados. Os resultados também deram uma compreensão sobra a tecnologia de produção de vidros romanos. Além disso, a comparação dos diferentes instrumentos Raman produziu resultados interessantes.

Palavras-chave: Arqueometria, mosaicos, Cástulo, Espectroscopia de Fluorescência de Raio X portável (hXRF), Espectroscopia Raman.

Acknowledgements

This master thesis, and the Master program as a whole, has been a time of learning, not only academically but on a personal level as well. Reflecting on the past two years, I would like to express some gratitude. I would like to thank ARCHMAT for accepting me in this Master program and all the professors from Évora, Thessaloniki and Rome who contributed in inspiring us to become archaeometric researchers. Thank you to my supervisor professor José Mirão for allowing me to do this thesis project with him. I would like to express my sincere gratitude to my co-supervisor, professor Peter Vandenabeele from Ghent University to welcome me as a thesis student and to allow me to participate in the project. The measuring campaign in Spain was a unique experience. At Ghent University, I would also like to thank Sylvia Lycke for all her support and the many hours she invested in me, especially when dealing with the XRF data. Thank you Anastasia Rousaki, for your assistance with interpreting the Raman data. A big thanks to Arianna, for the fun office times and the many laughs.

I would like to thank my parents, Mia and Rik, for always encouraging me in my studies and for giving me the opportunity to pursue my passions. Thanks to their support and encouragement, I had the chance to participate in this Master program. Without their help, I would not be where I am today. I would like to thank my friends for their support during these final months of the masters and especially Karel for always being there and calming me down when necessary. My friends and colleagues from the ARCHMAT 4th edition have made these past two years a memorable period during which we became incredibly close. A special thanks to Sriradha, Roshan, Sergio, Sylvia, Cecilia and Maisa. Mercedes, Guillermo and Amalia, I would like to especially thank you for inspiring me to do better in every aspect of my life. You have become my family during these two years, remember to always have Medium Fun.

Table of contents

List of Figures

List of Tables

1 Introduction

In spring 2018, Ghent University was invited by the University of Jaén to participate in a multi-technique study of the *Mosaico de los Amores*. The *Mosaico de los Amores* is part of the remarkable archaeological site of Cástulo in Jaén, Spain and has been recognized as an invaluable part of global cultural heritage. This thesis contributes to this multi-university collaboration and field campaign. The *Mosaico de los Amores* is well preserved and lends itself to conduct non-destructive, in-situ analyses. It was paramount to design a non-destructive protocol to be implemented at the site, since sampling was prohibited due to concerns regarding the preservation and conservation of the mosaic tesserae. Therefore, non-destructive, non-invasive handheld X-ray fluorescence (hXRF) and Raman spectroscopy were used to conduct compositional analysis of the Roman tesserae. Multiple instruments were employed during this field campaign to assure the quality and scientific validity of the results. Specifically, two hXRF instruments, four Raman spectrometers (three mobile and one handheld) and one digital microscope were used during this field campaign. This thesis focuses on the results of one hXRF, three different Raman instruments and the digital microscope to gain in-depth knowledge about the chemical and mineralogical composition of the tesserae in the *Mosaico de los Amores*.

The results from this thesis aim to determine the conservation state of the glass tesserae in the mosaic. By understanding the composition of the tesserae and identifying the possible weathering mechanisms, the mosaic can be protected from future decay. This thesis aims to contribute to preventive conservation of the *Mosaico de los Amores* and to its ability to be part of Jaén's future cultural heritage for many years to come. The main objective of studying tesserae is to understand the quality of the glass and possible weathering mechanisms through compositional analysis. Additionally, what are the (de)colouring agents and opacifiers used during production? And, can any conclusion be drawn on the manufacturing technology of the glass tesserae on the chemical and mineralogical data?

From a methodological point of view, this thesis aims to compare different Raman instruments and its lasers to test their suitability for the usage on the field and to the quality of the results.

This thesis is divided into three main parts. Chapter 2 consists of the geographic, historical and archaeological context of the mosaic. The geographical and geological context is delved into to determine the availability of local raw materials. The historical and archaeological background of the site of Cástulo is sketched to further understand the importance of the site in terms of Roman history and present Spanish cultural heritage. Next, the iconography, history and mythology behind the mosaic are discussed in detail. Finally, a discussion on the composition of Roman glass and recent research conducted on ancient glass tesserae are considered.

Chapter 3 focuses on the materials and methods used in this thesis. The samples under study are described in terms of their different colour hues, and their archaeological context. Next, different instruments and their main analytical features are discussed briefly but delved into in Chapter 4 (section 4.2). A short history of the techniques and their importance within archaeometry and archaeology as a whole is discussed. Furthermore, the rise of *in-situ* studies and their application is deliberated.

Chapter 4 consists mainly of this study's analytical results. The results from the scene of Paris myth and the scene depicting the season spring are discussed individually, both in terms of tesserae colour. In addition, a detailed comparison between the different Raman spectrometers is considered. These comparisons consist not only of spectroscopic evaluations, but also of practical features for the in-situ measurements. The last chapter situates the results in the geographical, geological and archaeological context and discusses their significance.

2 Context

2.1 Geographical and geological context

The mosaic from the *Sala del Mosaico de los Amores* is located in the archaeological site of Cástulo. This site is found in Linares, a town in the province of Jaén in southern Spain (GPS coordinates: 38°02'05"N, 3°37'29"W). The site is situated in the centre of a mining region between the towns of Linares, Lupión and Torreblascopedro. The city was founded in an ideal location. Enclosed by the mines of the Sierra Morena mountain range and the metalliferous outcrops of Linares, the ancient city is surrounded by natural resources. In addition, it held many political beneficial trade networks including the crossroads of an old road network and the last navigable port of the Baetis river. These conditions were ideal for the foundation of the city of Cástulo (López Martínez, 2015).

Figure 1 - Location Cástulo (Google Maps).

The archaeological site is located on a hilltop, a naturally elevated location above the landscape, on the northern banks of the Guadalimar river (Fig. 1), which is a tributary of the

Guadalquivir river (Rickard, 1928). From a geological perspective, the north eastern sector of the Quadalquivir Basin is developed between the Iberian Massif to the north and the Betic Cordilla to the south and is one of the largest Tertiary basins in the Iberian Peninsula (Fernàndez et al., 1998). The Quadalquivir carves into this Tertiary basin (Fig. 2). The lithological units of the area are represented in Figure 2 and are listed below (Jiménez-Espinosa et al., 2016; Perrone et al., 2006):

- to the north: the Hercynian basement of the Sierra Morena with Palaeozoic rocks such as granitic plutonic rocks and metamorphic rocks (slates, schists and hornfels);
- to the south: the Sierra Mágina belonging to the Subbetic domain of the External Zone of the Betic Cordillera with Mesozoic limestones;
- to the east: the Sierra de Cazorla of the Prebetic domain of the External Zone of the Betic Cordillera with Mesozoic carbonates, mainly dolostones.

The Guadalquivir River incises the Neogene basin, which consists of marl deposits, algal limestones, calcarenites and sandstones with carbonate cement (Jiménez-Espinosa et al., 2016). In general, the carbonate content is very high: calcite plus dolomite contents higher than 40%. The Olistostromic Unit forms the only anomaly within the lithology of the basin. It consists of clays, red sandstones, gypsum and dolostones from the Triassic era (Fernàndez et al., 1998). In Cástulo and along the banks of the Guadalimar River, alluvial Quaternary deposits cover the Mio-Pliocene lithological units. These deposits consist of conglomerates, gravels, sands and silts. The upper Quadalquivir River cuts into a thick dolomitic sequence of the Sierra Cazorla (Jiménez-Espinosa et al., 2016; Jiménez-Espinosa and Jiménez-Millán, 2003; Perrone et al., 2006). Analyses on the alluvial sediments determined different mineral phases of dolomite, calcite, quartz, clay minerals and feldspars. Calcite originates from the Mesozoic Subbetic sequences of Sierra Mágina. In contrast, dolomite stems from the Mesozoic Prebetic rocks of Sierra de Cazorla and blocks with Triassic sediments in the Olistrostromic unit (Jiménez-Espinosa et al., 2016).

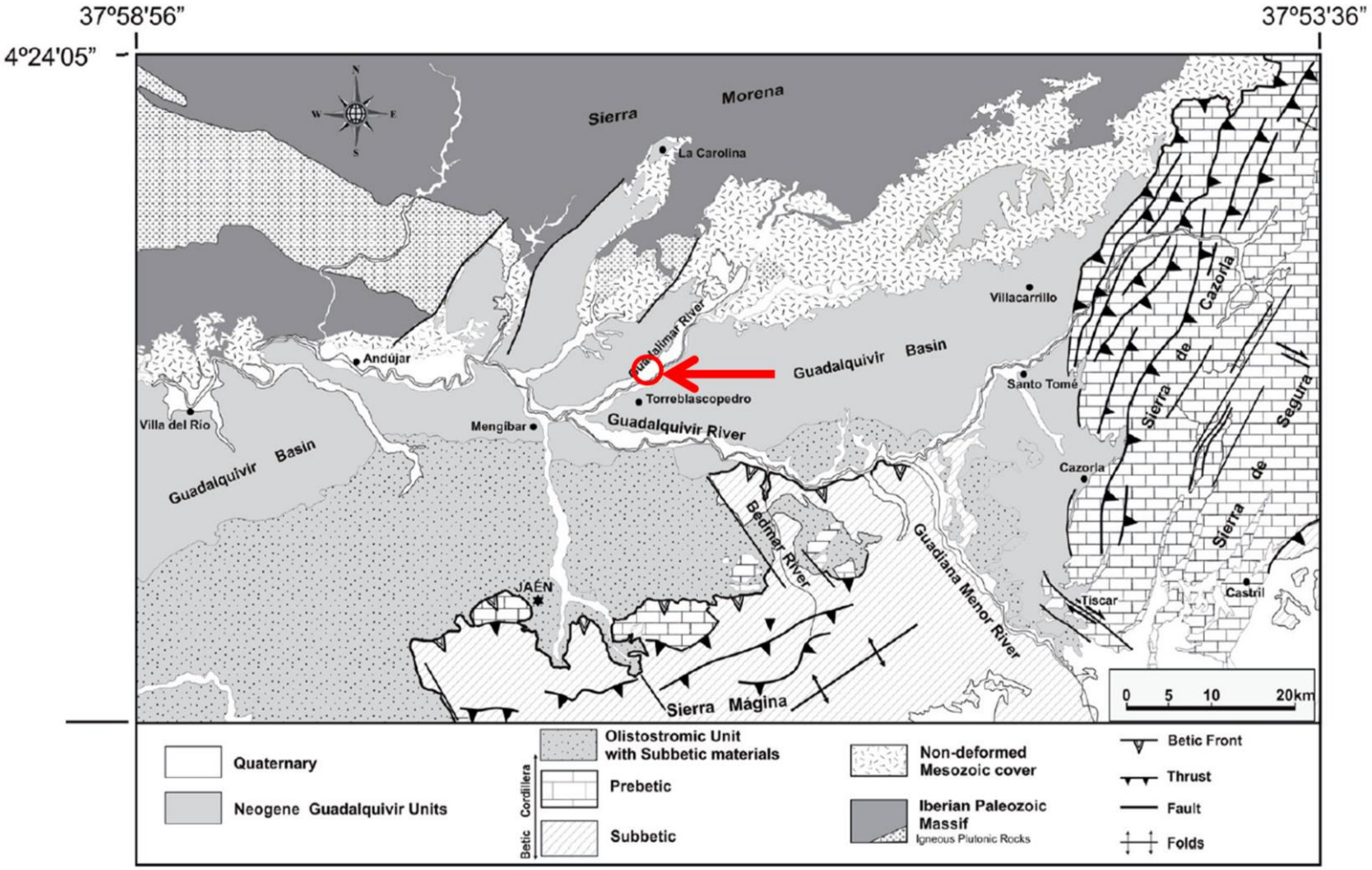

Figure 2 - Local geology map with lithological units and identification of Castulo in red (Jimenez-Espinosa et al., 2016)

2.2 Archaeological context Cástulo

The *Sala del Mosaico de los Amores* was constructed between the end of the 1st century and beginning of the 2nd century CE (López Martínez, 2015). The room was rediscovered in 2011 during excavations of the larger archaeological complex, Building D. However, the archaeological site of Cástulo was discovered long before that. Material evidence of human occupation on the site dates back to the final Bronze Age (8th century BCE). Older occupations are attested on the terraces of the Guadalimar river where evidence of a Paleolithic occupation was discovered during a surface survey conducted by Breuil (Blázquez and García-Gelabert, 2000). Hence, it is probable that this Paleolithic presence also occurred in Cástulo, however no proof of this has been found to date (Blázquez and García-Gelabert, 2000).

The most important pre-Roman habitation in Cástulo is situated at the foot of the *Cerro de la Muela*. The habitation settlement is from the Final Bronze Age, dating back to the end of the 8th century BCE. Traces of a smelting workshop were discovered together with some coarse ceramics, fired in a reducing atmosphere (Blázquez and García-Gelabert, 2000). This illustrates the transformation of the economy from an agricultural based economy to a metallurgy based economy. Similarly, the Phoenicians, Punics and Greeks base their exchange and trade on the exploitation of the same resources, which subsequently become a source of great wealth and power in the city. In Cástulo, and Andalusia in general, Greek pottery is mainly found from the first half of the 4th century BCE. The ceramics were low quality and were imported from the Phoenecians and Carthaginians. During the 4th century BCE, there is more pottery found in Cástulo than in Huelva, another important site in the region, proving the economic importance of the mines. The imported pottery demonstrates the relationship between Phoenicians and Carthaginians, and the rise of population in the city (García-Gelabert Pérez and Blázquez Martínez, 1994).

The new economic activity from the mines near Cástulo illustrates social change. A newly emerged upper class appeared. These elites controlled the mining activities and trade as evidenced in the historical and archaeological record (Blázquez and García-Gelabert, 2000).

Consequently, during the 5th and 4th centuries BCE an urban society that fuelled the workforce for the mines developed (Blázquez Martínez, 2000). This economic prosperity led to demographic growth, attested in the increased size of the necropolis. This led to socio-political changes, consisting mainly in the institutionalisation of social inequality. Relics of social stratification are evident in the tombs surrounding Cástulo. Clear economic differentiation in the material culture in the graves and the artefacts found with certain individuals in positions of power are attested (García-Gelabert Pérez and Blázquez Martínez, 1994).

During the Roman period, Cástulo was conquered in 206 BCE as a *fides accepta* in which the city remained its own governmental institution. Later, during Augustan times (27 BCE – 14 CE), the city became a *municipium* (López Martínez et al., 2016). Because of the booming mining activity and the concomitant agricultural expansion, the city of Cástulo underwent a period of great prosperity. The Romans exploited the silver mines located near Cástulo in the eastern Sierra Morena. Furthermore, lead ingots quarried around Cástulo were distributed all over the western Mediterranean Roman Empire (Keay, 2003). It is evident that Cástulo was of great importance to the Romans (Rickard, 1928).

The city kept flourishing during the next couple of centuries until the 3rd century CE, when the city fell into decline. Due to the over exploitation and exhaustion of the mines, the mineral resources ceased to be the main income of the city. Although the mines were still in use, the mining was minimal, resulting in an economic collapse. This economic setback and the Barbaric invasions during that period, led to a power vacuum from which Cástulo did not recover. From the 4th century onwards, there is no evidence of the peaceful and economically prosperous city that thrived during the Republican period. Instead, there is evidence of construction of infrastructure with materials from previous periods, a clear indicator of the absence of readily available construction materials. The re-use of materials and the poverty evident in the tombs in the necropolis are just a few indications of the aforementioned economic decline. This decay continues until the town is abandoned in the Middle Ages (Blázquez and García-Gelabert, 2000; López Martínez et al., 2016).

2.3 Sala del Mosaico de los Amores

The *Sala del Mosaico de los Amores* is part of a monumental public building complex (Building D) that dates back to the end of the 1st century CE, in the Roman Imperial period (Fig. 1). This archaeological complex was first detected in a geophysical survey in 2009. Initially, it was believed that the building complex was part of the city's forum since it is located in the centre of the city. However, this theory was falsified during excavations in 2011 and 2012. These excavations revealed two large buildings that could be linked to a the imperial cult (Morillas, 2011). The *Sala del Mosaico de los Amores* is discussed in terms of its conservation, ancient function and the factors behind its abandonment in the 1st century CE.

Building D is 33 m long and 13 m wide. In the southern part of the building, the identification of the different spaces is complicated by the re-use of construction materials during late-Roman times (Castro López, 2014; Morillas, 2011). Although several areas of the site cannot be identified with certainty, the function of the *Sala del Mosaico* is probably related to the imperial cult practices. The room measures approximately 6 x 12 m and is located in the northern part of the building complex (Fig.3). The walls of the room were covered with extensive wall paintings and were approximately 3,80 m high. The architecture of the room is conserved incredibly well because of the collapse of the eastern wall. This wall has covered, almost in its entirety, the mosaic floor since the end of the 1st century CE. Therefore, the mosaic has remained covered and protected until the recent excavation of the room in 2011. This good state of conservation led to a detailed 3D reconstruction of the room (Fig.4). The collapse did not only preserve the mosaic floor, but it also conserved the wall paintings and decoration motifs (Castro López, 2014).

The majority of construction elements of the building were recovered, such as the floor and a large part of the walls. It is particularly interesting to note that no archaeological artefacts were found within the mosaic room despite its high level of preservation. Only one iron key was found at the foot of the main door (Fig.5). The general lack of material evidence, complicates the dating of the room and the construction of the mosaic, as well as discerning the room's function. Currently, it is believed that the room offered an imperial and public use. This was determined through following factors. Firstly, it does not appear to be a

domestic environment. Secondly, it is close to the geographical centre of Cástulo. Lastly, the wall paintings and mosaics can be interpreted as imperial propaganda. The theme and style of the mosaic are attributed to the imperial style. It is believed that the mosaic, and the building complex in general, is dedicated to Emperor Domitian (López Martínez et al., 2016). The high quality of the mosaic, both technically and figuratively, is typical of this time period.

Consequently, no information can be discerned about the function of the room, or its role in Roman society. The collapse of the eastern wall raises important questions since the room was not used again after this occurred. The ruins remain intact, until the 4th century, where cut marks are evidenced on walls constructed above the layers of the Roman construction. This has been interpreted as the foundation of a more recent building. However, this recent structure never reached the stratigraphic levels of the Roman occupation. This is the key reason that the *Sala del mosaic de los Amores* remained in such a good conservation state for centuries (Castro López, 2014).

The fall of the wall in the historical context makes it very plausible to assume that this was a case of intentional demolishment (Morillas, 2011). The collapse of the wall was not the result of deterioration or natural decay, but a deliberate action that took place when the structure was still in perfect shape. The destruction of the building and the collapse of the eastern wall, could be what Romans term the *Damnatio Memoriae*, an intentional condemnation of historical and communal memory. Given the time of destruction around the end of the 1st century CE, the complex is linked to the emperor Domitian, the last emperor of the Flavian Dynasty (Castro López, 2014). The assassination of the emperor in 96 CE encouraged the Senate to condemn and destroy any relics of his authority and legacy (Roldán et al., 1999)

Figure 3 - Building D with identification of the Sala del Mosaico de los Amores (Morillas, 2011)

Figure 4 - Reconstruction Sala del mosaico de los amores (López Martínez et al., 2016)

Figure 5 - Iron key (Morillas, 2011)

2.4 Mythology

The mosaic owes its name to the presence of six Eros or Amores represented in half circles along the sides of the mosaic. The mosaic theme and style are attributed to the imperial style. The main themes of the mosaic are represented by two central circles: the northern circle depicting the myth of the judgement of Paris and the southern circle depicting the goddess Luna.

The myth of the judgement of Paris consists of a contest between the three most beautiful goddesses Minerva, the goddess of wisdom, Juno, the goddess of marriage, and Venus, the goddess of love. These roman goddesses are parallel in Greek mythology with Athena, Hera and Aphrodite, respectively. The prize given by Paris, a Trojan mortal, for 'the fairest' goddess was a golden apple. Consequently, each goddess tried to bribe Paris with their seductive powers. At the end, Paris chose Venus since she promised to concede him the most beautiful woman of the world, who at the time was known to be Helen of Sparta (Rodney, 1967; Walcot, 1977). The goddesses are represented in the upper plane. Athena is on the right and displays her fierce warrior attributes (Fig.6, right). Hera is depicted in the middle and is usually portrayed as being majestic and solemn. In this image she is wearing a *polos*, a cylindrical crown. Aphrodite, shown half-naked, is on the left. This embodies her further as the goddess of love and seduction. Paris is represented in the lower plane sitting on a rock and accompanied by an oxen and a dog, typical animals depicted with shepherds. In the centre of the scene, Paris is receiving the apple from Hermes who is represented on the lower right panel. Hermes is shown naked, only covered by a very colourful mantle loosely hanging from his body and his characteristic winged crown. The environment in the scene contains by four bushes, which symbolizes nature (Lopéz Monteagudo, 2014). The representation of the Judgement of Paris is attested in two other Spanish Roman mosaics in Casariche (Seville) and in Noheda (Cuenca) (Blázquez Martínez, 2014).

The myth of Luna and Endymion is depicted in the other full circle (Fig.6, left). Luna is the goddess of the moon and she can be seen driving a moon chariot across the heavens. In antiquity, Luna is usually depicted with her horse driven moon chariot. In this mosaic she also has a stunning half moon on her head. She is on her way to visit her mortal lover

Endymion, who is shown sleeping in his cave in the lower part of the circle. According to the Roman myth, Endymion fell in love with Juno and asked Jupiter to grant him eternal sleep, in which he became immortal and ageless (Pilar San Nicolás, 2014). Parallels to this Roman myth exist in Greek mythology with Hera and Zeus.

Figure 6 - Central scenes Mosaico de los Amores (left - myth of Luna; right - myth of Paris)

Besides these two full circles, the mosaic has four quarter-circles in each corner, representing the four seasons. These are personified with each character displaying a different attribute according to the season. The winter scene is depicted with mistletoe, a mantle covering the person's head from the cold and by the subdued colours. On the other hand, the spring scene is depicted by an abundance of flowers and plants in a bright, vibrant colour scheme. The presentation of the seasons is a symbol of the continuity of time and the different stages in life, going from childhood, youth, maturity and old age (Lopéz Monteagudo, 2014). In the six half circles between the corner scenes, Cupid, depicted hunting, is the protagonist. In the different scenes, Cupid is hunting different animals including a hare, a partridge, a pheasant and a rabbit. Lastly, the spaces between the circles, shaped like diamonds, show different animals such as a horse, a lion, a wild boar and a deer.

Figure 7 - Mosaico de los Amores, all scenes.

In general, the high quality of the mosaic's iconography stands out, not only due to the good state of preservation but also the high technical quality. The technique of using very small tesserae in the images in comparison to the rest of the floor mosaics of the room is a common practice during the Roman period (Izzo et al., 2016). This mosaic is unique because of the rich and varied colour palette and the different uses of material (stone, ceramic, glass-paste). Furthermore, the level of accuracy in the depiction of the human form shows a deep knowledge of anatomy. This gives the scenes dynamic movement. In addition, the shading of the figures enhances the dynamic movement, as seen in figures 6 and 7.

2.5 Roman mosaics and historical glass studies

The practice of using glass tesserae in mosaics has existed for over 2000 years and is an important component of cultural heritage around the world. A mosaic is defined as a collection of small fragments of different materials and colours embedded in a mortar, usually to form a pattern or an image. The earliest occurrence of the mosaic technique is

found in Mesopotamia and Egypt using polished natural stones placed in a deliberate order (Verità, 2000). Later, the use of shells and marble chips was attested. As the technique developed in the Mediterranean basin, the necessity for a larger and richer range of colours became apparent and is believed to have led to the introduction of cut glass tesserae. In addition to aesthetics, glass tesserae are favoured for their water resistance and their large range of colour intensities (Verità, 2000). Roman floor mosaics consisted of stone tesserae and opaque glasses. Since coloured glass was considered a luxury good, adding this expensive material enhances the elite status of the mosaics. Glass tesserae began to appear in pagan or religious monuments all over the Mediterranean. The evolution of this technology is still not clear and more studies are needed to fully comprehend the technological practices and to determine the best restoration and conservation techniques to be applied. To understand the material properties of the glass tesserae, the chemical composition of the glass and the conservation environment need to be understood (Brems et al., 2012; Izzo et al., 2016; Ricciardi et al., 2009b). Below, this thesis will delve deeper into the most important material properties of glass tesserae.

Glass is an amorphous, solid material. The three main elements necessary for making a raw glass are a glass former, a flux and a stabiliser. The glass former is silica (SiO_2), for which sand was used. A flux is added to this to reduce the melting temperature. In antiquity, this flux was added in the form of natron, a sodium carbonate (Na_2CO_3), (most common in Roman times) or plant ash. Finally, the mixture needs a stabilizer, for which lime (CaO) was added (Barca et al., 2016). This combination produces translucent glasses and they were produced in a limited number of primary production sites, known as glassmaking sites, in the Levant and Egypt and later traded all over the Mediterranean in chunks or ingots. The glasses were then re-melted at secondary production sites, termed glass working sites, where additional elements were added to produce the desired glass product. These additional elements were colouring agents, decolouring agents and opacifiers (Arletti et al., 2006; Caggiani et al., 2017; Verità, 2000). Roman glass tesserae are usually of the soda-lime type, which is chemically very stable, and they are usually opaque (van der Werf et al., 2009).

The existing information about Roman glass originates from different sources. Historical sources such as Pliny the Elder describe the glass production technique in his *Naturalist*

Historia XXXVI in 70 CE. Archaeological excavations and archaeometric analyses conducted over the past decades provide more information concerning Roman glass. Although archaeometric studies on Roman glass have significantly increased over the last decades, they have focussed mainly on translucent glasses and primary production sites (Abd-allah, 2010; Ceglia et al., 2013; Gallo et al., 2013; Ganio et al., 2012). Most of the glass studies involve sampling and destructive techniques (Arletti et al., 2006; Barca et al., 2016; Boschetti et al., 2017). Therefore, this thesis study hopes to contribute to understanding glass tesserae technology through non-destructive analysis and provide a methodology to employ in future non-destructive studies.

3 Materials and methods

3.1 Materials

The goal of the study was to do a full-coverage study of the mosaic. In total 227 tesserae were measured with 5 instruments which resulted in a total of 1175 measurements. For this thesis, we focused on two mythological scenes of the mosaic: the Paris scene, which is the largest one measured, and the Spring scene. These scenes were chosen due to their diverse colour palette. In the Paris scene, 96 tesserae were analysed and 48 tesserae in the Spring scene. Each mosaic tesserae piece was measured with the different instruments. The mosaic was measured *in situ* without any major sample preparation. The only sample preparation was the cleaning of the mosaic tesserae with a brush and with a sponge drenched in cleaning ethanol.

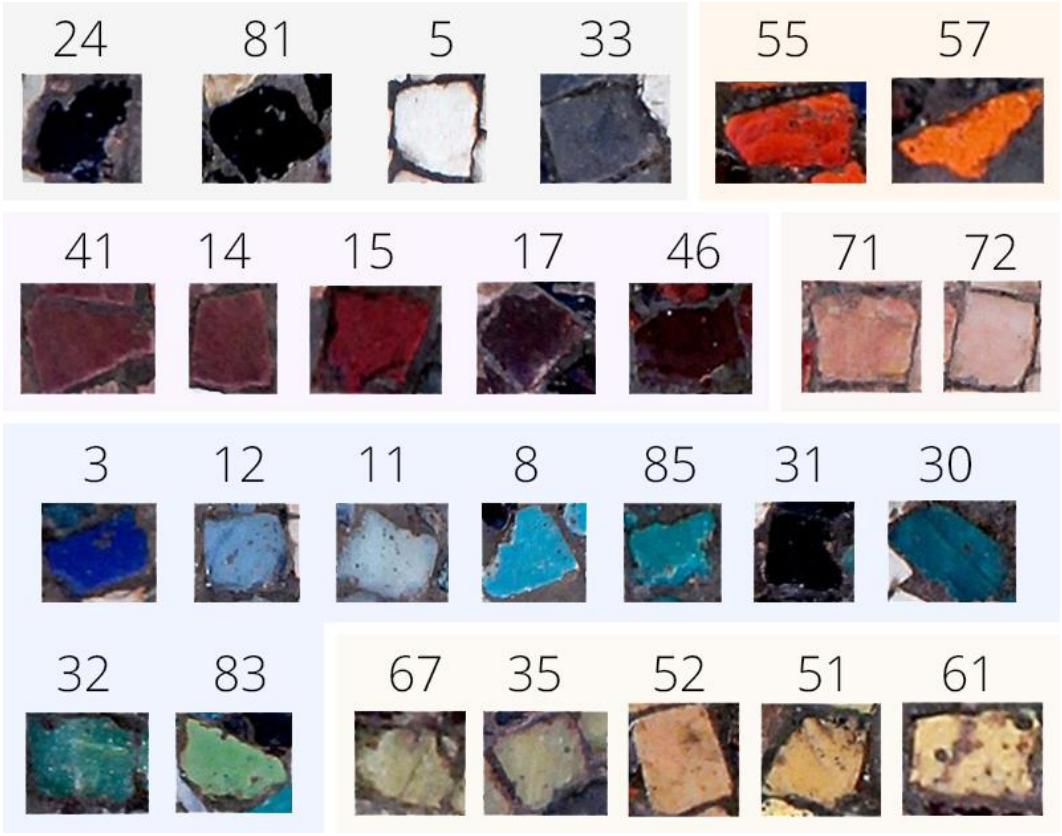

Figure 8 - Paris colours: Black (24, 81), white (5), grey (33), orange (55, 57), red (41, 14, 15), dark red (17, 46), pink/nude (71, 72), dark blue (3), blue (12), light blue (11), baby blue (8), turquoise (85), dark green (31), green (30), light green (32), bright green (83), yellowgreen (67, 35), yellow (52, 51, 61).

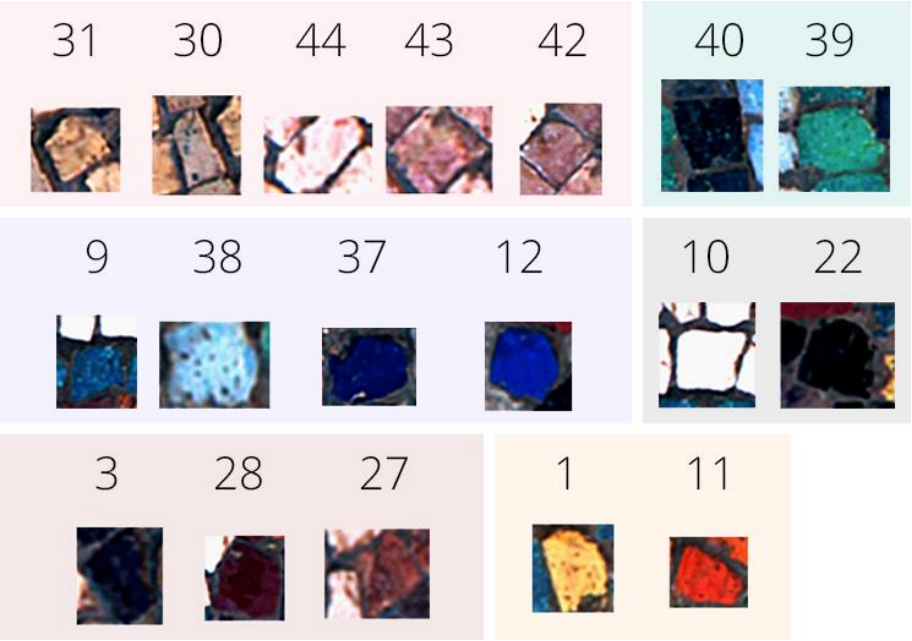

Figure 9 - Spring colours: Light orange (31), brown (30), nudes (44, 43, 42), dark green (40), green (39), turquoise (9), light blue (38), dark blue (37), blue (12), white (10), black (22), dark red (3, 28), red (27), yellow (1), orange (11).

Table 1 - Number of tesserae

Number of tesserae	
summer	20
eros1	18
spring	***48***
paris	***96***
Eros 2	40
apple paris	5
Total	**227**

Table 2 - Number of measurements

MEASUREMENTS	***hXRF***	***BWtek***	***enwave GR***	***enwave R***	***Bravo***	***TOTAL PER SCENE***
Summer	20	20	20	20	25	105
eros1	22	26	20	35	26	129
spring	***47***	***49***	***52***	***53***	***59***	***260***
paris	***87***	***103***	***99***	***99***	***111***	***499***
eros2	0	43	42	40	48	173
apple paris	9					9
TOTAL PER INSTRUMENT	185	241	233	247	269	**1175**

3.2 hXRF

XRF is a widespread elemental technique that can be non-destructive, meaning that the sample is undamaged during analysis. Furthermore, minimal sample preparation is necessary and in the case of handheld XRF, no sample preparation is needed. It is a relatively fast analytical technique, especially portable and handheld instruments, and has been applied widely in archaeometric studies (Colomban et al., 2012; Licenziati and Calligaro, 2016; Miriello et al., 2010; Pincé et al., 2016; Van Pevenage et al., 2014). This technique is user-friendly since it is computer operated. By using the appropriate software, the procedure can be almost completely automated. Different types of materials can be analysed using XRF such as liquids and solids. All the elements are detected in one single measurement making it a multi-elemental analysis. The main advantages of portable and handheld XRF instruments are the low operation costs and fast analysis. It can be used for conducting measurements *in situ*, for example in a museum or on the field, and has commonly been used on irreplaceable cultural heritage artefacts. Not only can the major elements be detected, but also the trace elements, which can provide information on technology and provenance (Shackley, 2011).

X-rays are energetic waves with a wavelength between 0,001 and 100 nm in the electromagnetic spectrum. They were discovered by Wilhelm K. Röntgen in the 19th century (Pollard et al., 2007). The basic principle of X-ray fluorescence spectroscopy is that X-rays coming from an X-ray source will hit and irradiate the sample. When the energy of the incoming X-rays is high enough, they can excite and eject an electron from one of the inner shells of the atom. This leaves a vacancy in the shell during which the atom is unstable. To return to a stable state, an electron from the outer shells of the atom will occupy the vacancy during which energy is released under the form of X-rays. This will lead to the emission of secondary X-Rays or characteristic fluorescence that is detected by an energy dispersive or wavelength dispersive XRF spectrometer. These secondary X-Rays have an energy that is characteristic for each element, thus the elements in the sample can be detected (Del Castillo and Strivay 2012; Scholze, 2006).

3.2.1 Instrumentation

A commercial hXRF instrument (Olympus InnovX Delta Premium) was used in order to obtain qualitative elemental information of the mosaics. The measurements were conducted in air under conditions listed in Table 3. The silicon drift detector is thermo-electrically cooled. The diameter of the X-ray is 10 mm in normal conditions but can be reduced to 3 mm when using a collimator. During this field campaign, the measurements were conducted under collimated conditions with a beam size of 3 mm. Furthermore, the instrument is equipped with a camera making it easier to choose and determine the zone to be measured (Coccato et al., 2017; Lauwers et al., 2014).

Elements are detected from Mg onwards (Z=12). The analyser produces two different energetic X-beams, one of 10 kV and one of 40 kV. The 10 kV beam makes it easier to detect low Z-elements from Mg to Mn (Pincé, 2018). The instrument was not connected to a field laptop during the measurements but at the end of each day the data were transferred from onto a laptop using a USB connection. The instrument does not require electricity and was battery operated. Multiple Li-ion batteries were available and recharged every night.

Table 3 - Conditions Olympus InnovX Delta Premium

Parameter	***Conditions***
Tube voltage	40 kV, 10 kV
Tube current	79 µA
Detector	Silicon drift detector (SDD)
Measuring time (life time)	150 s
X-ray tube /source	Rh
Beam size	10x10mm^2 or 3x3mm^2

The ideal life time conditions were determined by testing different life times on the same spot. The spectra were compared in order to choose the best option. Taking into account the practical limitations such as the quantity of tesserae to be measured and the available time of the field campaign, we opted for a final life time of 150 seconds for each measuring mode. The noise reduction of a lifetime of 150 seconds compared to 100 seconds can be observed in Fig.10. The life time is the time during which the detector is actually measuring the X-rays. In reality the sample will be irradiated with X-rays for a longer period than 150 seconds, but the secondary X-rays will be detected by the detector during 150 seconds. This phenomenon

occurs at the 10kV beam as well as the 40 kV beam. Besides the life time (LT), there is a death time (DT), a time during which the secondary X-rays are not detected by the detector. The relation of the real time (RT), DT and LT is:

LT = RT (1-DT), in which LT and RT are expressed in seconds and DT is expressed in a percentage

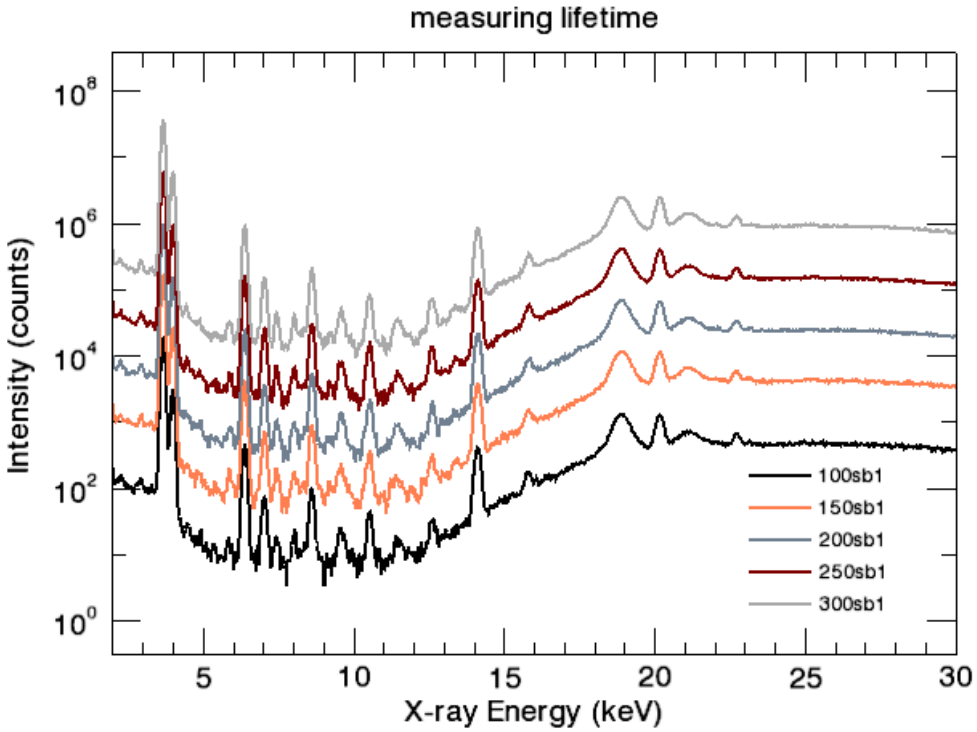

Figure 10 - Testing different lifetimes.

For each analysed mosaic piece, one point measurement was conducted. For the Paris scene 87 mosaics were analysed and 47 for the Spring scene (Table 1). In the Paris scene, not all mosaics are incorporated in the hXRF measurements. This was due to a strict time schedule during the field campaign. It was opted to skip some tesserae of colours that were already well represented in other measurements. In order to control the safety during the analyses, a minimum distance of a few meters was maintained from the measuring area (Fig.11).

Figure 11 - hXRF instrumentation in the field

3.2.2 Data processing

The recorded spectra were analysed with the "Analysis of X-ray spectra by iterative least squares" (AXIL) software (Van Espen et al., 1986; Vekemans et al., 1994). This technique allows obtaining qualitative elemental information, which can help in distinguishing groups within the mosaics. It detects the elements that are present in the sample as well as the intensity. The basic principle of the quantitative analysis of the spectrum is that there is a relation between the intensity of the peak and the concentration of that specific element in the sample (Van Espen et al., 1986; Vekemans et al., 1994). The area under the peak is related to the concentration of the element in the sample. However, no absolute values are known. Even if only relative values are obtained with hXRF, this gives us a good primary look into the elemental information of the analysed materials and allows for a first comparison between the data.

For each measurement, a unique fitting model was created. By producing a unique fitting model per spectra the spectral artefacts could be easily identified. Apart from the peaks of the measured elements, other peaks are present in the spectra. Some of the primary X-rays are scattered by the sample instead of absorbed. When these scattered rays are elastic, they keep the same wavelength as the incoming rays and no energy is lost. This is called coherent or Rayleigh scattering and is usually a peak represented by the element of the source of X-ray, in this case rhodium. When these scattered rays are inelastic, they have a lower energy

and longer wavelength than the incoming X-rays, and this is called incoherent or Compton scattering. The Compton peak is broader and has a lower energy than the Rayleigh peak (Pollard et al., 2007). Besides these scattering peaks, sum peaks and escape peaks are also identified in some samples. This is case for elements with a very high intensity. A sum peak is the result of the method of detection of the secondary X-rays. When two photons arrive close to each other, the detector is unable to differentiate the two photons and will register one photon with an energy that is the sum of the two single photons (Pollard et al., 2007). Escape peaks are found when a photon interacts with the detector. When the detector is a Si solid state detector, the photon can excite Si atoms to release Kα X-rays. If these X-rays escape from the detector, the peak will not appear at the original energy of the incoming photon but at an energy lowered by the Si Kα energy, 1,74 KeV (Tanaka et al., 2017). Fig.12 demonstrates the escape peaks from Fe in a sample with high Fe intensities. At last, the instrumental interferences should also be taking into account. The spectral quality of the instrument was tested (Pincé, 2018) and revealed interference of Ni, Cu and Au. Especially the Au interference was clear in the spectra, giving false peaks while no gold was detected. Caution should be taken when dealing with these elements, though we can assume that this interference is similar in all the spectra. Thus, when comparing spectra the effect of the instrumental interference can be equal. The peak X-ray intensities are used for further data processing.

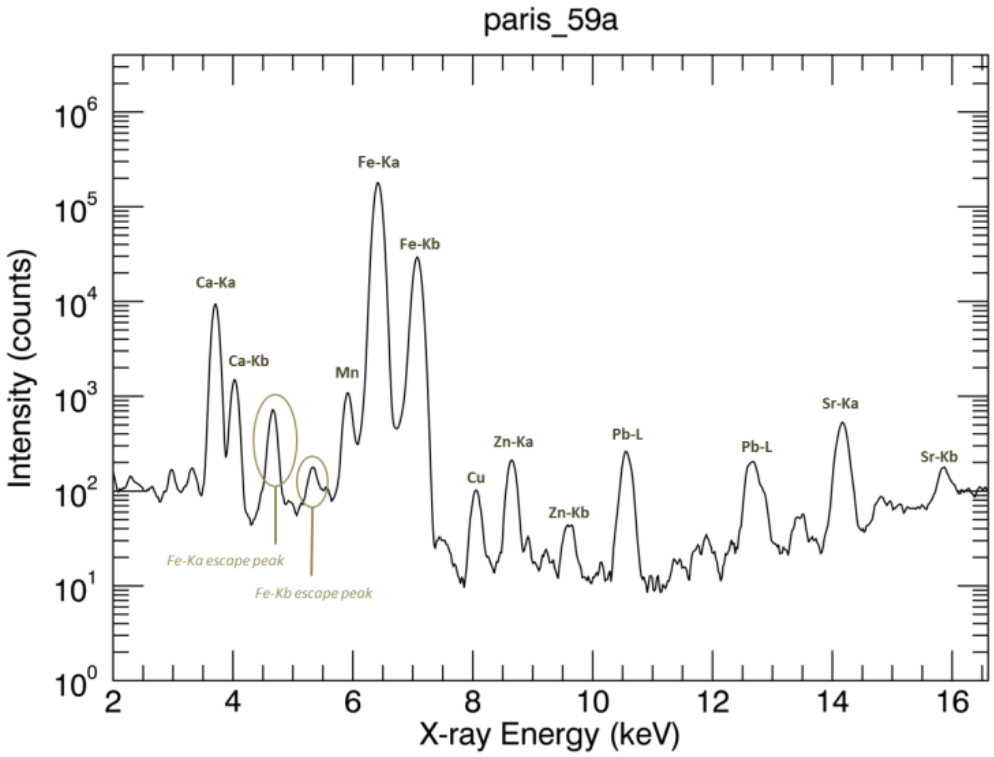

Figure 12 - Example hXRF spectrum indicating escape peaks of iron

Since the database exists of varied data because we are dealing with different types of materials, a first step was to divide the large dataset in subsets. By plotting the values of Ca and Si against each other, normalised by Rh, obtained with the 10 kV mode, it was able to see a clear division in two groups: stone and glass mosaics. The glass mosaic tesserae were normalised over Si for both modes. The best relative standard deviation percentage was calculated to find an internal standard for the stone tesserae and finally the data were normalised over Ca for both modes. Further compositional information is obtained with bivariate plots. Even though hXRF has its limitation and no absolute values are attained, it is semi-quantitative and some patterns can be observed.

3.3 Raman Spectroscopy

Raman spectroscopy is a molecular spectroscopic technique that is employed widely in archaeometry, cultural heritage studies and conservation science. Mobile instruments are designed for conducting analyses *in situ*. The uses of Raman spectroscopy go from the identification of pigments, the study of degradations products, corrosion processes and organic materials (Cosano et al., 2017; Rousaki et al., 2018; Vagnini et al., 2017; Vandenabeele, 2004; Veneranda et al., 2017). The technique has several advantages that make it popular in art and archaeology research. Firstly, the non-destructive character allows for wider application in archaeology and art studies. Secondly, the analyses can be conducted rather quickly. Thirdly, no or limited sample preparation is necessary. Lastly, Raman spectroscopy provides molecular information of organic and inorganic materials, depending on the laser source, and therefore provides complimentary information to XRF analysis (Bersani et al., 2016; Lauwers et al., 2014; Vandenabeele, 2004).

The basic principle in Raman spectroscopy is that incoming light is absorbed which leads to an excitation of a molecule. During the de-excitation of the molecule, light is emitted. It is the inelastic scattering of this light that is known as the Raman effect. The Raman effect was discovered in 1928 by Sir C. V. Raman and K. S. Krishnan by demonstrating the inelastic scattering of a light by a fluid for which he was awarded the Nobel prize for Physics in 1930. Most of the emitted energy has the same wavelength as the incoming energy: the Rayleigh scattering. However, Raman scattering occurs when the emitted energy has a different wavelength as the incident energy. Raman spectroscopy determines the modes of molecular motions: vibrations. When a chance in the molecular polarizability occurs during these vibrations, the Raman effect is observed (Vandenabeele et al., 2014).

As mentioned the use of portable and mobile Raman instrumentation has increased in popularity since it eliminates the need of bringing artefacts to laboratories. A distinction between different types of mobile instrumentation has been made by Lauwers (Lauwers et al., 2014). A transportable instrument can be carried from one site to another although it is not designed to be moved frequently. Most bench-top Raman instruments are transportable. A mobile instrument is designed for mobile use and can be brought on site

rather easily. They usually have a stable spectrometer. A portable instrument is carried on the field by a single person. Finally, a handheld instrument can be operated by holding it in one hand and it is usually battery operated.

Bench-top instruments have some features that have an advantage over mobile/handheld instruments. For one, the laboratory is a stable environment where microscope images can also be obtained. Secondly, bench-top instruments have an improved sensitivity. The large focal length of the instruments results in an improved resolution. In some cases, when the object has a rather flat surface, Raman mapping is possible. Thirdly, and most importantly, it is possible to have multiple lasers in the instrument, which enables the reduction of fluorescence background. Though, in some cases characteristic photoluminescence can help identifying the materials (Bersani et al., 2016; Vandenabeele et al., 2014).

However, *in situ* analyses are performed with mobile or handheld equipment. In this case, no chemical or mechanical sample preparation is possible. Therefore, it is important to be able to work with an adjustable laser power. Another useful aspect in mobile or handheld instruments is the ability block the laser beam during the work, which increases the safety of both the user and the artefact. By blocking the laser beam during positioning, the artefact is exposed to less laser irradiation (Vandenabeele et al., 2014). During *in situ* analysis the speed of the analysis is of great importance because it is related to the sensitivity of the instrument. During this research, three different mobile and handheld instruments were employed.

3.3.1 EZRAMAN-I-DUAL Raman system (Enwave Optronics, Irvine CA, USA)

This mobile fibre-optic-based spectrometer from TSI Inc is equipped with two lasers: a red diode laser (785 nm) and a green Nd:YAG laser (532 nm) and spectra are recorded in the range of 100 and 2350 cm^{-1} and 100 and 3200 cm^{-1}, respectively (Fig. 13). The spectral resolutions are 6 cm^{-1} and 7 cm^{-1} for the 752 and 532 nm lasers, respectively. The instrument is equipped with three interchangeable lenses for each wavelength. To conduct the measurements during this campaign, the standard lens (STD) was used with a focal length of ca. 7 mm and a circular spot size of 74 ± 2 µm and 88 ± 2 µm for the 785 nm and 532 nm

laser, respectively. The instrument is equipped with a CCD detector and an adjustable power controller for each laser with a maximum power outlet of 400 mW and 100 mW for the 785 nm and 532 nm laser, respectively. The spectrometer can be used by applying 230 V AC or by using an internal or external Li-battery (Lauwers et al., 2014). During the research, the battery was the main way of using the machine although in some cases it was possible to connect it to a generator.

Figure 13 - Set up EZRAMAN-I-DUAL Raman spectrometer in the field.

3.3.2 i-Raman® EX (B&WTEK)

The i-Raman® EX portable Raman spectrometer has an excitation laser of 1064 nm and covers a spectral range from 100-2500 cm^{-1} with a resolution of less than 10 cm^{-1} at 1296 nm (Fig. 14). The instrument is equipped with a high sensitivity InGaAs array detector with deep TE cooling. In addition, it is equipped with a fibre optic Raman probe and probe holder and an adjustable laser power controller with maximum laser power of 499 mW. The laser has a spot size of 85 µm. The spectrometer delivers a high signal to noise ratio without inducing auto-fluorescence. A voltage of 100-240 VAC can be applied. During this measuring campaign the instrument was power operated using a generator that was available on site.

Figure 14 – i-Raman® EX Raman spectrometer

3.3.3 BRAVO handheld Raman spectrometer (Bruker)

This handheld Raman spectrometer by Bruker is equipped with two excitation lasers (DuoLaser™) ranging from 700 to 1100 nm during acquisition. Spectra are collected in the spectral range of 300 – 3200 cm^{-1}. The second laser is not intended to try to mitigate fluorescence, as in common in commercial handheld or portal Raman spectrometers, but it is a way to collect spectra up to 3200 cm^{-1}. In this way, the CH stretching region is accessed. Thus, the first laser is used to obtain data in the fingerprint region, while the second laser obtains data from the CH region. BRAVO uses a new technology called Sequentially Shifted Excitation (SSE™), a patented fluorescence mitigation, in which they mitigate fluorescence without reducing sensitivity. Furthermore, BRAVO comes with an automated inbuilt wavelength calibration. It has a wavenumber accuracy of ± 1 cm^{-1} in the fingerprint and ± 2 cm^{-1} in the CH-stretching region. The applied laser power is less than 100mW for both regions. No fibre cable is available for the BRAVO and the laser exits the instrument through a measuring tip. This tip is interchangeable with a measuring tip for vials, which was used for measuring the reagents. Measurements on the samples were performed using the standard measuring tip (measuring tip for bags). The instrument is operated using a touchscreen. The instrument was battery operated and was recharged overnight by placing it in the docking station. The docking station requires a voltage of 100 – 240 VAC, has a size of 36 x 15 x 13 cm and weighs 1.9 kg. By using the two lasers from 700 to 1100 nm, the sensitivity to inorganic green en blue is reduced in comparison with a 532 nm laser (Jehlička et al., 2017; Vagnini et al., 2017).

The Raman spectra collected with the i-Raman (B&WTEK) and the EZRAMAN-I-DUAL (Enwave) are processed in GRAMS (ThermoFisher Scientific). The Raman spectra collected with the Bravo are processed in OPUS^{TM}.

3.4 Digital Microscopy

Apart from the hXRF instrument and Raman spectrometers, a digital microscope was employed during this field campaign (Fig. 15). The model used was a HIROX model KH-8700. The main unit has a weight of around 15kg. The instrument can be used with a power of AC100 to 240V and was connected to a generator. The Dual Illumination Revolver Zoom Lens was used (MXG-2500REZ) allowing magnification from 35x up to 2500x (Table 4). Furthermore, the instrument has triple objective turret. Due to the dual illumination mechanism, both co-axial and ring lighting are possible. Three objective lenses can be accessed with an optical zoom range of over 70 times the minimum magnification providing a field of view from 8 mm up to ca. 0.12 mm. The three lenses and here magnifications are mentioned below (Table 4).

Table 4 - Features digital microscope HIROX KH-8700

Model	***MXG-2500REZ***		
	Low-Range	**Mid-Range**	**High-Range**
Magnification	35~250x	140~1000x	350-2500x
Field of View	8.17~1.22mm(H)	2.18~0.31mm(H)	0.87~0.12(H)
Operable distance	10.0mm	10.0mm	10.0mm

https://www.hirox-europe.com/products/microscope/index8700.html

Figure 15 – Set up HIROX microscope in the field

4 Results and discussion

4.1 Material composition

As discussed in the introduction, Roman mosaics could be produced from different materials including stone tesserae, glass tesserae, glazed stone, ceramics, etc. Based on the Ca/Si ratio's obtained with the hXRF analysis, the mosaics are divided into two groups for further analyses (stone and glass tesserae). This is an assumption and not a strict division and caution is advised, since the hXRF results do not comprise absolute values. For example, it is possible to find aluminosilicate rich rocks within the glass. However, coupling the hXRF data with the Raman results can confirm the composition of the tesserae. Together with the visual information (on the field) and the microscopy pictures, the distinction between glass and stone mosaics can be assumed.

On figures 16 and 17 the division in the two material groups is clear. The stone mosaics have a higher calcium and lower silica content while the glasses separate themselves with a lower calcium and higher silica content. In what follows, the Raman and hXRF results will be discussed per scene and per colour to discuss the material composition of the tesserae. In the second part of the results, the comparison between the different Raman instruments will be discussed.

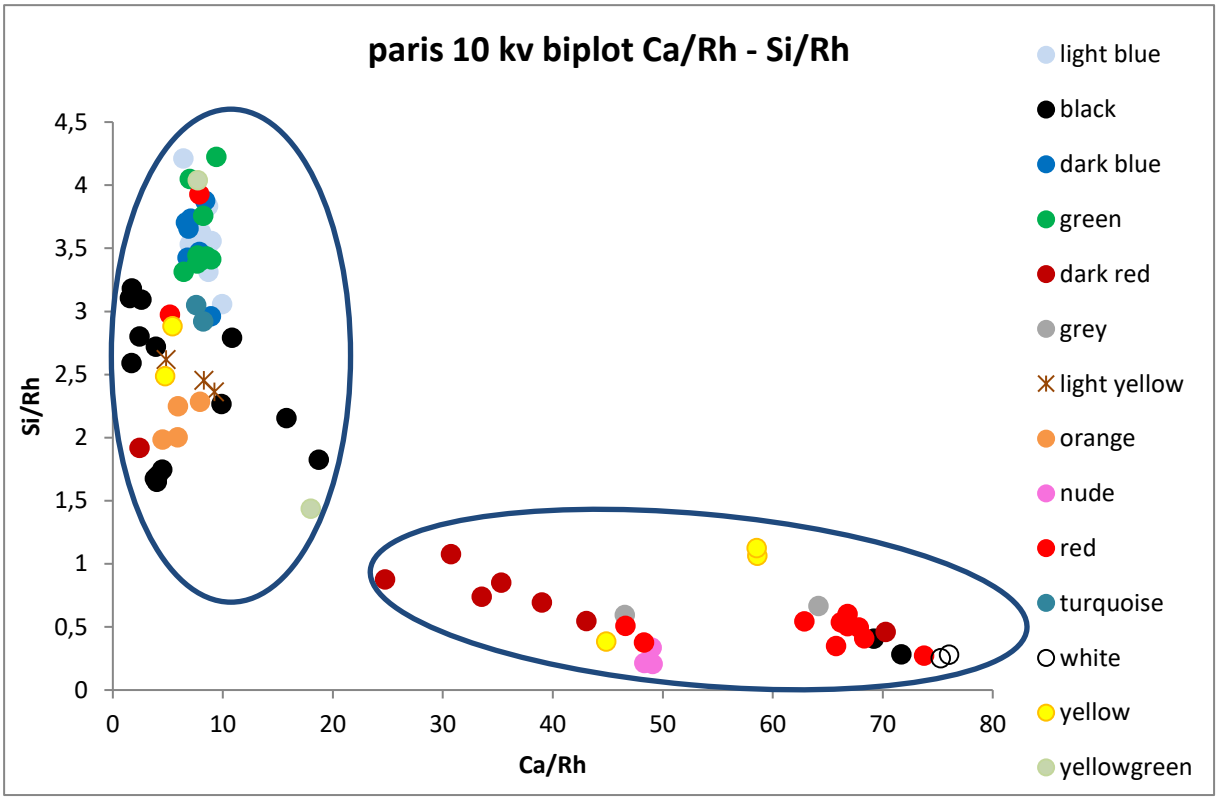

Figure 16 - Bivariate plot Ca/Rh and Si/Rh of the Paris scene in the 10 kV mode

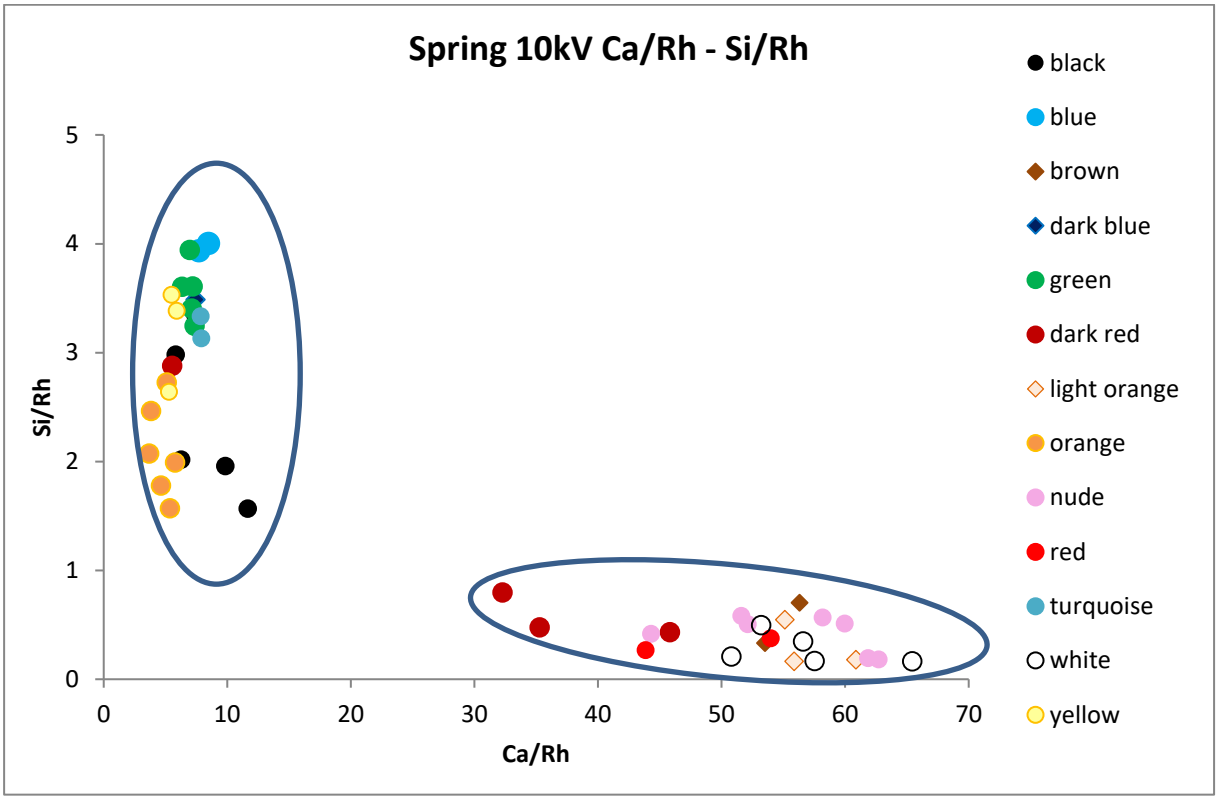

Figure 17 – Bivariate plot Ca/Rh and Si/Rh of the Spring scene in the 10 kV mode

4.1.1 Paris

Table 5 - Identification Raman signals Paris scene

Colour	*signal 1064 nm*	*signal 785 nm*	*signal 532 nm*
black	Calcite + titanium dioxide + carbon black	Calcite + titanium dioxide + carbon black + α-quartz	calcite
white	Calcite + dolomite	Calcite + dolomite	Calcite + dolomite
grey	Calcite + dolomite	Calcite + dolomite	Dolomite
pink/nude	Calcite	Calcite + dolomite	Calcite + dolomite
red			
dark red	Calcite + haematite	Calcite + haematite	Calcite
red	Calcite + dolomite + haematite + α-quartz + anatase	Calcite + dolomite + haematite + α-quartz + anatase	Calcite + dolomite
orange			
yellow	Calcite + dolomite	Calcite + dolomite	Dolomite
blue			
dark blue	Calcite (fade) + $CaSb_2O_6$	$CaSb_2O_6$	
blue			
light blue	Gypsum		
baby blue			
turquoise			
green			
dark green			
green		Calcite (fade)	
light green			
yellowgreen			

White

The white tesserae are produced with calcareous stones. Raman signals for calcite and dolomite are identified with all four lasers. No white glass tesserae are identified. White tesserae are used in the background of the mosaic and in the figures as well: in the clothes, as skin colour, in attributes of the figures. The signal is usually the strongest in the 1064 nm laser.

Nudes

In the mosaic a variety of colours are categorized as “nude”. These represent different skin tones but are also used for the representation of animals (the ox’s) and of clothes. The different hues go from light pink, pink, beige, light brown and darker brown. The nude tesserae have a similar Raman spectrum, with either calcite or dolomite (Fig. 41 and 42). The same is observed in the grey tesserae: only calcite or dolomite signals are identified. The strongest signals are the bands at 1086 and 1099 for calcite and dolomite respectively (Edwards et al., 2005). As seen on Figure 16, all the nude hues and the grey tesserae are located in the group with stone tesserae. The stones chosen were of calcareous nature, which is the case for most analysed stone tesserae of the mosaics and which was common during Roman times (Capedri et al., 2001; Galli et al., 2004; Izzo et al., 2016; Miriello et al., 2017). The different nude hues are naturally occurring in the different rocks. None of these colour tesserae consist of glass pieces.

Red

The red tesserae are divided in two categories: dark red tesserae and red tesserae. In general, both groups have a higher calcium and lower silica content and can therefore be attributed to stone tesserae. However, the dark red tesserae have remarkable lower calcium contents than the red tesserae. Instead, they contain more Si, K, Ti and mostly more Fe compared to red tesserae (Fig. 18). Furthermore, the dark red tesserae have a higher Mn, Cu, Zn and Pb content.

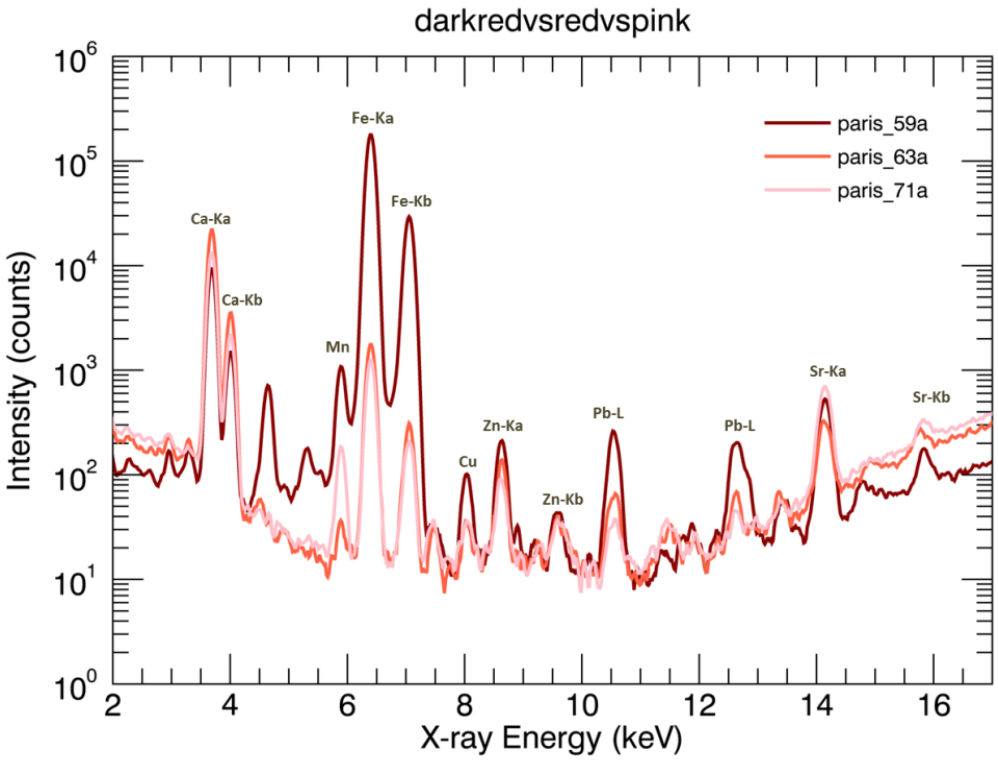

Figure 18 - hXRF spectra of dark red, red and pink tesserae

The two subcategories in red tesserae are visible in the Raman results as well. For the red tesserae the only phases identified are calcite or dolomite (Fig.19). In one case both calcite and dolomite were identified together (Paris 63, Fig.19c). For the dark red tesserae, Raman results identified calcite or dolomite with haematite (Fig.20). The high Fe content in the hXRF data confirms this (Fig.21). The haematite identified with the red 785 nm laser is shifted compared to the one identified with the infrared 1064 nm laser (Buzgar et al., 2013; Caggiani et al., 2016). Raman spectroscopy can differentiate between the ordered and disordered structure of haematite and the haematite spectrum depends on the energy of the exciting radiation (Rousaki et al., 2015). The shift can be due to the difference in size, morphology and orientation of the haematite crystallites as well (Prinsloo et al., 2008). Moreover, a shift of 5 cm^{-1} to 15 cm^{-1} is possible due to difference in laser power. Cosano et al. attested a shift of haematite towards lower wavenumbers by increasing laser power (Cosano et al., 2017; de Faria et al., 1997). Consequently, haematite bands in literature can show substantial shifts.

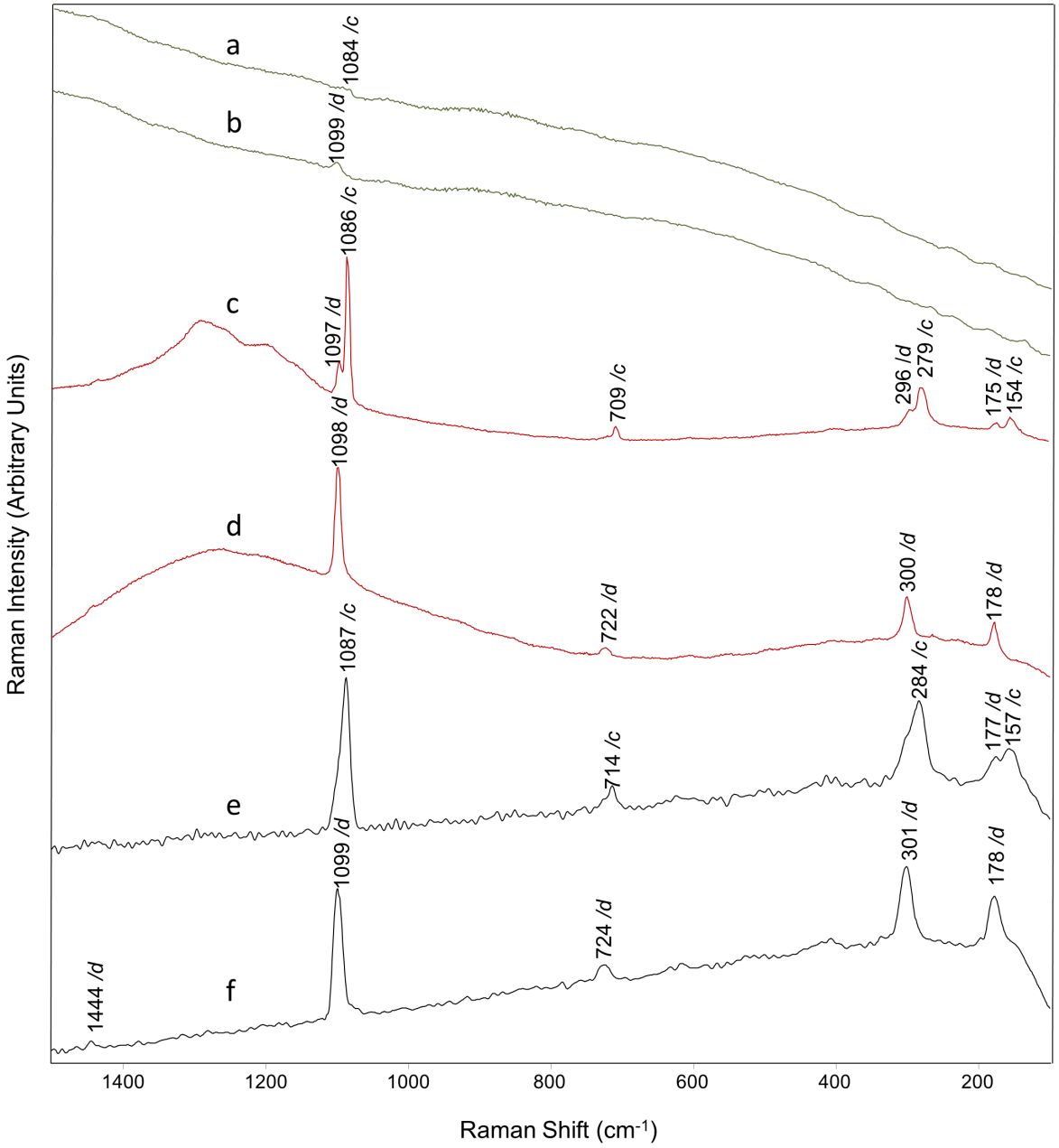

Figure 19 - Raman spectra of Paris 63 and Paris 14, a (Paris 63 with 523nm), b (Paris 14 with 532nm), c (Paris 63 with 785nm), d (Paris 14 with 785nm), e (Paris 63 with 1064nm), f (Paris 14 with 1064nm), obtained between 100 cm^{-1} and 1500 cm^{-1}

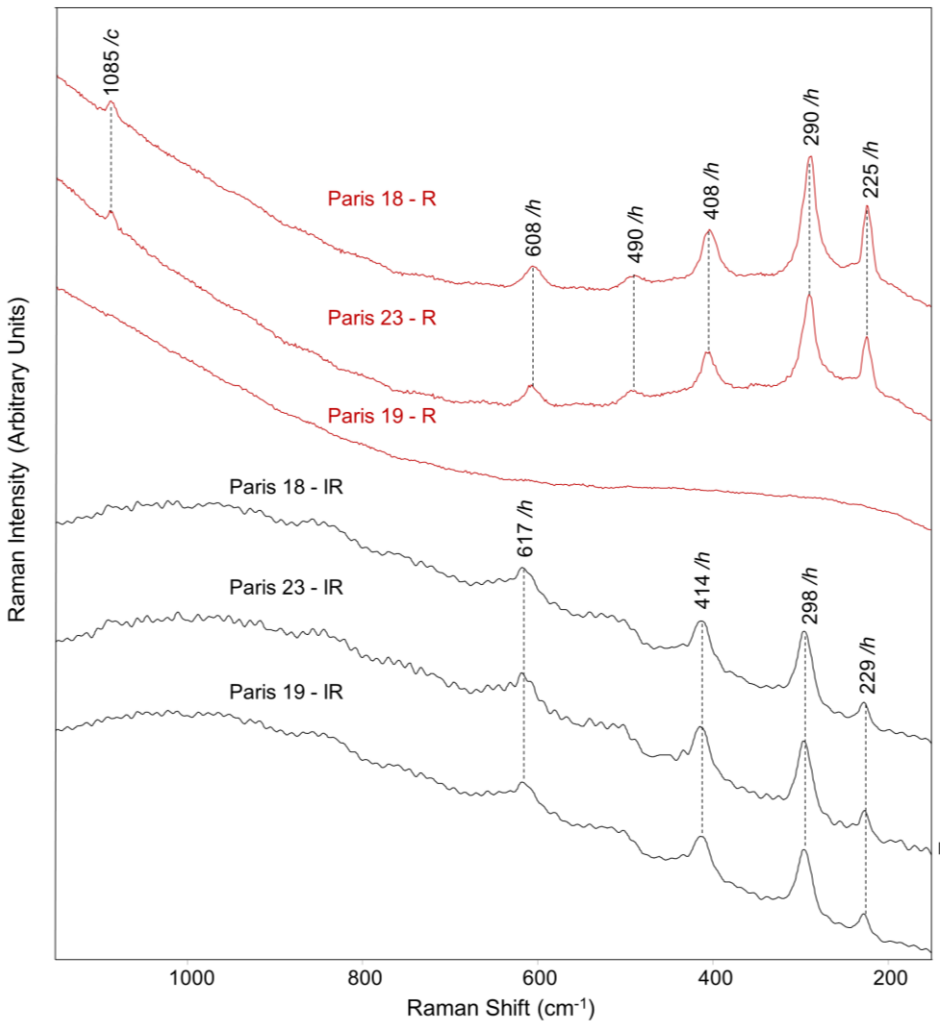

Figure 20 - Raman spectra of Paris 18, 23 and 19 with 785 nm (R) and 1064 nm (IR) obtained between 150 cm^{-1} and 1150 cm^{-1}

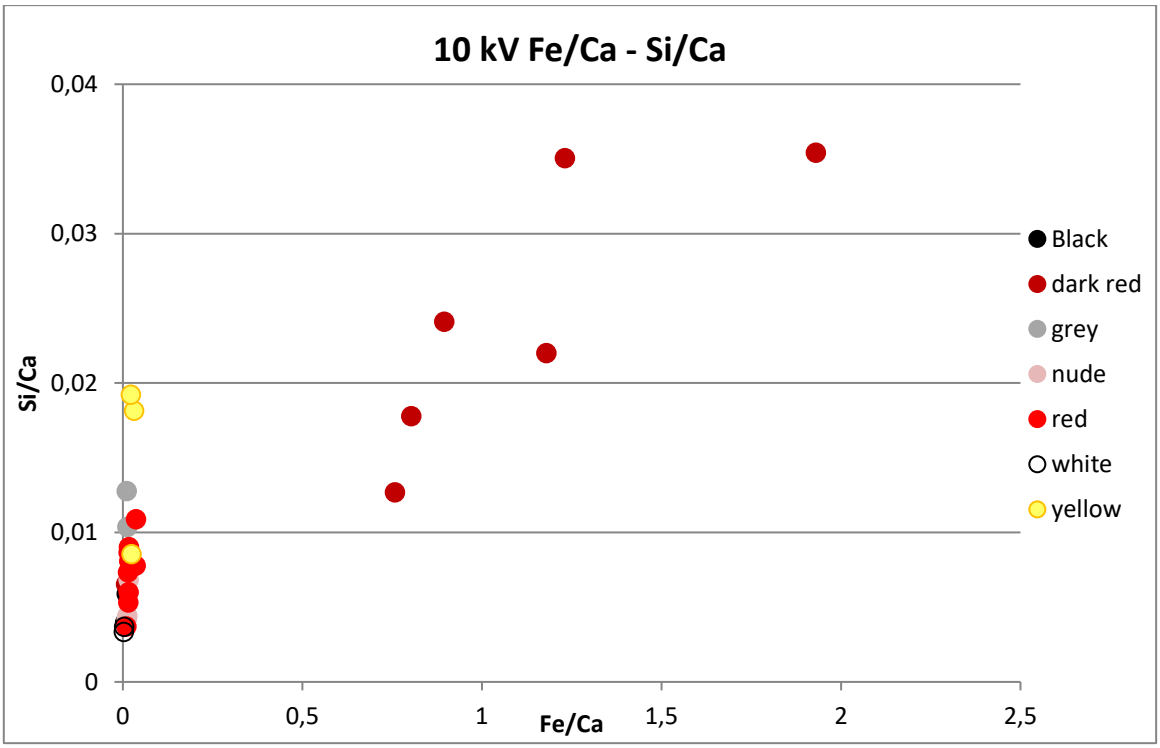

Figure 21 - Bivariate plot Fe-Si, Paris scene, 10kV

Although the majority of red and dark red tesserae seem to be made from stone, a few exceptions can be seen (Fig 16). Two red and two dark red tesserae in the Paris scene consist of glass: Paris 13 and 15 (red), Paris 17 and 46 (dark red). For Paris 17 no hXRF data is available. Most of these red glasses did not give good Raman signals relating to crystalline phases belonging to the origin of the colour. Ancient red glasses are usually produced using copper and iron in a lead-rich matrix (Ricciardi et al., 2009a). The hXRF results reveal a higher Fe and Cu content in the red tesserae, while the dark red tesserae have significant higher lead content (Fig.22). The red tesserae also contain more Ca compared to the dark red tesserae.

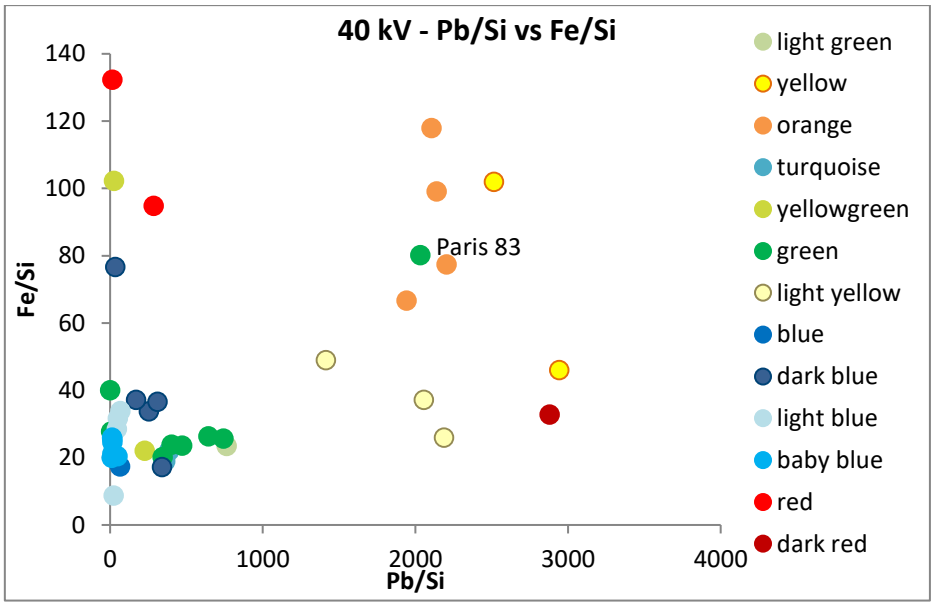

Figure 22 – Bivariate plot Fe-Pb, Paris scene, 40 kV

The presence of lead creates a reducing condition enabling copper to transform to the cuprous state: Cu^{2+} to Cu^{+}. However, to obtain metallic copper (Cu^{0}), an even stronger reducing atmosphere is necessary, for which Fe was usually added (Arletti et al., 2006). The combination of lead and iron was necessary to create the reducing atmosphere to create the Cu^{0} state and to maintain this state as well (Basso et al., 2014). This dispersion of metallic copper particles in the glass matrix generated red opaque coloured tesserae during Roman times (Arletti et al., 2006). Different hues of the red are the result of different dimensions of the copper particles and the differences in distance between the copper nanoparticles (Colomban and Schreiber, 2005).

There is a consensus that copper is responsible for orange, red and brown colour and opacity in Roman glasses, and that these colours are produced under reducing conditions (Silvestri et al., 2014). Yet, the nature of the copper phase is still disputed. Some studies attribute the process to the presence of cuprite while others believe metallic copper is responsible for the colouring of the glass (Freestone, 1987; Padovani et al., 2006). When copper and lead are both present in high quantities in the glass, cuprite dendrites are developed. In glass with a low copper content, independent from the lead amount, metallic copper nanoparticles would be the producing colorant. However, the coexistence of both phenomena is attested as well (Barber et al., 2009). More cuprite crystals of constant small sizes and homogeneity

of the cuprite distribution creates a more intensive and heterogeneous colour (Gedzevičiute et al., 2009). Since no clear Raman signals were obtained in the red tesserae, it was not possible to determine the colour to cuprite or metallic copper nanoparticles.

Raman analysis on glasses coloured by metallic particles are challenging and depend on the laser wavelength and the experimental setup. The colour is determined by the light absorption because of the Surface Plasmon Resonance (~400 nm for Cu^0), which complicate the generation of a good spectrum (Ricciardi et al., 2009a). The SPR is the oscillation of free electrons on the surface (Basso et al., 2014). These electrons cause a strong absorption of the incoming energy range of the laser resulting in a decrease of the laser beam. The penetration depth is decreased and the Raman signal of the opaque red glasses is actually a surface phenomenon. The Cu^0 interacts with the exciting laser and generates a resonant Raman spectrum (Colomban and Schreiber, 2005).

The microscopy images of the red tesserae show linear bands with some bands appearing darker, black even (Fig. 45). In literature the red bands are described as containing more copper nanoparticles while for the red bands only a small amount or no copper has been attested. Copper particles dissolve quickly, meaning they lose their colour if the glass comes into contact with air. These darker bands are probably areas of partially oxidized glass, which is a result of uneven or incomplete mixing of the glass (Santagostino Barbone et al., 2008).

One clear Raman spectra obtained of a dark red glass tesserae is represented below. With the 785 nm laser (Fig.23a) bands at 146, 396 and 634 cm^{-1} can be attributed to anatase, while bands at 352, 462 and 1375 cm^{-1} can be attributed to α-quartz. A fade signal of calcite is identified at 1087 cm^{-1}. In the 1064 nm laser anatase bands are identified at 144 and 514 cm^{-1}, while α-quartz bands are identified at 208 and 466 cm^{-1}. Weak bands at 300 and 406 cm^{-1} are attributed to haematite (Fig.23b). The haematite bands are not sharp but broader, which could be due to the differences in particle size or morphology of the crystallites (Prinsloo et al., 2008). Finally, two broad weak bands at ca. 1305 and ca. 1597 cm^{-1} are identified in the 1064 nm laser. These could be attributed either to amorphous carbon, haematite or α-quartz (Buzgar et al., 2013; Hernanz et al., 2008).

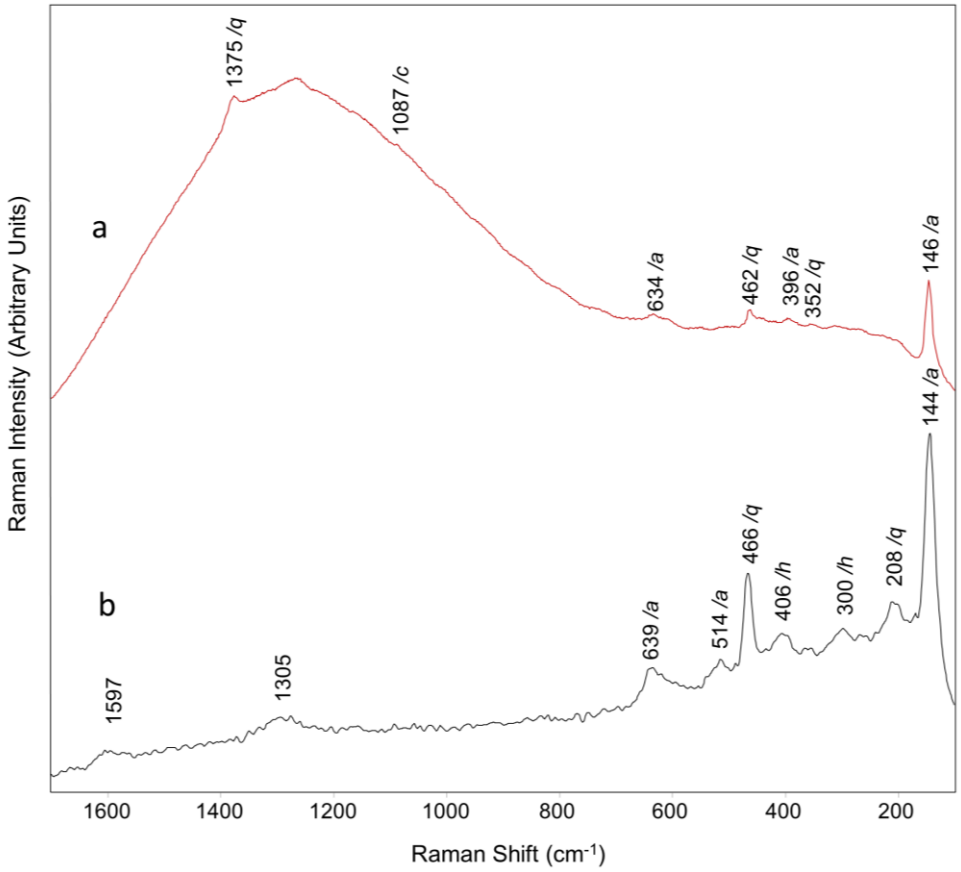

Figure 23 - Raman spectra of Paris 17 (dark red):
a (785 nm), b (1064 nm) obtained between 100 cm^{-1} and 1700 cm^{-1}

Orange

The orange coloured tesserae in the Paris scene are all glass mosaic tesserae and are a variant on the red opaque glass, discussed above. The colour is determined by cuprite crystals or by the presence of metallic copper nanoparticles. Cuprite crystals of a larger size are said to produce a redder colour whereas an increase in crystal particles would produce an orange colour (Gedzevičiute et al., 2009; Santagostino Barbone et al., 2008).

Comparable to the red opaque glass tesserae, the orange tesserae also show linear bands of lighter and darker orange (Fig. 49). No clear Raman signatures could be obtained for the orange tesserae in the Paris scene. Pb is present in high amounts together with Sn (Fig. 25). Figure 26 shows the presence of Pb and Cu. The orange tesserae also have a higher Fe amount, which was needed to create a more reducing atmosphere as discussed for the red tesserae. The high amount of copper, together with iron and lead, in the orange tesserae is shown in Figure 24 (top), while the high amount of tin is seen in Figure 24 (bottom).

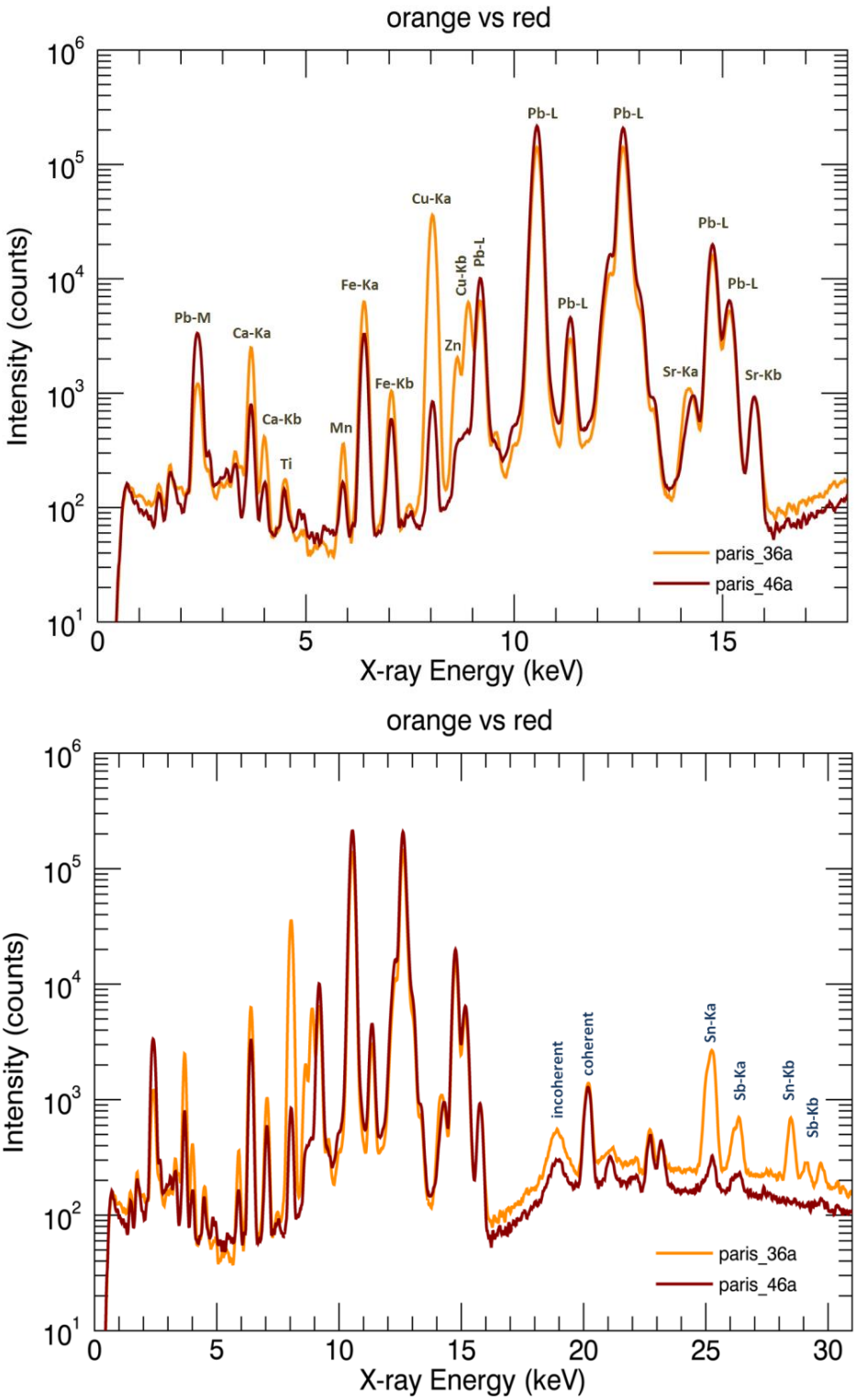

Figure 24 - hXRF spectra of dark red and orange tesserae (top: 10kV, bottom: 40kV)

Yellow

Yellow tesserae are made of two material groups: the duller yellow mosaics are made from stone while the more intense yellow colour appears to be glass. The stone yellow tesserae have Raman signals for calcite and dolomite, similar to the white and nude tesserae (Table 5). No good Raman signatures could be obtained for the yellow glasses, however the hXRF data provides some information regarding the colorants in the glasses. The yellow glass tesserae have a high lead and tin amount (Fig. 25). The lighter yellow glasses have a slightly lower lead and tin amount. The detection of lead and tin, together with antimony suggest the presence of lead antimonate (bindheimite or Naples yellow, $Pb_2Sb_2O_7$) or lead-tin antimonate ($Pb_2Sb_{2-x}Sn_xO_{7-x/2}$) (Arletti et al., 2006; Basso et al., 2014; Ricciardi et al., 2009a). The lead yellow acts as an opacifying and colouring agent (Gedzevičiute et al., 2009). However, the Raman features of these phases are not identified.

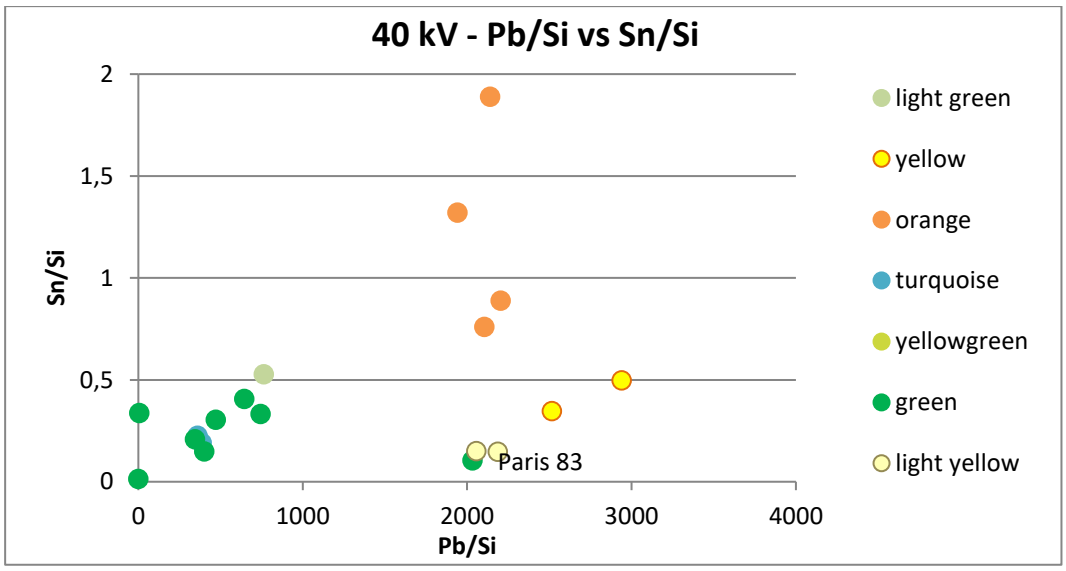

Figure 25 – Bivariate plot Pb-Sn, Paris scene, 40 kV

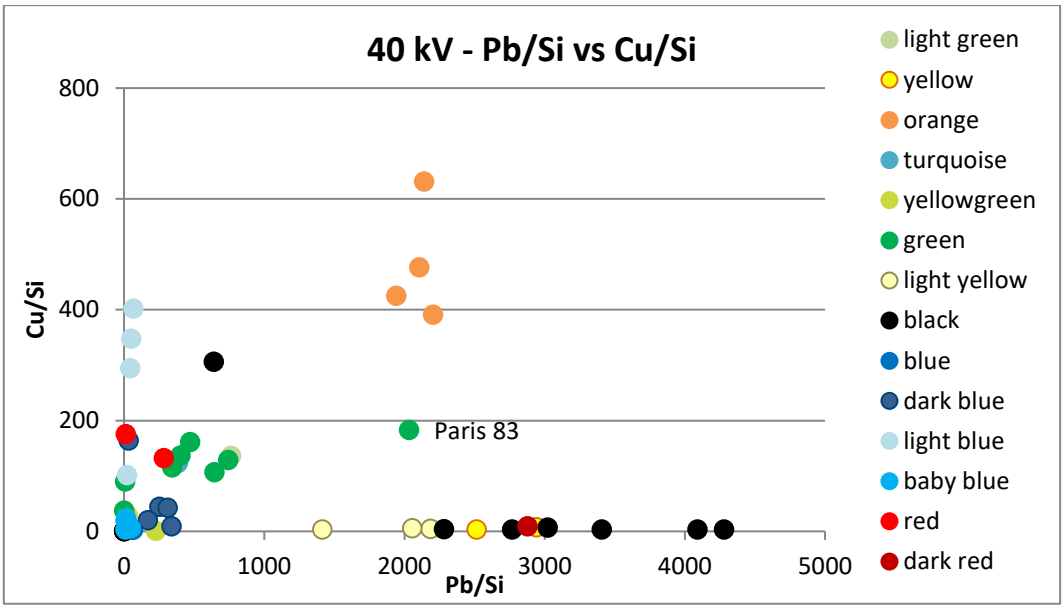

Figure 26 – Bivariate plot Pb-Cu, Paris scene, 40 kV

Blue

The blue tesserae in the Paris scene are divided in different colour categories and are all made of glass. The blue colour is due to the presence of cobalt and copper (Fig. 29A and 29B).

Dark blue

The dark blue tesserae are characterised by the presence of Co, while the other blue hues have less cobalt in their composition (Fig. 29A). Cobalt ions (Co^{2+}) are a strong chromophore and can produce a deep blue colour even when present in low amounts. This is due to the strong absorption in the yellow regions of the visible spectrum (Basso et al., 2014). Additionally, the amount of Sb and Ca suggest that Ca antimonate was used as an opacifier in the dark blue glasses. The presence of the opacifier does not affect the colour of the glass. The hXRF result of the dark blue glasses correspond to other studies performed on Roman glasses (Arletti et al., 2006; Boschetti et al., 2008; Caggiani et al., 2013; Gedzevičiute et al., 2009; Gliozzo et al., 2010; Verità, 2000). The Raman spectra of the dark blue tesserae do not give good signals apart from a weak band at 670 cm^{-1} and 699 cm^{-1} in the 1064 and 785 nm laser wavelengths, respectively (Fig. 27). This band could possibly be attributed to calcium antimonate. However, in the 532 nm wavelength, a weak band at 655 cm^{-1} is unidentified.

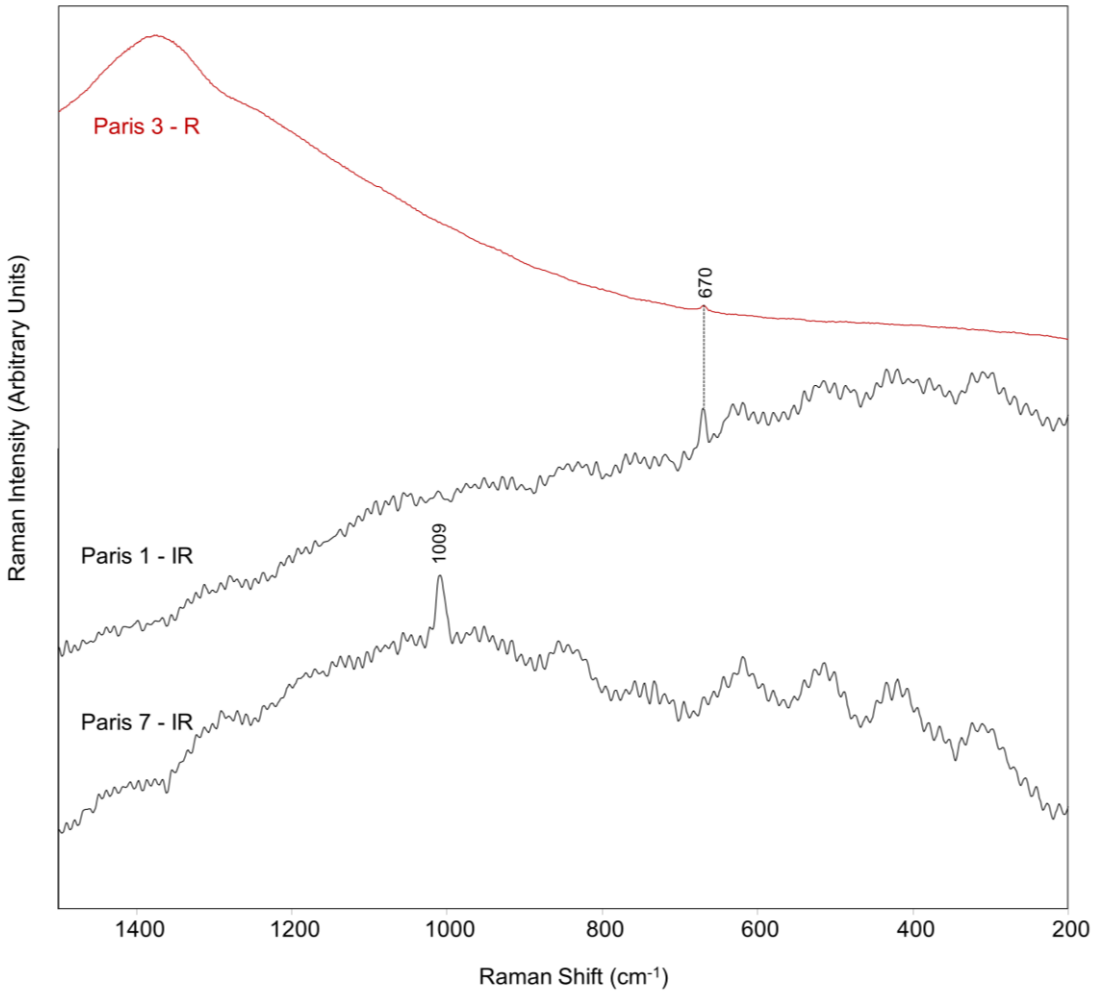

Figure 27 - Raman spectra blue tesserae: Paris 3 - R (785 nm), Paris 1 - IR (1064 nm), Paris 7 - IR (1064 nm), obtained between 200 - 1500 cm^{-1}

Light blue

The light blue colour is due to the presence of copper (Fig. 29B). Cu^{2+} is a common colorant for producing a light blue translucent glass (Gedzevičiute et al., 2009). The presence of antimony and calcium indicate the use of calciumantimonate as opacifier. The presence of copper in combination with specific elements can identify the raw material that contained the copper. When copper is present in combination with a significant amount of tin, bronze or bronze scraps were added to the glass batch as colourants (Polikreti et al., 2011). This could be the case for the light blue tesserae in the Paris scene since tin is also identified in the hXRF data (Fig. 28 bottom).

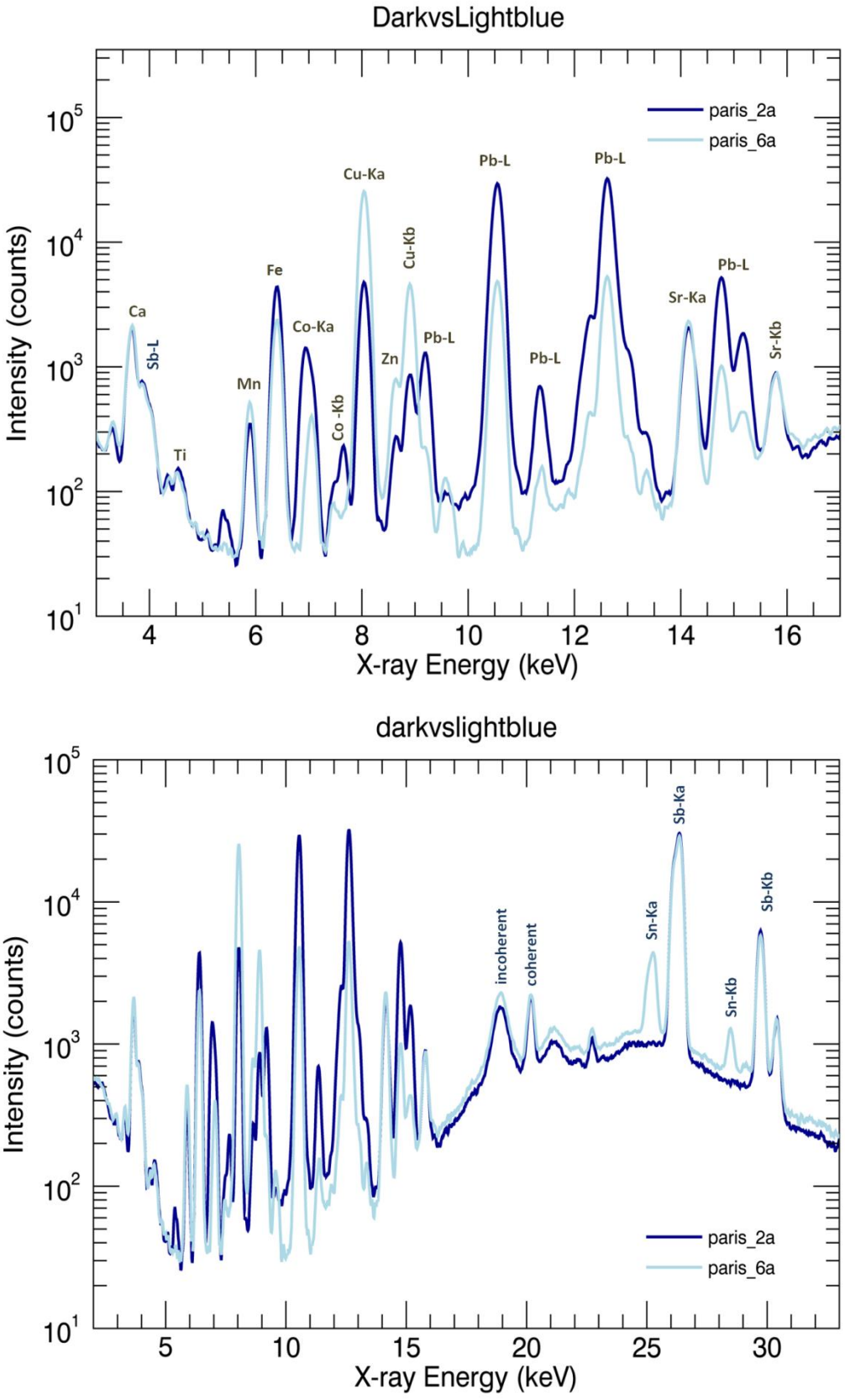

Figure 28 - hXRF spectra of dark blue and light blue tesserae (top: 10 kV, bottom: 40 kV)

Baby blue

The baby blue tesserae have a similar cobalt amount as the light blue tesserae, but have a lower amount of antimony (Fig. 29A). Further, the hXRF results indicate they have a lower copper amount compared to the light blue colour (Fig. 29B). The low amount of Co present could be enough to produce the blue colour (Basso et al., 2014).

Blue

Only one tesserae was ascribed as 'blue' and it shows similar amount of Co and Cu as the baby blue colour (Fig. 29). The Sb amount is slightly lower than the amounts observed in the baby blue colour. Since antimony is related to the opacifier calcium antimonate, the reduction of Sb could mean a lower amount of opacifier present in the glass, resulting in a slightly darker blue hue compared to the baby blue tesserae. No good Raman signals were obtained of the blue coloured tesserae.

Turquoise

Turquoise coloured tesserae are usually obtained by mixing green and blue colourants together. In this case the colour could be attributed to the mix of cobalt (creating a blue colour) and iron and copper (creating a green colour) (Boschetti et al., 2008). Copper in the divalent state (Cu^{2+}) forms the light blue colour. The colour is usually obtained by melting the glass in oxidizing conditions (Lima et al., 2012). As seen figures 29B and C, the turquoise tesserae have a similar Cu and Sb content as the green tesserae, however the turquoise tesserae also have a small amount of Co present in the glass. One dark blue tesserae, Paris 37, stands out with a low Co and Sb amount and higher Cu content. It is possible that this tesserae should be grouped with turquoise tesserae and was wrongly categorized as dark blue in the field.

The Cu content of the turquoise tesserae is lower than the light blue tesserae, but higher than the baby blue and dark blue tesserae (Fig. 29B). There is a small amount of Sn present, which could be due to the recycling of opaque glass (Lima et al., 2012), or by the mixing of a blue Cu-coloured glass with a yellow glass (Gedzevičiute et al., 2009). No good Raman signals were obtained of the turquoise coloured tesserae.

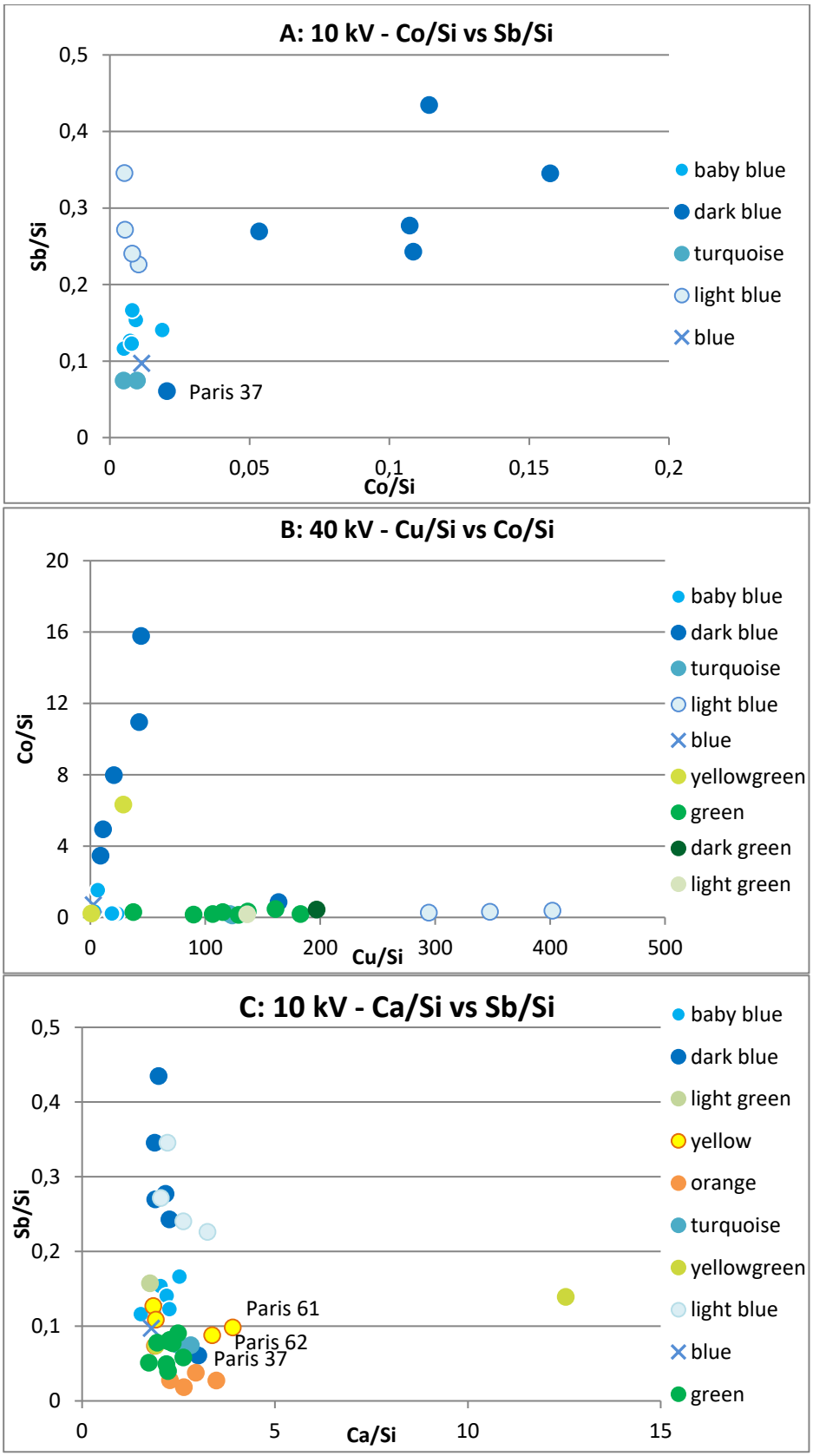

Figure 29 – A – Bivariate plot Co-Sb-L, Paris scene, 10 kV; B – Bivariate plot Cu-Co, Paris scene, 40 kV; C – Bivariate plot Ca-Sb, Paris scene, 10 kV

Green

Green

In general, the hXRF results of the green tesserae place all the green tesserae in the glass tesserae group. The elemental results show a high amount of copper but antimony and tin are present as well (see figures 30 and 31 top). The green colour is probable ascribed to the presence of a blue colorant together with a yellow-based opacifier (Arletti et al., 2006; Licenziati and Calligaro, 2016). Given the presence of lead and antimony, the possible yellow opacifier could be lead antimonate, however no Raman signals for this opacifier have been identified in the Raman measurements. Cu and Fe could be responsible for the blue colorant, and small amounts of Co were also detected in the green tesserae (Fig. 29B). The presence of tin in association with copper might propose the use of bronze scraps as a raw source for copper (Basso et al., 2014).

Dark green

The dark green tesserae are chemically pretty similar to the other green hues. The tessera has a slightly higher concentration of Cu, Fe and Mn. No Raman signals were identified in the dark blue tesserae.

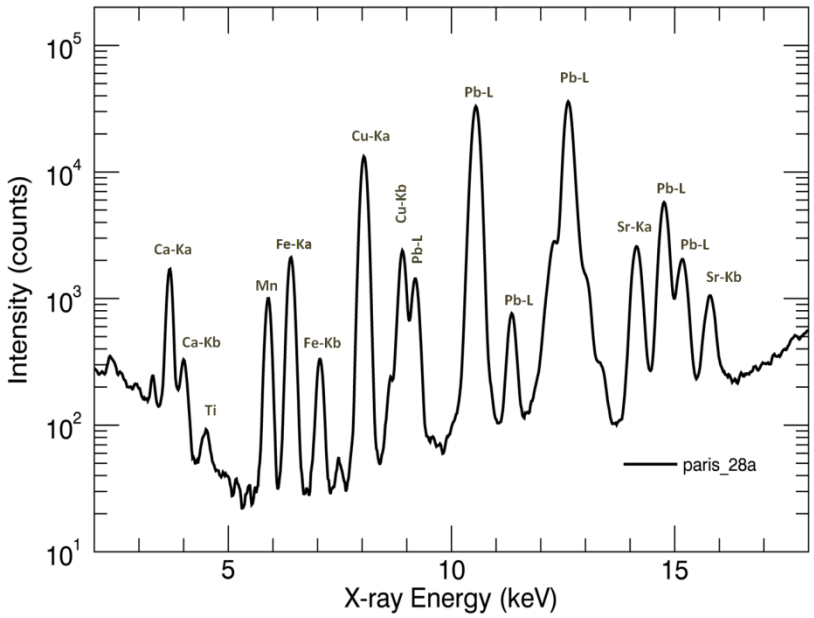

Figure 30 - hXRF spectra of green tessera, 10 kV

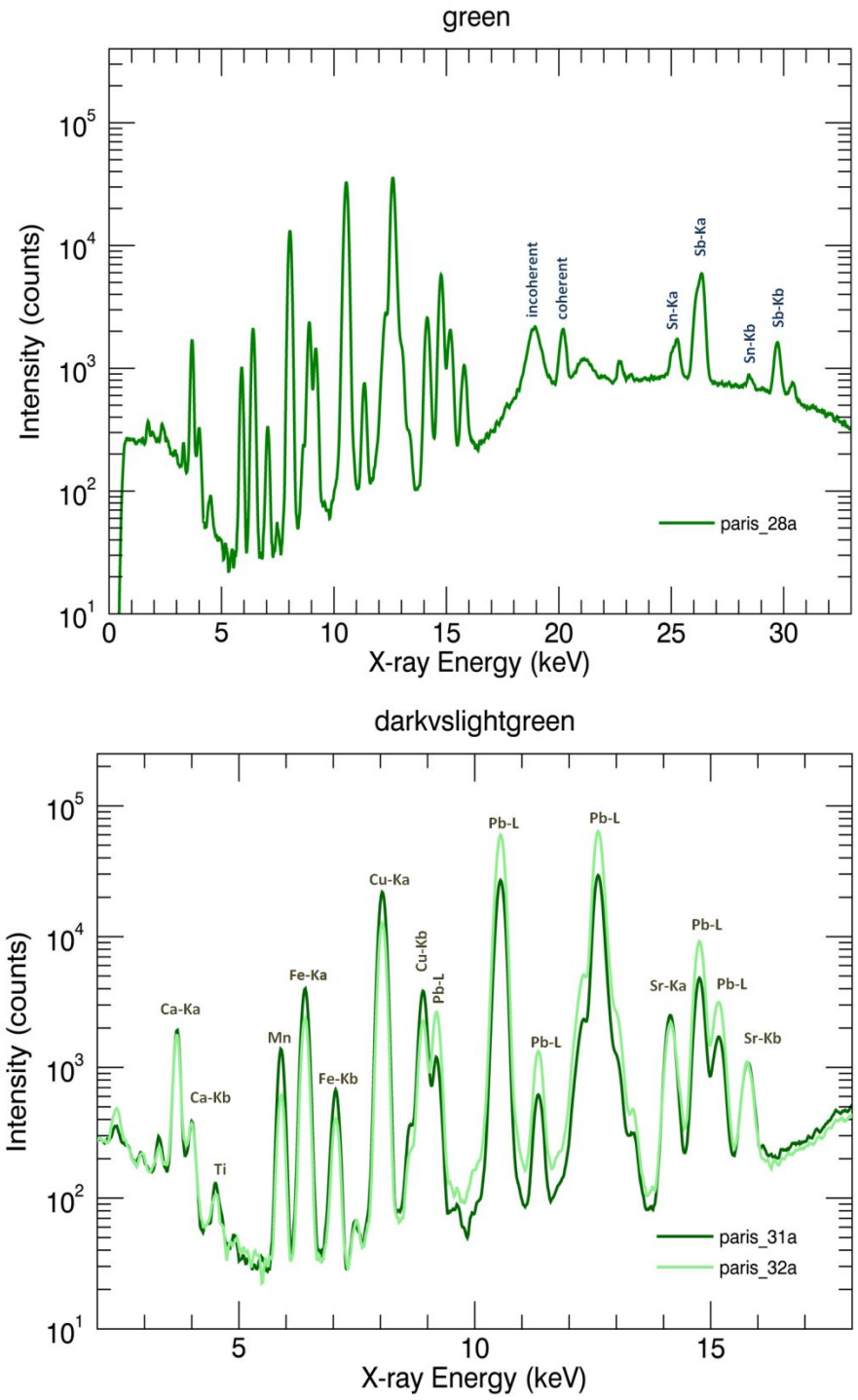

Figure 31 - hXRF spectra of green tessera (top - 40 kV), dark and light green tesserae (bottom - 10 kV)

Bright green

One tessera, Paris 83, can be distinguished from the other green tesserae. This is due to the intense green colour of the tesserae, emerald green. The bright green tessera shows a significant higher amount of Pb compared to the other green tesserae (Fig. 32 and 26). Furthermore, the Cu and Fe content is higher compared to the light green and green tesserae. The relationship of Pb with higher amounts of Sb creates the crystallisation of lead antimonates, which is used to form the emerald green shade (Barca et al., 2016). Paris 83 did not yield good Raman signals.

Light green

A slightly higher Sn, Pb and Sb content are present in the light green tesserae compared to the other green glasses, except for the bright green tesserae, which is discussed above. Fe, Mn and Cu are lower than the other green tesserae (Fig. 31 bottom). No clear Raman signals were obtained in the light green tesserae.

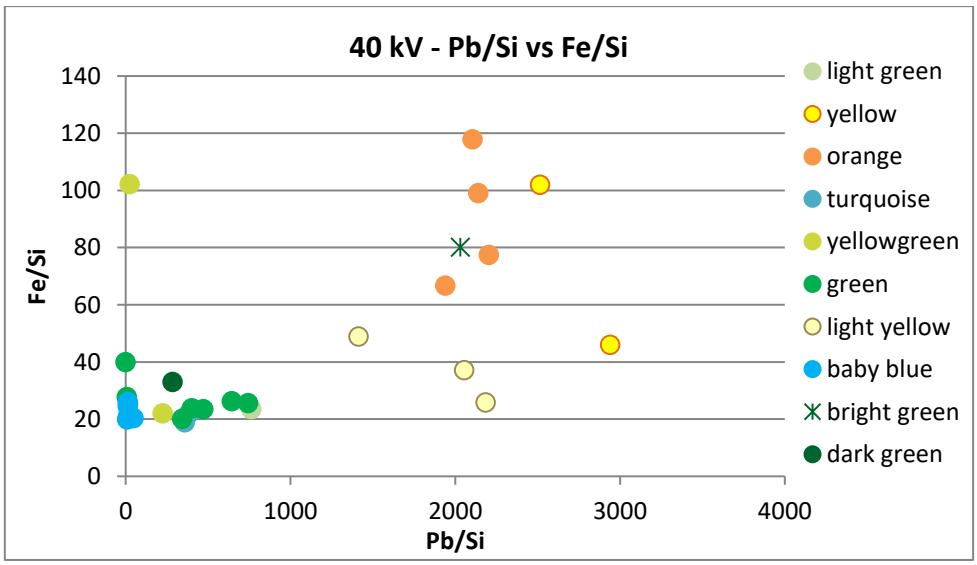

Figure 32 - Bivariate plot Pb-Fe, Paris scene, 40 kV

Yellowgreen

The yellowgreen tesserae have a significant lower amount of Cu compared to the green tesserae. Furthermore, the Mn and Pb content is lower. In literature, yellowgreen Roman tesserae are attributed to the presence of large particle aggregates of lead and antimony (Arletti et al., 2006; Basso et al., 2014). No clear Raman signals were identified in the yellowgreen tesserae.

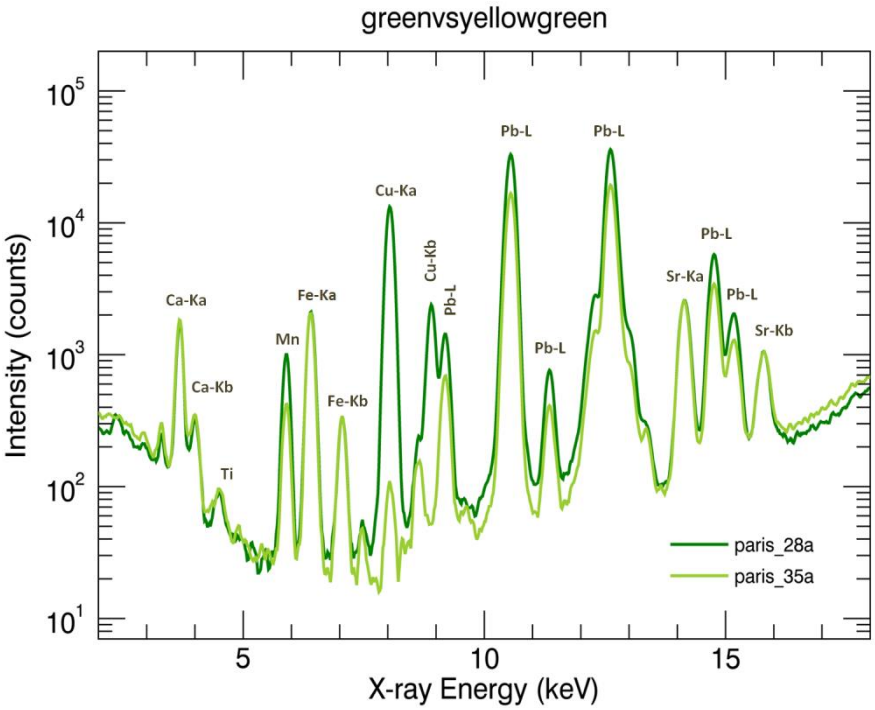

Figure 33 - hXRF spectrum green and yellowgreen tesserae, Paris scene, 10kV

Black

In the black coloured tesserae in the Paris scene, there was a difference in intensity and colour hue noticed during the field campaign. This difference is reflected in the chemical and Raman data. Some of the black mosaic pieces are made from stones while other are glass mosaics (Fig. 16). The high Ca and low Si amount separate the stone tesserae from the glass tesserae.

Black stone

In the Paris scene, two stone black tesserae were identified. It consists of a dark, blackish mosaic at the mouth of the ox and a dark, blackish mosaic at the shadow near the foot of Hermes. It must be noted that their colours are very similar to the two dark mosaics measured in the dark circle surrounding the Paris scene (Paris 33 and 34), which were categorized as "grey". The Raman signals for these tesserae show the typical signal produced by the stone tesserae in this mosaic and the hXRF results are similar for the stones as well (Fig. 34). However, the calcite signals in the Raman spectra are less clear than the calcite signals in the white and nude tesserae. The main calcite peak at 1086 cm^{-1} is the only observed in 1064 nm and 785 nm laser, while in the 523 nm laser, the main peak is only present as a fade signal. Moreover, in the 1064 nm laser, a lot of fluorescence is present in the lower wavenumber region of the spectra (Fig. 35).

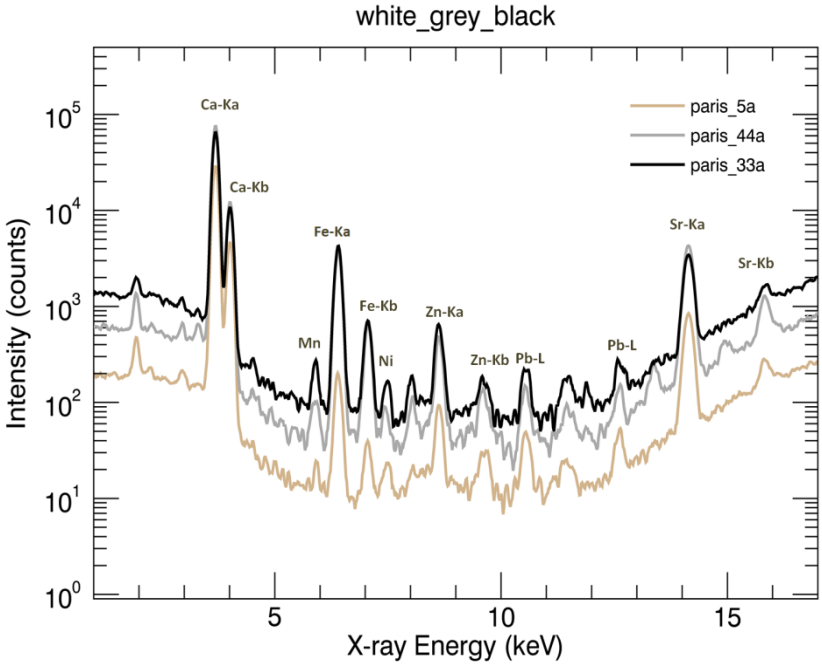

Figure 34 - hXRF spectra white, grey and black stone tesserae, Paris scene, 10 kV (Paris 5 – white, Paris 44 – grey, Paris 33 – black).

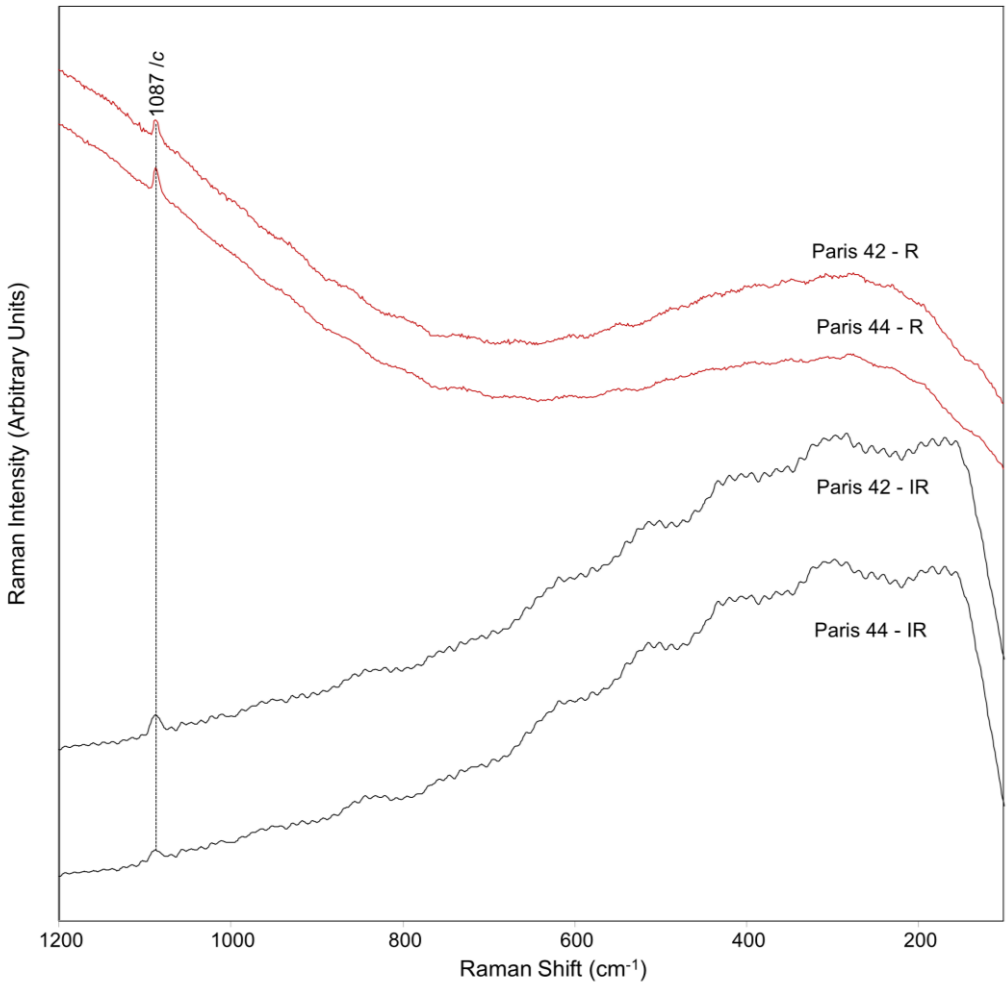

Figure 35 – Raman spectra of black stone tesserae, (Paris 42 – R and Paris 44 – R with 785 nm, Paris 42 – IR and Paris 44 – IR with 1064 nm), obtained between 100 and 1200 cm^{-1}

Black glass

Based on the hXRF results, three groups can be distinguished in the black glasses:

- Group 1: Paris 24, 27, 49, 77, 81, 82 and 38 (but a bit separate)
- Group 2: Paris 78, 79, 80, 43
- Group 3: Paris 93, 94, 95

Table 6 - Groups black tesserae Paris scene

Paris blacks	***Al***	***K***	***Ca***	***Ti***	***Fe***	***Pb-L***
Group 1	Low	Low	Low	Low	Low	High (except 38 – med.)
Group 2	High	Med.	Low	High	Med.	Low
Group 3	High (except 93)	High	High	High	High	Low

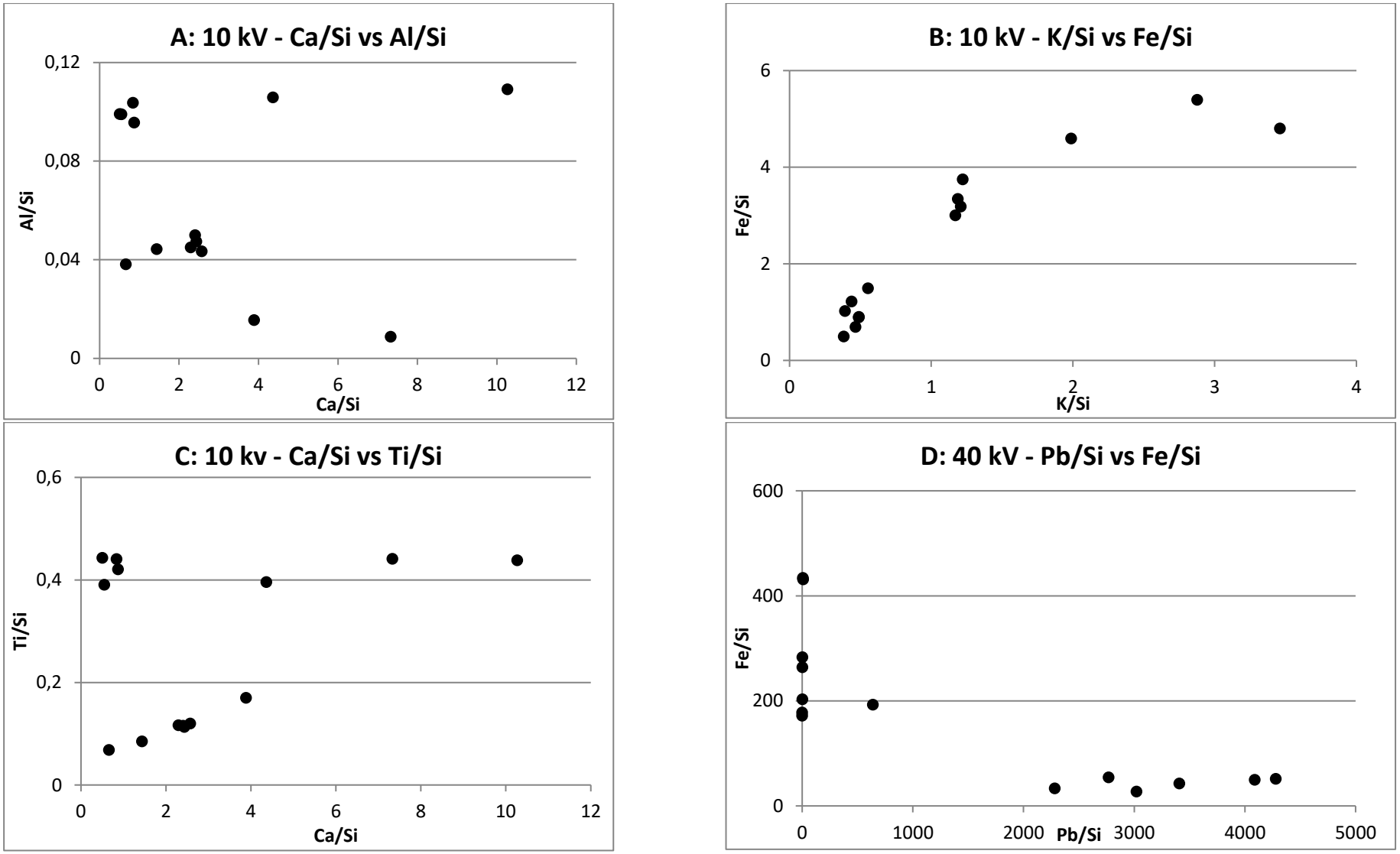

Figure 36 – Bivariate plots black tesserae Paris scene: A – Ca-Al, 10 kV; B – K-Fe, 10 kV; C – Ca-Ti, 10 kV; D – Pb-Fe, 40 kV

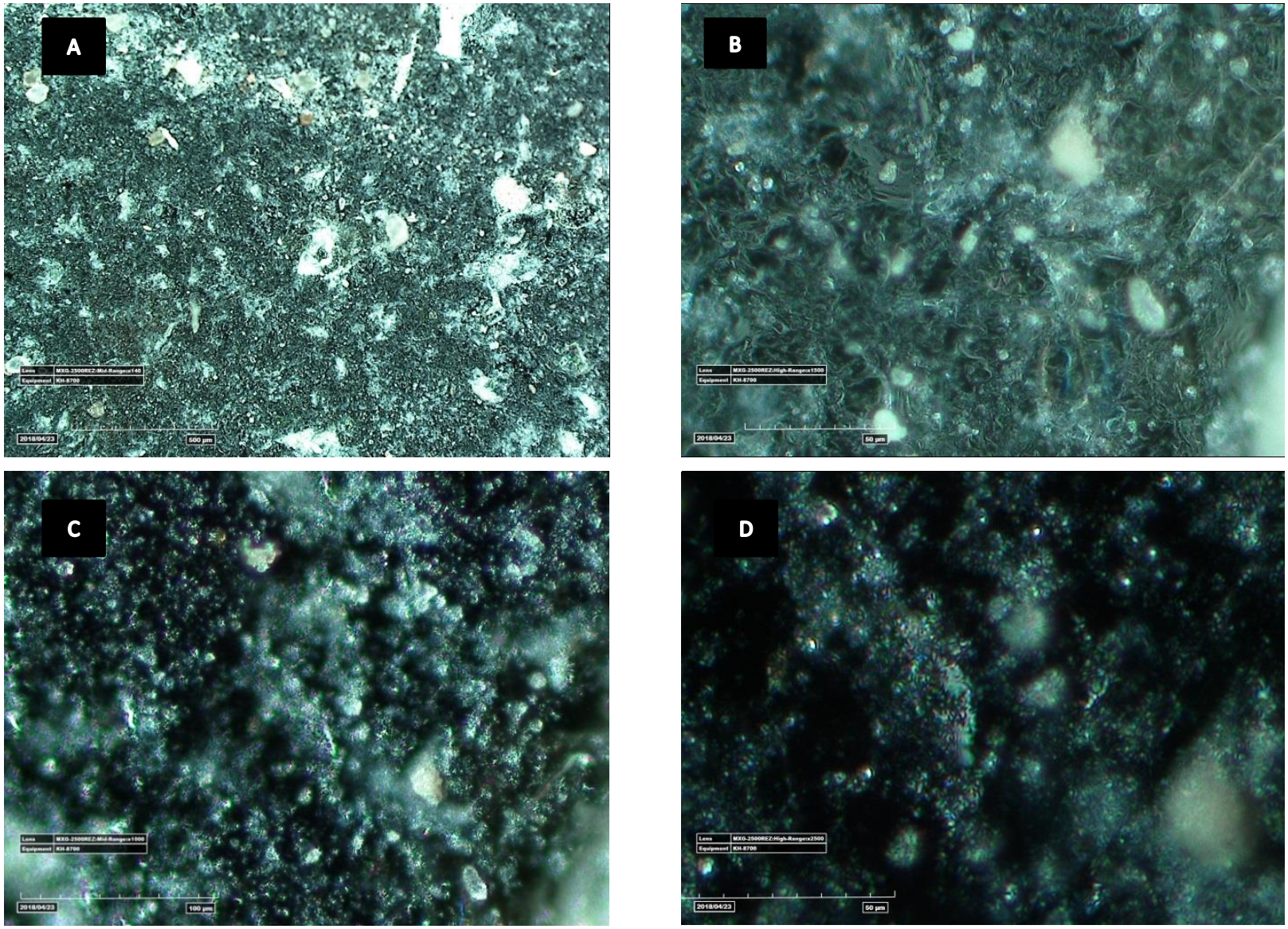

Figure 37 – Microscopy images of Paris 24 (black): A (Mid-Range, x140) B (High-Range, x1500), C (Mid-Range, x1000, racking light) D (High-Range, x2500, racking light).

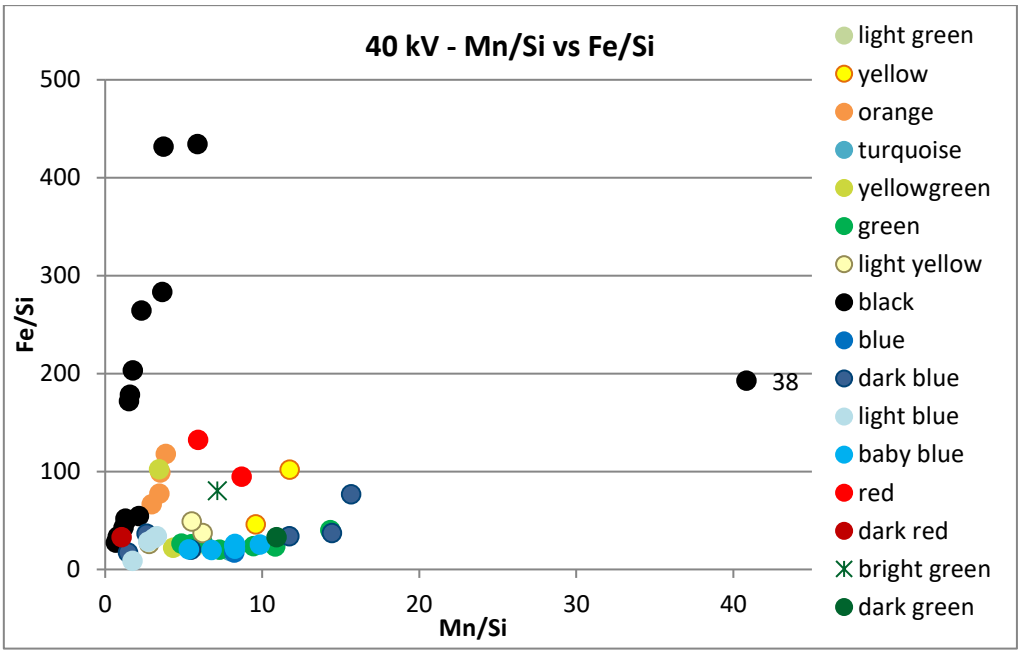

Figure 38 - Bivariate plot Mn-Fe, Paris scene, 40 kV

It is possible that these glasses identified as “black” appear black to the human eye due to the thickness and a high dopant concentration of Mn and Fe. Since the measurements were conducted in situ, it was not possible to cut smaller pieces to identify the hue glass. Black appearing glasses can actually have a purplish or brownish hue when looking at fragments with a lower sample thickness (Möncke et al., 2014). Not only does the thickness of the glass determine the dark (black) colour, so does the concentration of Mn_2O_3 present in the glass (Gedzevičiute et al., 2009). A higher manganese-oxide concentration leads to a darker hue of purple, which might appear black. Gliozzo et al. 2010 studied black glasses in which the role of Mn and Fe are discussed as colorants. Mn^{4+} is known as a decolourant as well. Given the dark black colour, the levels of Mn were low enough to not decolour the glass, but probably high enough to oxidize Fe^{2+} to the Fe^{3+} state. The combination of Fe^{2+} and Fe^{3+} ions could produce a dark olive green tint, but since the non-invasive aspect of the study, the hue could not be studied in detail. The presence of Fe^{2+} and Mn^{2+} creates a reducing atmosphere. In the Raman spectrum of a black glass obtained with the BRAVO spectrometer, a band at 635 cm^{-1} can be possibly attributed to γ-Mn_2O_3 (Buciuman et al., 1999; de Faria et al., 1997).

Looking at the hXRF data, a high amount of lead and iron are found in the black samples, but contents are not very high. The presence of Pb and Sb could indicate the use of lead antimonate as an opacifier. The presence of Ca and Sb on the other hand could suggest the use of calcium antimonate as opacifier (Coccato et al., 2017). The dark (black) hue could be obtained due to relevant amounts of Fe and Cu and Pb (Ricciardi et al., 2009b). The tesserae belonging to group one are characterised by a very high lead amount (Table 6). An example is Paris 24 (Fig. 37), present in the coat of Paris. These tesserae stand out from the other blacks due to their intense black colour.

The Raman spectra of the glass tesserae do not yield good signals except for tesserae from group two: Paris 43, 78, 79 and 80. These spectra show an intense band at ca. 144 cm^{-1} and two broad bands at ca. 1287 cm^{-1} and 1595 cm^{-1} in the 1064 nm laser. The first band can be attributed to titanium dioxide and possibly anatase. The two broad bands can possibly be attributed to carbon black (Ferrari and Robertson, 2000). The band at ca. 1287 cm^{-1} corresponds to the D peak and the band at ca. 1595 cm^{-1} to the G peak. These peaks are attributed to nanocrystalline or amorphous carbon. Carbonaceous material is detected more clearly in the 1064 nm laser. It is possible that fluorescence in the 532 and 785 nm lasers, resulting in a more background, masks the carbon signals (Harris et al., 2015). However, the absence of the carbon signal in the 532 and 785 nm lasers could also be due differences in laser footprint size and penetration depth between the lasers. Carbon signals have been identified in the BRAVO spectra of these black glasses as well. The automatically calibrated spectrum obtained with two lasers (785 – 1100) is baseline corrected and Raman bands of carbon (D and G peaks) are detected at 1310 and 1600 cm^{-1}. The other glass tesserae produce high fluorescence Raman spectra (Fig. 39).

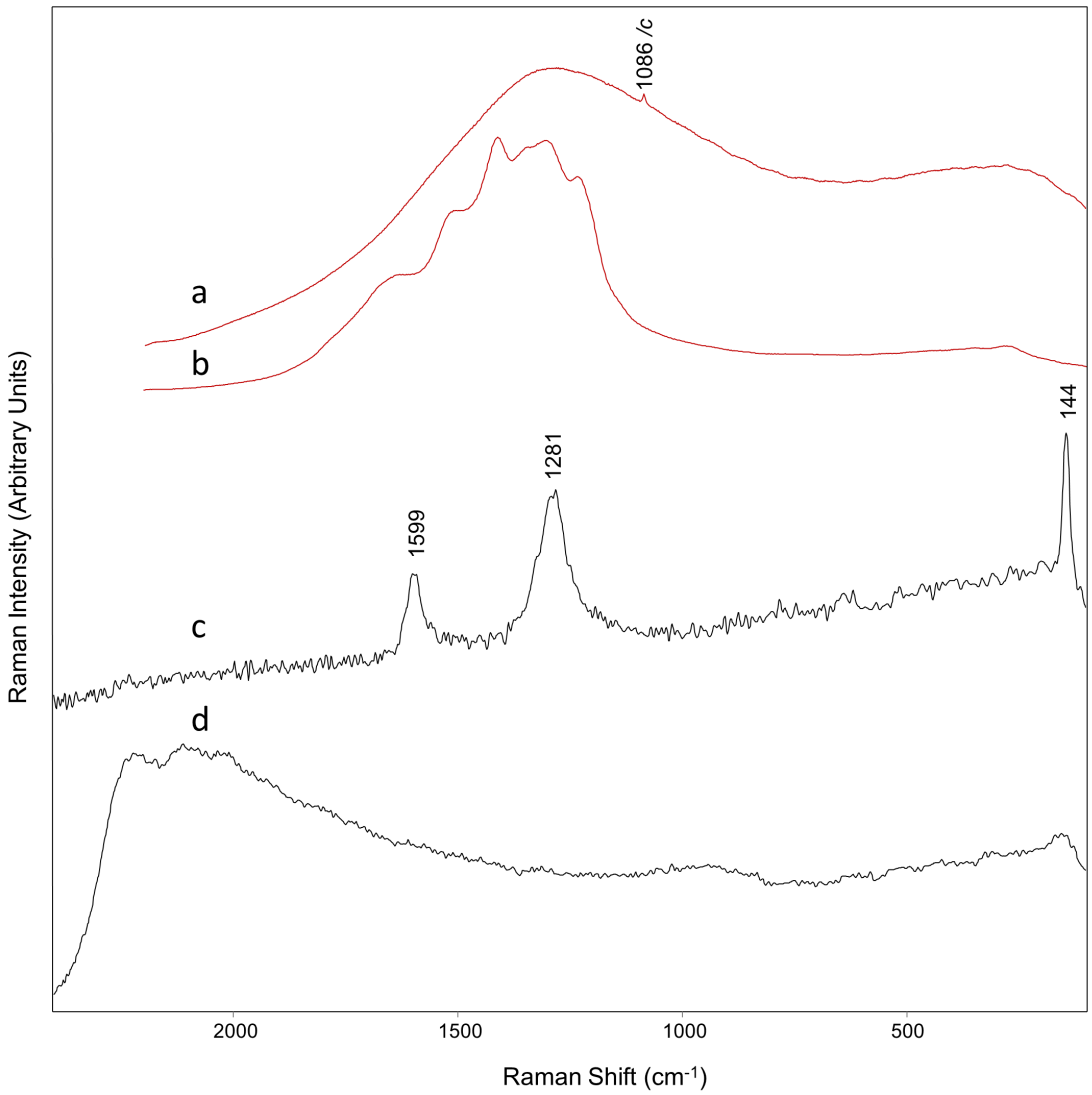

Figure 39 - Raman spectra black glasses: a (Paris 44, 785 nm) and b (Paris 95, 785 nm) obtained between 100 and 2200 cm^{-1}; c (Paris 78, 1064 nm) and d (Paris 81, 1064 nm) obtained between 100 and 2400 cm^{-1}

4.1.2 Spring

Table 7 – Identification Raman signals Spring scene

Colour	*signal 1064 nm*	*signal 785 nm*	*signal 532 nm*
black			
white	Calcite	Calcite	Calcite
pink/nude	Calcite + dolomite	Calcite + dolomite	Calcite
Brown	Calcite + dolomite	Calcite	
red			
dark red	Calcite + haematite	Calcite + haematite	
red	Calcite	Calcite	
yellow	Titanium dioxide	Calcite (fade)	
orange		Calcite (fade)	
blue			
dark blue			
blue			
light blue			
turquoise			
green			
dark green			
green			

White

The white tesserae in the Spring scene are all made of stone, like in the Paris scene. Here, only calcite signals were identified in the Raman spectra (Fig. 40).

Nude and brown

As in the Paris scene, different hues of nude are grouped together in the Spring scene. These hues go from beige and light pink, to light brown and dark pink. Theses nude tesserae are all made of stone and signals of calcite and dolomite are identified in the Raman spectra (Fig. 41 and 42).

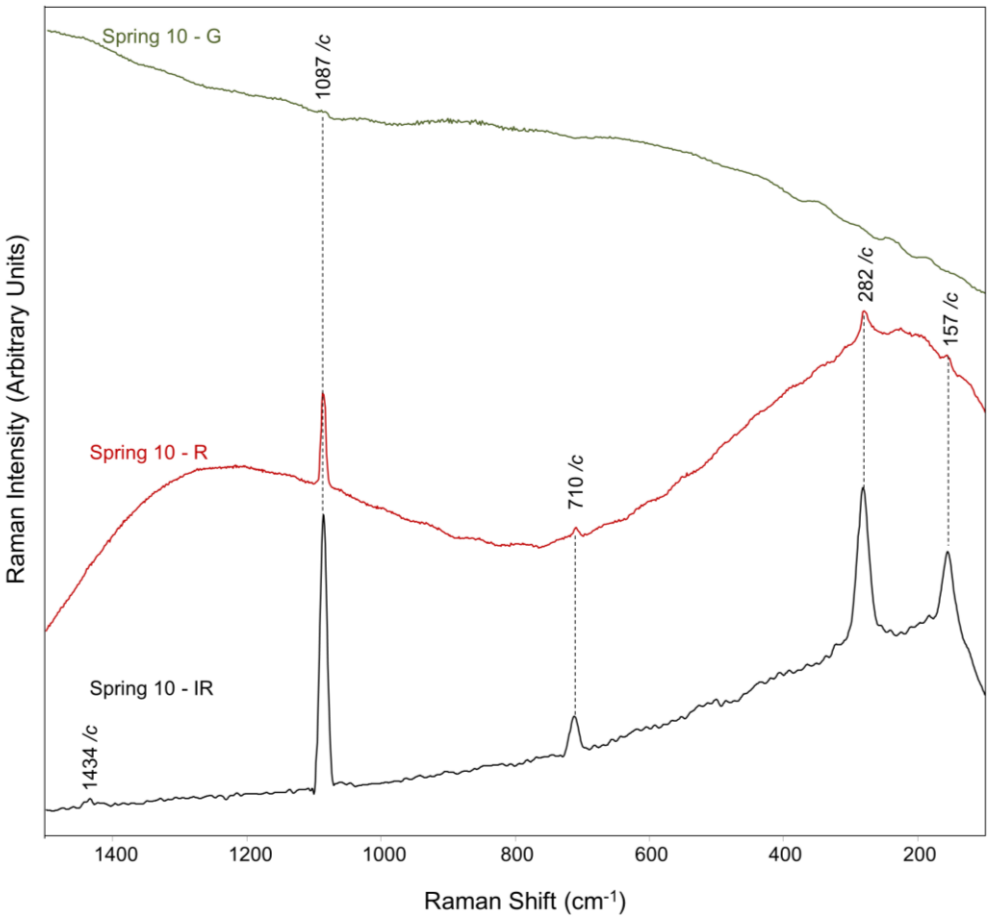

Figure 40 - Raman spectra of Spring 10 (white) obtained with 532 nm (G), 785 nm (R) and 1064 nm (IR) between 100 cm^{-1} – 1500 cm^{-1}

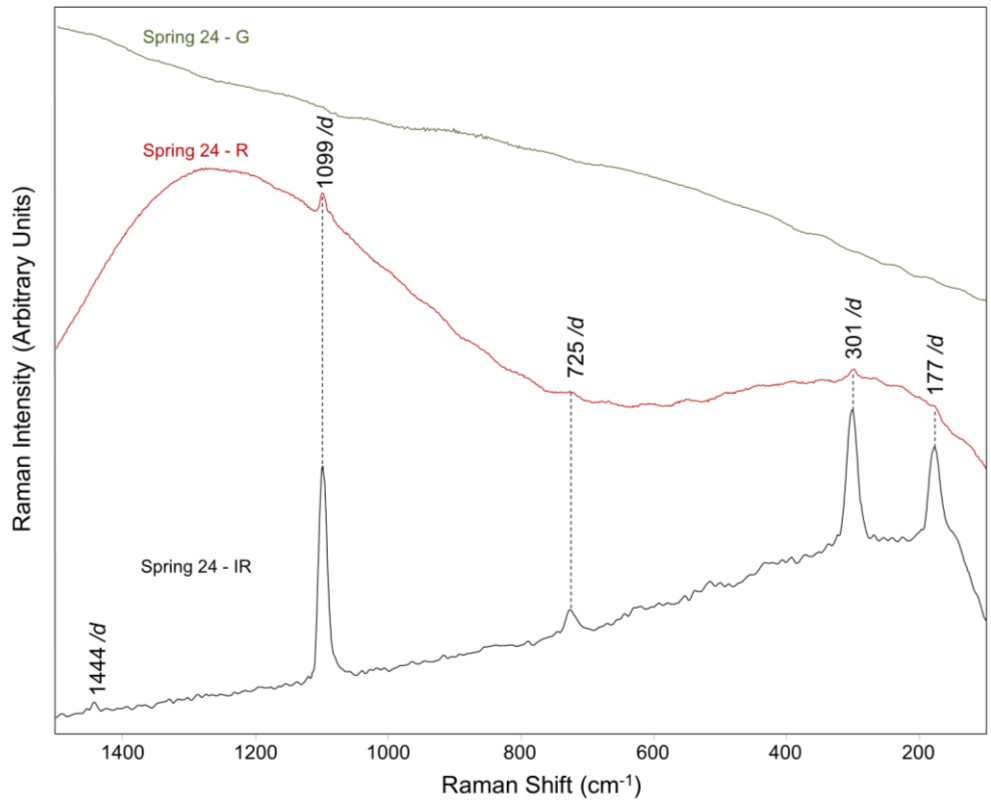

Figure 41 - Raman spectra of Spring 24 (nude) obtained with 532 nm (G), 785 nm (R) and 1064 nm (IR), between 100 cm^{-1} – 1500 cm^{-1}

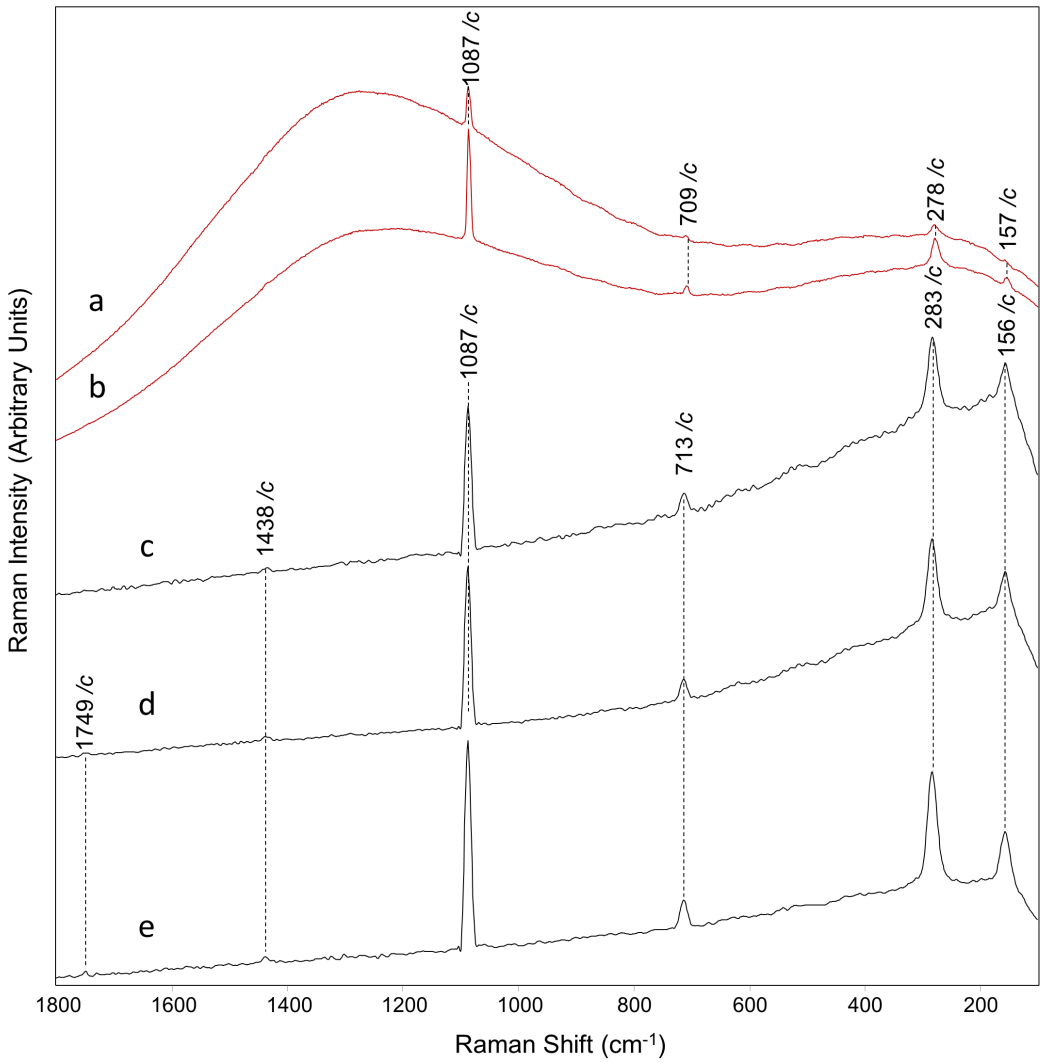

Figure 42 - Raman spectra of nude tesserae (Spring scene): a (spring 28, 785 nm), b (spring 47, 785 nm), c (spring 26, 1064 nm), d (spring 44, 1064 nm), e (spring 48, 1064 nm) obtained between 100 cm^{-1} - 1800 cm^{-1}

Red

As in the Paris scene, the red tesserae from the Spring scene are divided in red tesserae and dark red tesserae. The red tesserae analysed in the Spring scene are all made from stone, no glass tesserae are identified. The signal identified with Raman spectroscopy is that of calcite. However, these spectra have a high fluorescence in the lower wavenumbers compared to the white and nude tesserae (Fig. 43).

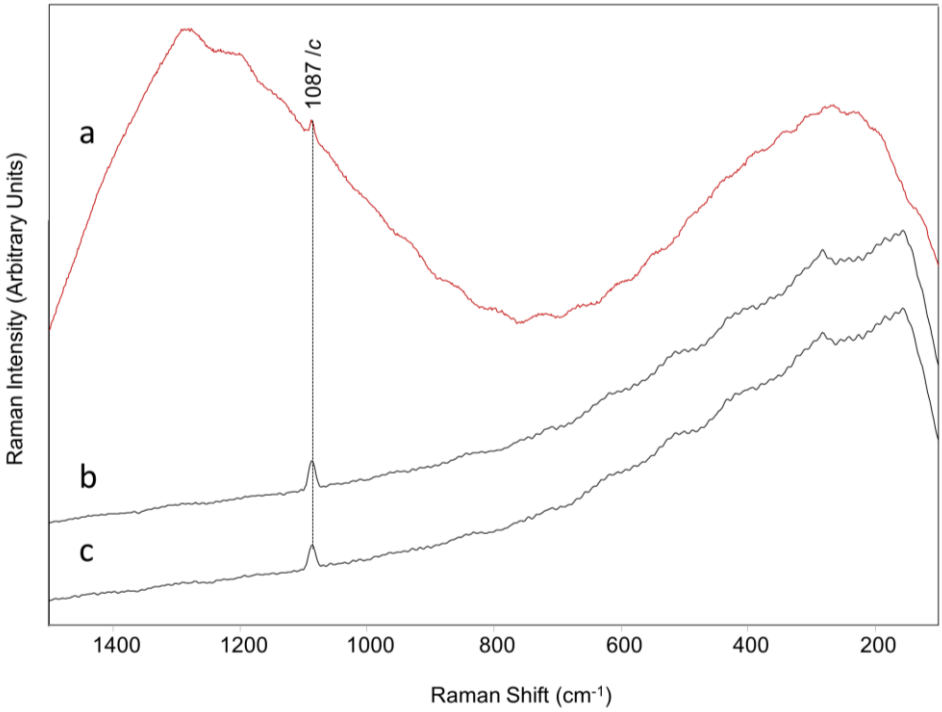

Figure 43 - Raman spectra red tesserae (spring scene): a (spring 15, 785 nm), b (spring 15, 1064 nm), c (spring 27, 1064 nm) obtained between 100 cm^{-1} and 1500 cm^{-1}

The dark red tesserae in the Spring scene are made of stone with exception of one tesserae, spring 3. The latter is made from glass and no Raman signals were identified from this tesserae. The stone tesserae display the same signals as the red tesserae from the Paris scene with a combination of calcite and haematite. No signals were identified in the 532 nm laser (Fig. 44). Corresponding to the results of the dark red tesserae from the Paris scene, the haematite signals are shifted between the 785 and 1064 nm laser. Haematite bands are identified at 224, 240, 295, 407, 493 and 606 cm^{-1} in the 785 nm laser and at 228, 295, 414 and 618 cm^{-1} in the 1064 nm laser (Buzgar et al., 2013; Caggiani et al., 2014; Košařová et al., 2013). In the red laser (785nm), a calcite band is identified at 1087 cm^{-1}.

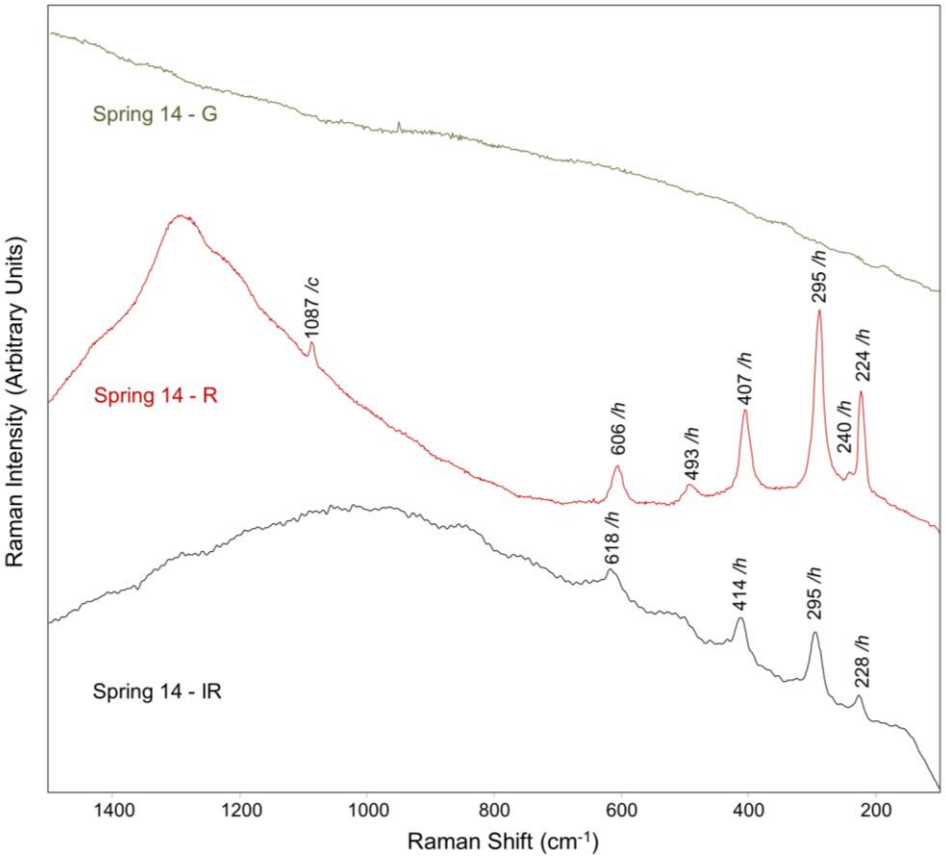

Figure 44 - Raman spectra Spring 14 (dark red): 532 nm (G), 785 nm (R), 1064 nm (IR) obtained between 100 cm^{-1} and 1500 cm^{-1}.

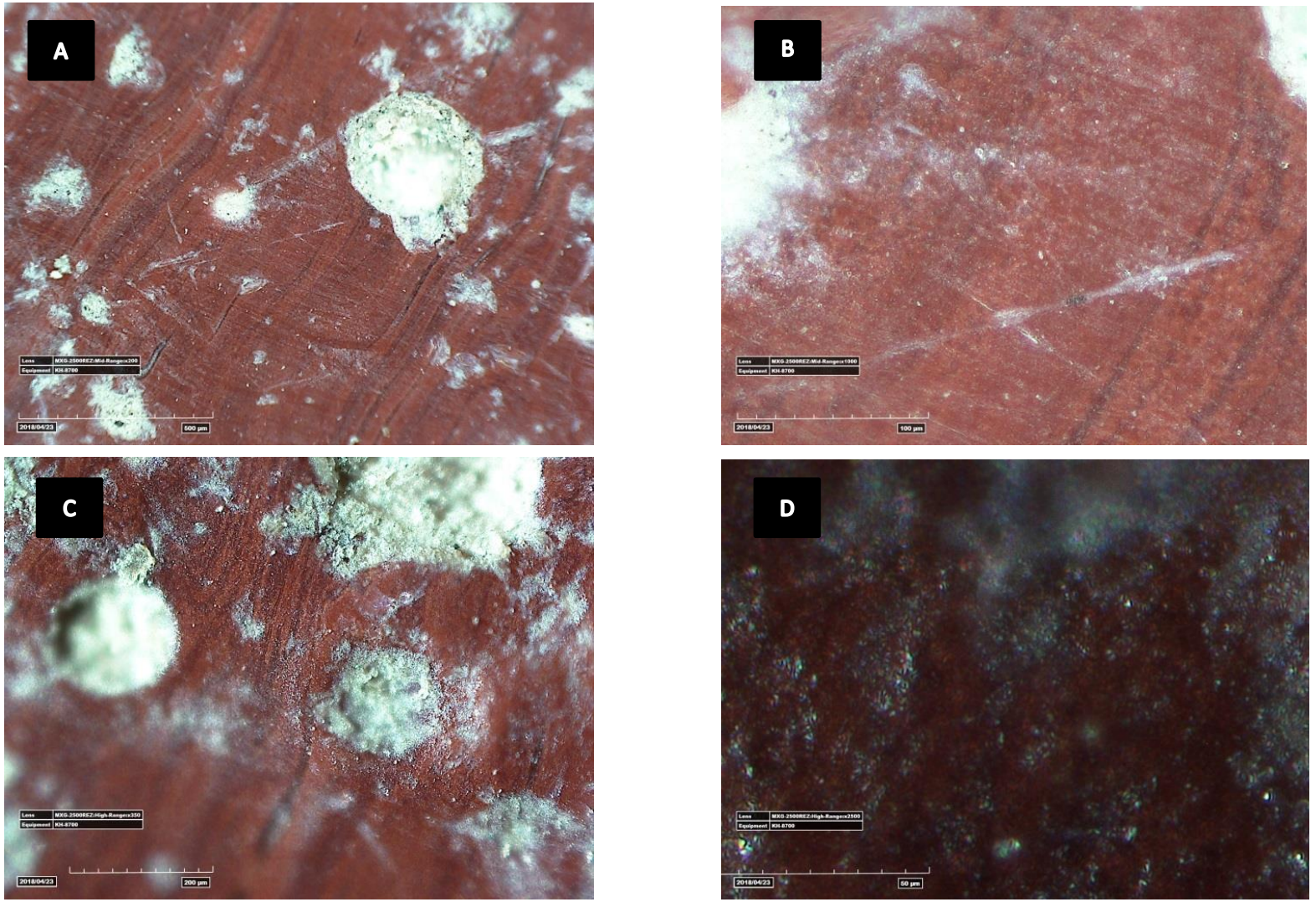

Figure 45 - Microscopic pictures of red tesserae (spring scene): A (Mid-Range, x200), B (Mid-Range, x1000), C (High-Range, x350, racking light), D (High-Range, x2500, racking light).

Yellow

The three analysed yellow tesserae in the Spring scene are glass tesserae (Fig. 46). Their Raman spectra show a high level of fluorescence in all lasers. A weak signal of titanium dioxide is identified in all samples with the 1064 nm laser at ca. 143 cm^{-1} but due to the absence of other bands no further distinction between anatase and rutile was possible. A fade signal of calcite is identified at 1086 cm^{-1} with the red 785 nm laser in sample Spring 17. However, the hXRF results identify Spring 17 as a glass. Pb and Sb contents in the yellow glasses indicate the use of lead antimonate as colorant and opacifier. Even though tin has been found in the yellow glasses, this is in lower amounts than antimony. This excludes the probable use of a tin-based opacifier (lead stannate yellow), which was common for a short period of time during the first and second century BCE (Tite et al., 2008).

Orange

The orange tesserae originating from the Spring scene have an elemental composition of glass. Most orange samples generate a resonance Raman spectrum. A fade signal of calcite is identified in sample Spring 2 at 1086 cm^{-1} with the 785 nm laser. As discussed in the Paris scene, the orange tesserae have a high amount of copper, lead and tin (Fig. 47 and 48). The colouring and opacifying agent is due to the presence of copper, either cuprite or metallic copper nanoparticles (see Paris red). However, no cuprite signals are identified in the Raman spectra. Darker bands of orange and red are visible in the glass (Fig. 49) together with some larger crystals. These darker bands in the glass are previously discussed in Paris red.

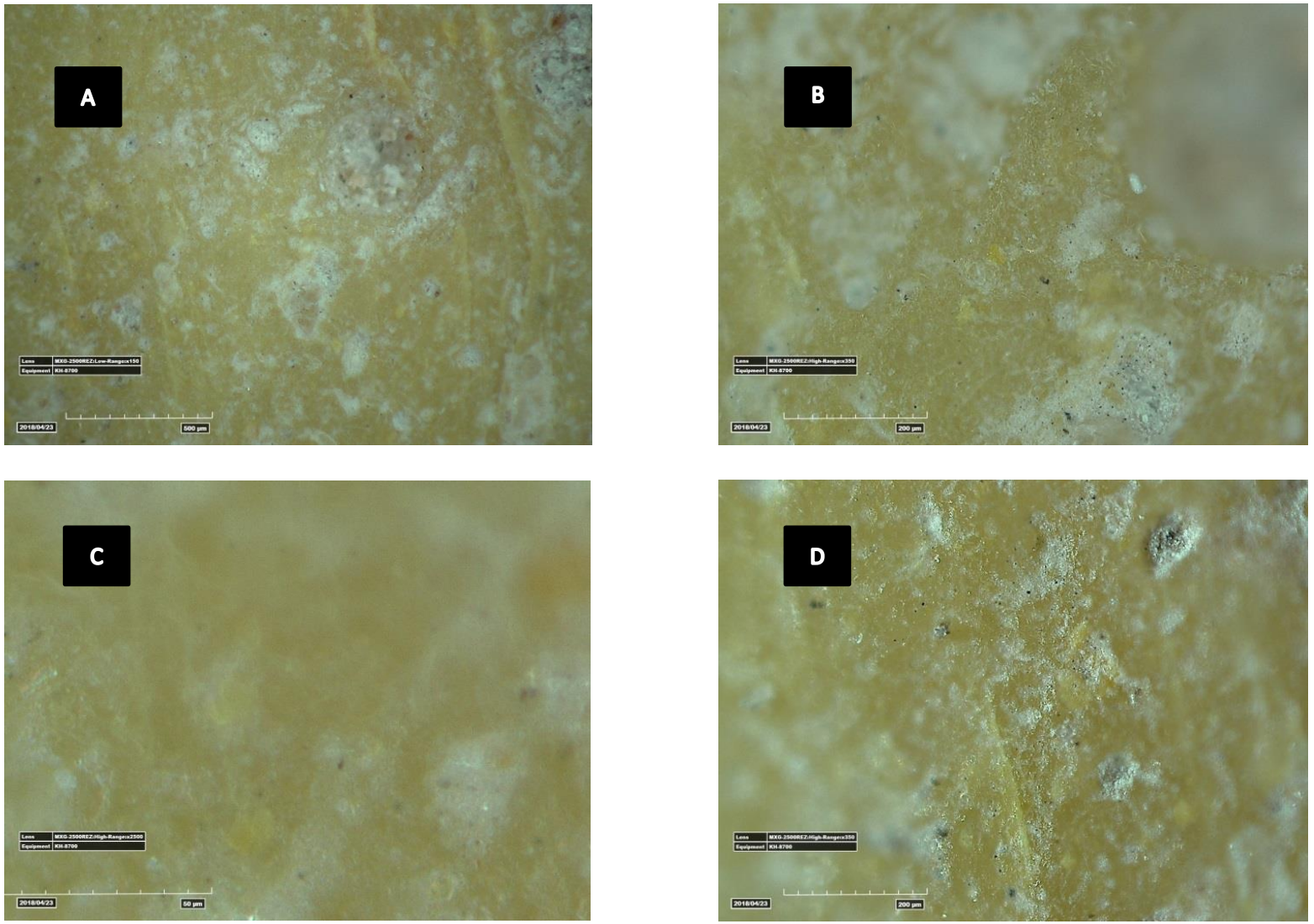

Figure 46 - Microscope image of yellow tesserae (spring scene): A (Low-Range, x150), B (High-Range, x350), C (High-Range, x1500), D (High-Range, x350, racking light)

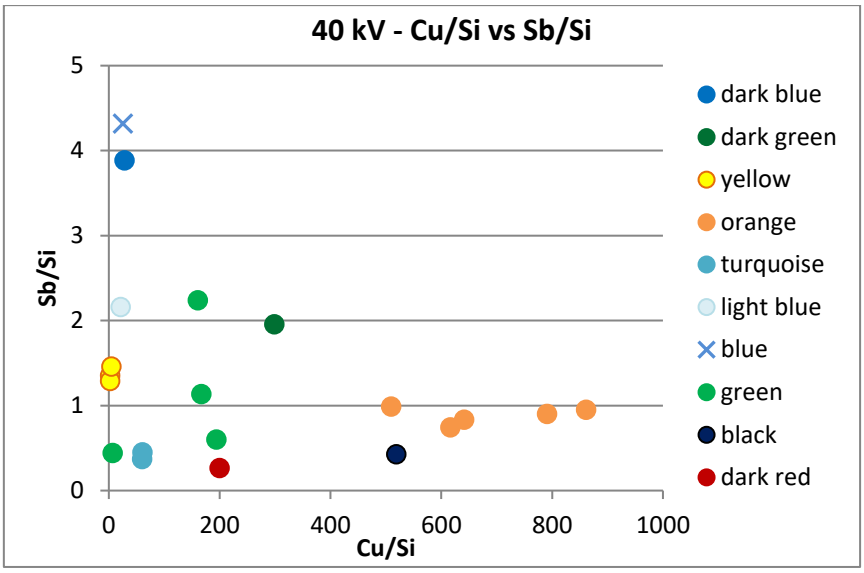

Figure 47 - Bivariate plot Cu-Sb, Spring scene, 40 kV

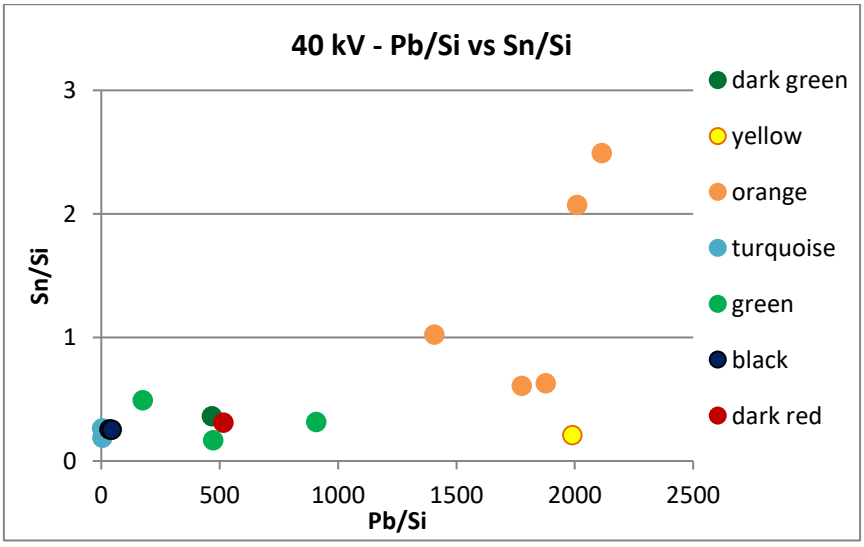

Figure 48 - Bivariate plot Pb-Sn, Spring scene, 40 kV

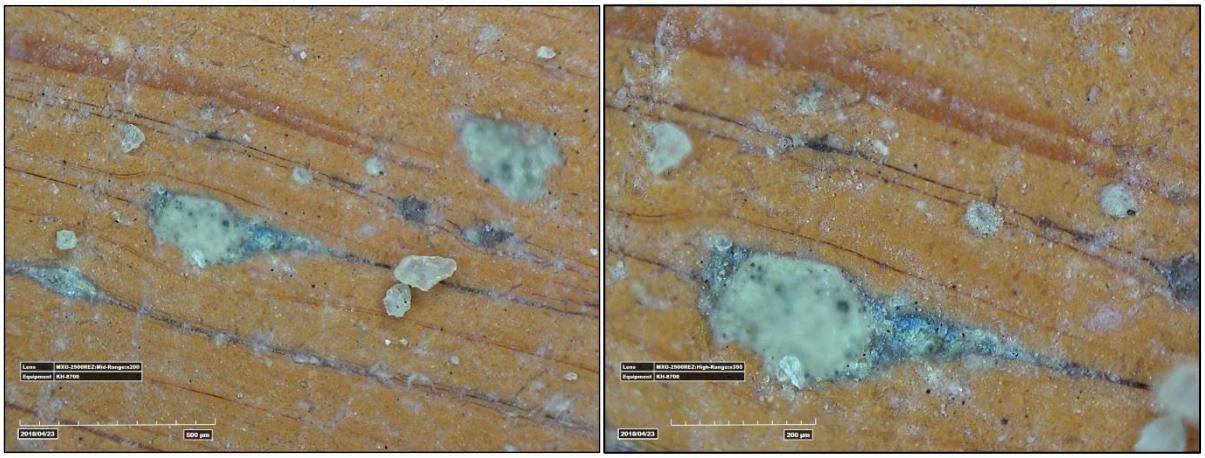

Figure 49 - Microscopy picture of orange tesserae (Spring scene): left (Mid-Range, x200), right (High-Range, x350).

Blue

The blue tesserae in the Spring scene are subdivided in dark blue, blue, light blue and turquoise. All the blue tesserae have a glass composition and no stone tesserae are identified. The blue colour is obtained by the presence of Co and Cu. The dark blue and blue glass have a high Co content compared to the other blue glasses (Fig. 50). The high presence of Sb suggests the use of calcium antimonate as an opacifier. White crystals have been identified with microscopy (Fig. 51). The combination of antimony and cobalt produced the blue and the dark blue hue. The light blue sample has a low Co and Cu content, but more Sb is present in the light blue compared to turquoise glass, indicating calcium antimonate is used as opacifier. However, no Raman signals for calcium antimonate are identified in the blue samples of the Spring scene. The turquoise tesserae have a slightly higher Cu content and a lower amount of Sb. Small amounts of tin are identified in the turquoise, as was the case in the turquoise tesserae in the Paris scene. As discussed in the results of the Paris scene, a turquoise colour is obtained by mixing green and blue colorants together.

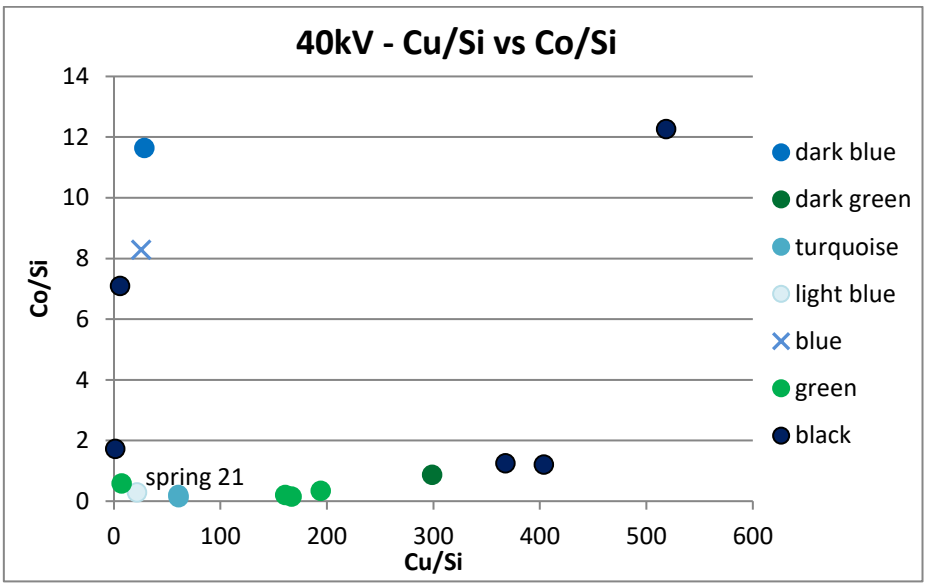

Figure 50 - Bivariate plot Cu-Co, Spring scene, 40 kV

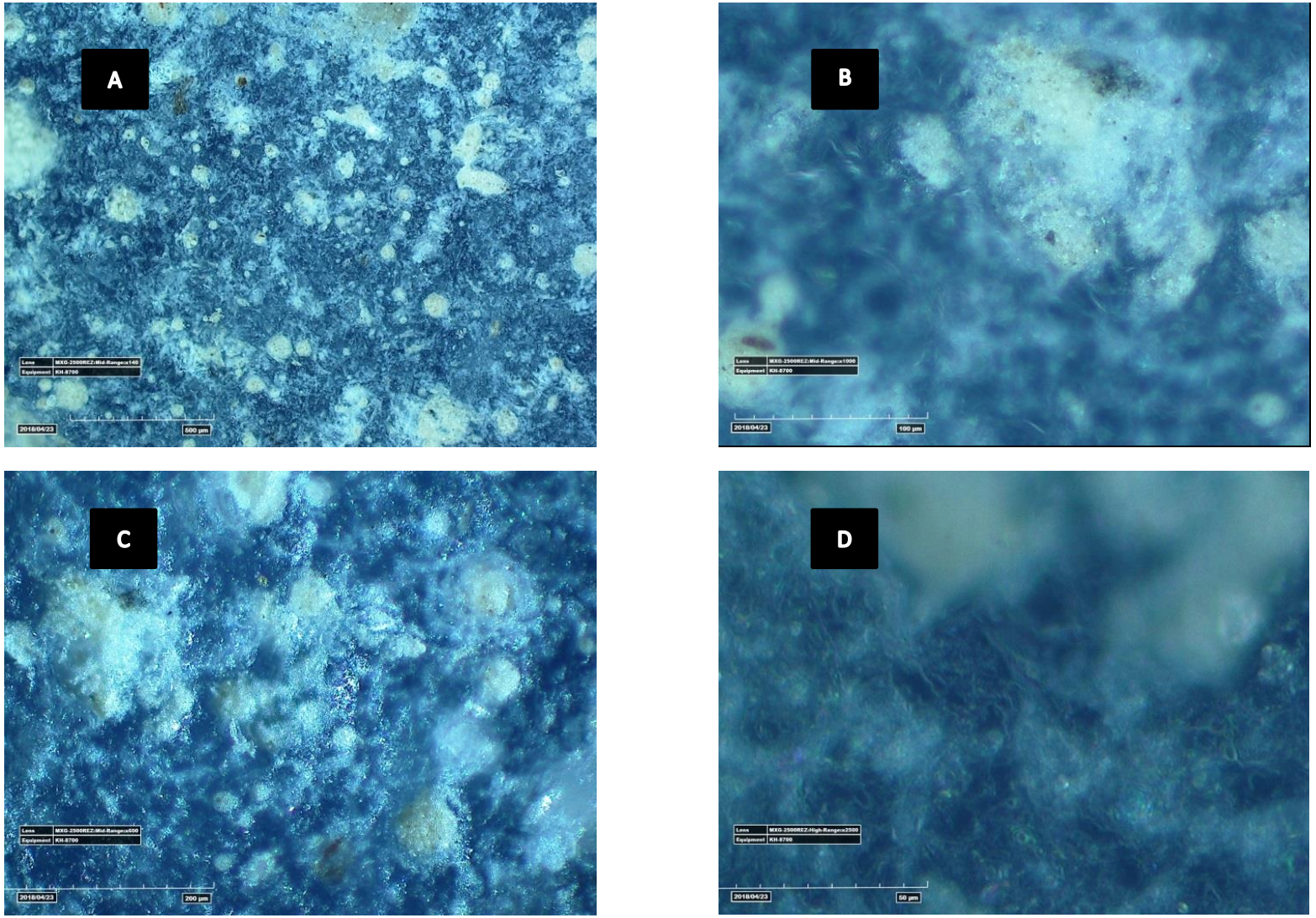

Figure 51 – Microscopy picture of blue tesserae (Spring scene): A (Mid-Range, x140), B (Mid-Range, x1000), C (Mid-Range, x600, racking light), D (High-Range, x2500).

Green

The green tesserae are divided in green and dark green, the latter comprising only one tesserae (Spring 40). No Raman signals are identified for the green glasses, but the hXRF results provide some information concerning the colouring agents. Copper is present in all samples and is responsible for the green colour. The dark green tesserae has a higher Cu content which could be responsible for the darker hue, together with a slightly higher presence of Mn. Besides Cu, significant amounts of Sb are present, suggesting the use of calcium antimonate as opacifying agent. Spring 21 is a lighter hue of green and this is reflected in the lower Cu amount identified (Fig. 50).

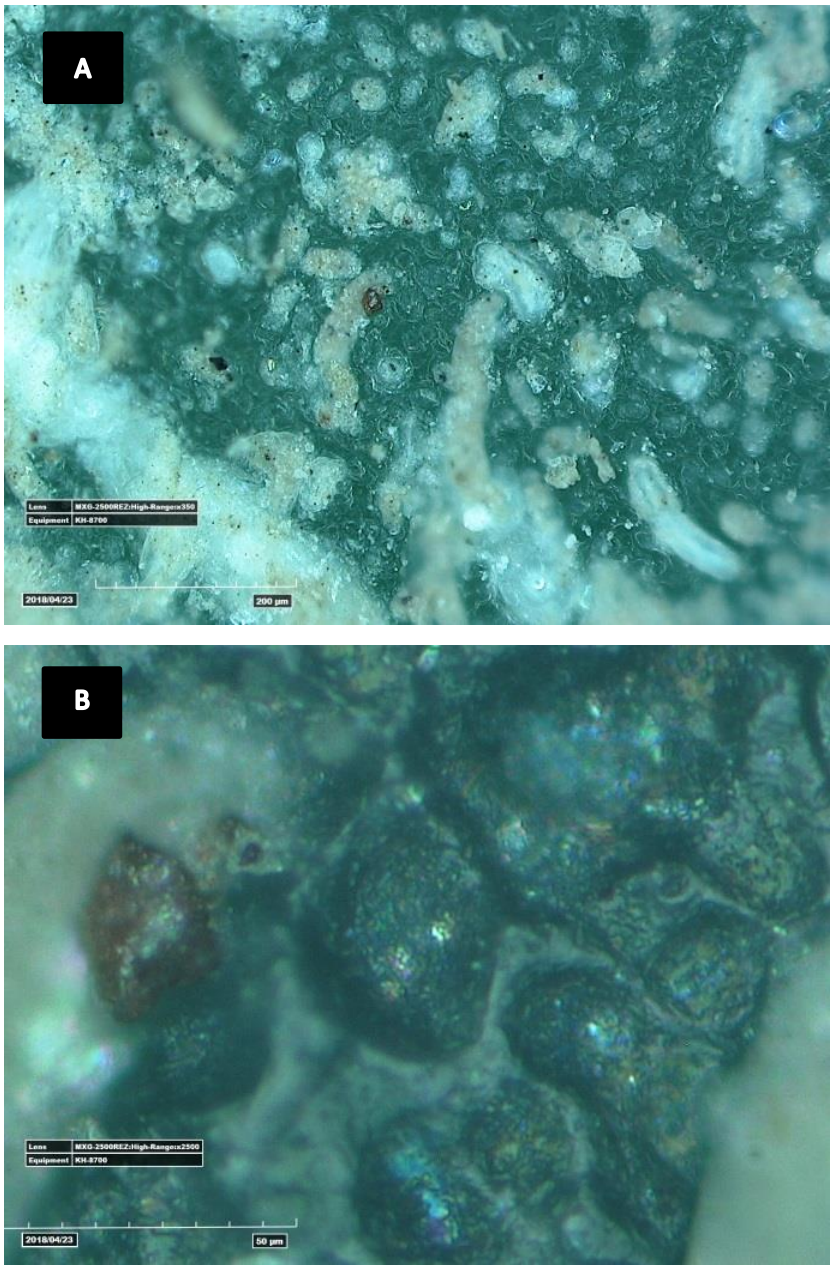

Figure 52 - Microscopy picture of green tesserae (Spring scene):
A (High-Range, x350), B (High-Range, x2500).

Black

The hXRF results of the black tesserae indicate that they have a glass composition. No Raman signals could be identified from the black glasses as they all show high fluorescence in different regions of the spectrum according to the laser wavelength. This fluorescence will be discussed further in chapter 4.2. The hXRF data of the black glasses reveal a high level of Fe, Mn and Ca (Fig. 53 and 54).

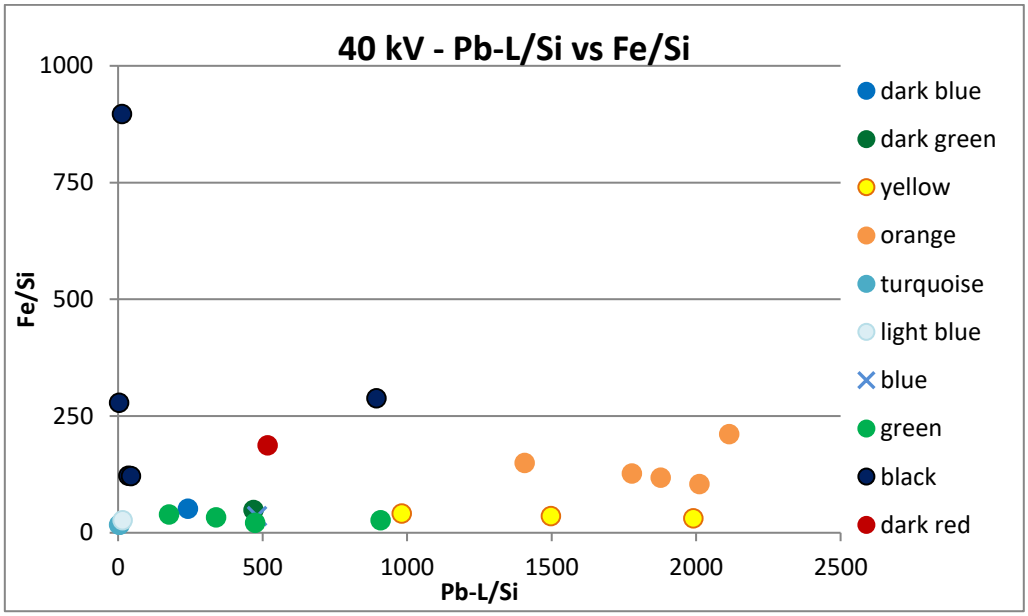

Figure 53 - Bivariate plot Pb-L - Fe, Spring scene, 40 kV

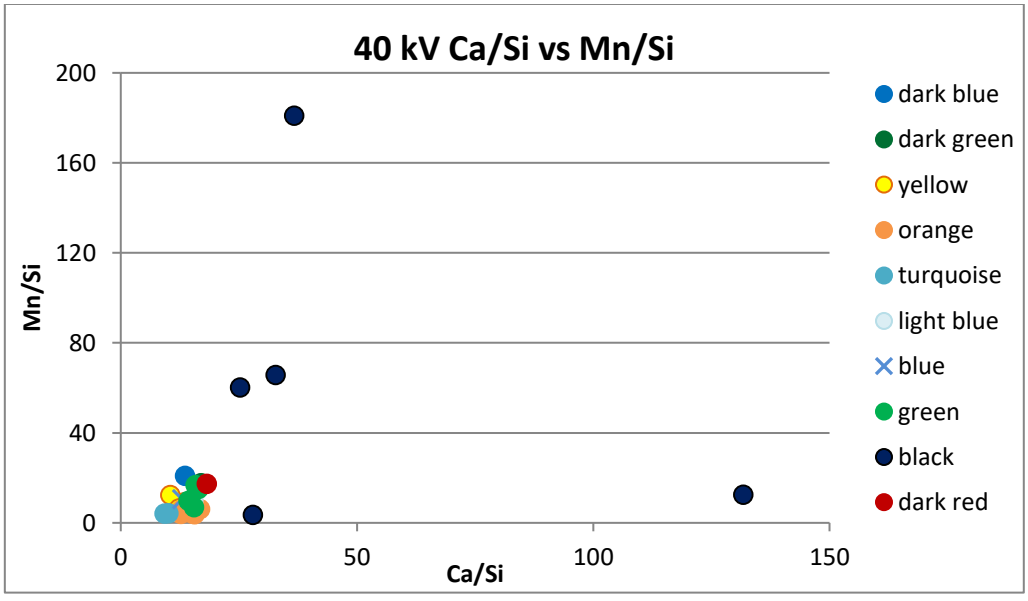

Figure 54 - Bivariate plot Ca - Mn, Spring scene, 40 kV

4.2 Comparison instrumentation

When comparing different Raman instruments, one should not only take the spectroscopic features in consideration, but the practical limitations as well. The features of the instruments employed during this campaign are listed in Table 8. The limitations of mobile and handheld Raman spectrometers compared to bench-top instruments are already discussed in chapter 3.3. The employment of different instruments with different laser energies allows for a better understanding of the material and for better controlling fluorescence.

The main advantage of the ENWAVE is the two incorporated lasers: in one single mobile instrument, spectra are obtained with both the 532 and 785 nm laser. Furthermore, the fiber optics probe of a length of 5 meters allows for more mobility on the field. The lasers were visible to the eye, which allowed for easier position on the area to be measured. To protect the probe head and to avoid interference from ambient light, plastic tubes with a protective foam layer were slid over the lens. During the measurements, the standard lens was used. The instrument is equipped with an incorporated laptop, which enables visualisation of the spectra. Moreover, the instrument enables to obtain a continuous scan, during which the ideal settings can be chosen for the measurement. Before using either one of the lasers, wave calibration was performed with following reagents: sulphur, epsilon-caprolactone, acetonitrile/toluene (mixed in 50/50% volume) and cyclohexane (Lauwers et al., 2014). During the field campaign, the ENWAVE was operated using the internal battery. Only in a few cases, the instrument was connected to the available generator on site.

The B&WTEK spectrometer with a laser wavelength of 1064 nm was not battery operated and access to the generator was necessary at all times when using this instrument. The instrument is a lot lighter compared to the ENWAVE (Table 8). However, a laptop needs to be connected to the instrument in order to visualise the spectra and control the settings. A continuous scan that allows determining the ideal laser power and measuring time could be obtained. The fiber optics probe of 1,5 meters allowed for a better mobility on the field. To protect the probe head and to avoid light interference a protective foam layer was used on

the probe heads. Wave calibration was performed with following reagents: sulphur and cyclohexane.

The handheld Raman spectrometer of Bruker (BRAVO) is a lightweight instrument that was battery operated. The instrument is equipped with built-in software and could be operated using a touch screen. Laser power and measuring time cannot be controlled manually and are selected by the instrument. The spectrometer did not come with a fiber optics probe and the instrument had to be placed on the measured area with the measuring tip on the area. Since no laser beam was visible and no camera is built in the instrument, this complicated the measurements. The instrument has automatic wavenumber calibration however, sulphur and cyclohexane were also measured as reagents. The spectrometer combines the spectra of both lasers (Fig. 55) and combines the spectra obtained with the sequentially shifted excitation (Fig. 57). The output file is a spectrum processed by the instrument that is automatically baseline corrected. The processing and visualising of the spectra is performed with the OPUS software. The spectra of each laser can be extracted from the data (Fig. 55). The red line corresponds to the first laser, obtaining data in the fingerprint region, while the blue line corresponds to the second laser, obtaining data in the CH stretching region. The spectrum displayed in Figure 55 is the baseline corrected spectra, provided by BRAVO.

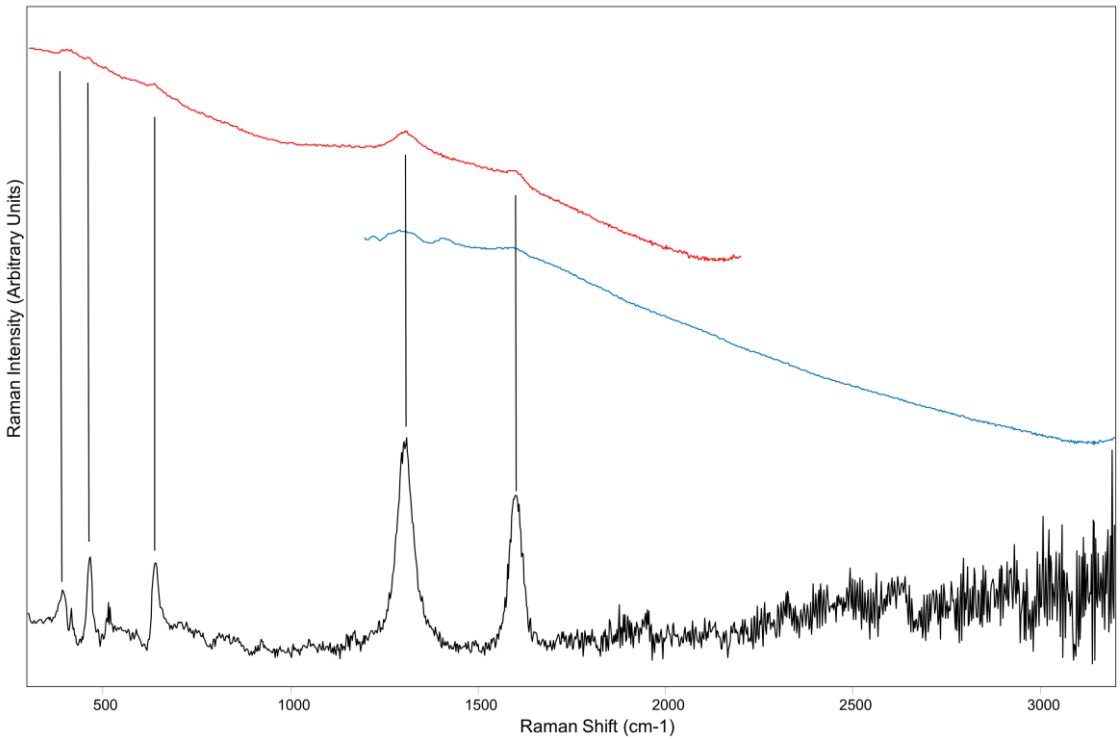

Figure 55 - Raman spectrum Paris 78 (black) obtained with BRAVO.

Table 8 - Parameters Raman instrumentation

parameter	i-Raman EX	EZRAMAN-I-DUAL (G - 532 nm)	EZRAMAN-I-DUAL (R - 758 nm)	BRAVO
company	B&WTEK	Enwave Optronics	Enwave Optronics	Bruker
mobile/handheld	mobile	mobile	mobile	handheld
laser(S)	1064 nm	532 nm	785 nm	Duolaser^{TM} 700-1100 nm
weight	3,4 kg (main unit)	17 kg	17 kg	ca. 1,5 kg
size	17 x 34 x 28 cm	43 x 33 x 18 cm	43 x 33 x 18 cm	27 x 15,6 x 6,2 cm
detector	TE cooled InGaAs	TE cooled CDD	TE cooled CDD	CCD
power supply	110 - 240 VAC	230 VAC	230 VAC	100 - 240 VAC (docking station)
battery	no	yes	yes	yes
power control	0 - 100%	0-100 %	0-100 %	no
maximum laser power	499 mW	100 mW	400 mW	< 100 mW
range	100 cm^{-1} - 2500 cm^{-1}	100 cm^{-1} - 3200 cm^{-1}	100 cm^{-1}-2350 cm^{-1}	300 - 3200 cm^{-1}
resolution	<10 cm^{-1} @ 1296 nm	7 cm^{-1}	6 cm^{-1}	± 1-2 cm^{-1}
spot size	85 µm	88 ± 2 µm	74 ± 2 µm	2 mm
lenses		STD, LWD, HiNA	STD, LWD, HiNA	
focal length		3,7 - 15 mm	3,7 - 15 mm	
fiber optic probe	yes	yes	yes	no
probe length	1,5 m	5 m	5 m	/
computer	no, connect to laptop (usb)	yes, integrated	yes, integrated	Integrated software
operating temperature	0 - 35 °C			5 - 35 °C
storage temperature	-10 - 60 °C			
humidity	10 - 85 %			0 - 95 %

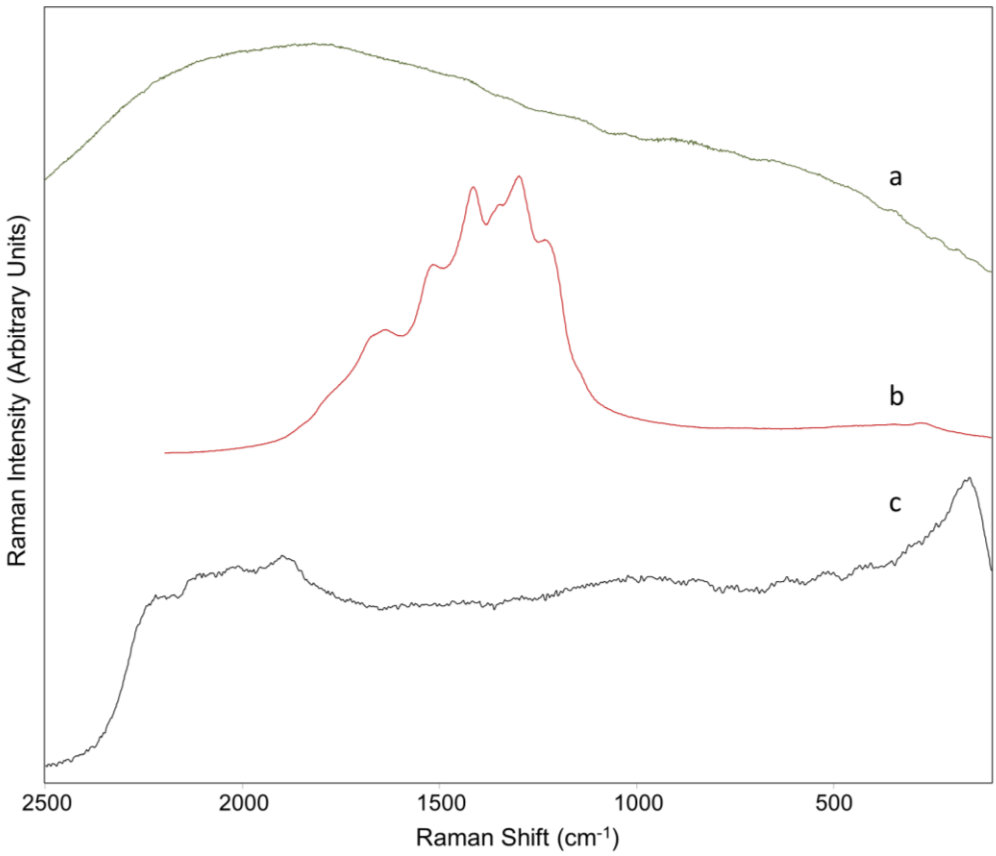

Figure 56 - Raman spectra of Spring 34 (black): a (532 nm), b (785 nm), c (1064 nm). A and b obtained between 100 cm^{-1} and 2500 cm^{-1}; c obtained between 100 cm^{-1} and 2200 cm^{-1}.

The i-Raman EX spectrometer with a laser wavelength of 1064 nm could detect organics in the higher wavenumbers (Fig. 58). A similar spectrum is obtained for other black tesserae. Fluorescence often increases towards the lower wavenumbers (Fig. 56), which made identification difficult in some cases. However, fluorescence in the larger wavenumbers is largely decreased, enhancing the organic signals as discussed above. The spectrometer provided good quality signals of calcite and dolomite. It was possible to not only detect the strong bands, but medium to weak ones as well. The 785 nm laser of the EZRAMAN-I-DUAL displayed high fluorescence in the larger wavenumbers (organics). Identification of calcite and dolomite was possible with the 785 nm laser and in one sample both signals have been attested. In this case, the differentiation between calcite and dolomite was most clear in the 785 nm laser, compared to the 1064 nm laser (Fig. 19). This might be related to the resolution of the instrument. The best spectra of calcite and dolomite are obtained with the 1064 nm laser, fluorescence increases in the 785 nm laser.

The 532 nm laser of the EZRAMAN-I-DUAL overall did not give good results. In some cases calcite or dolomite was identified in which the strongest band only gave a weak signal with a

lot of noise. Though recent studies with mobile Raman on glasses have been and yielded good results, this was not the case for this field campaign. It was not possible to perform baseline subtraction on the spectra (Colomban et al., 2006; Colomban and Slodczyk, 2009). It is possible that light interference results in a high noise signal. However, the probe head was covered with protective black foam to eliminate light. Glass is typically more translucent compared to stones so maybe the light interference did play a role. Another possibility is that the bad spectra are due to a problem with the instrumentation.

Haematite is detected with the 785 nm and 1064 nm lasers with multiple bands. However the Raman bands slightly shifted between the lasers as discussed in chapter 4.1. No haematite is detected in the 352 nm laser since the laser light is usually absorbed by the red coloured haematite (Harris et al., 2015). The BRAVO spectrometer could identify haematite as well with bands at 411, 496, 610, 1350 and 1555 cm^{-1}. The signal at 1087 is ascribed to calcite (Fig. 57).

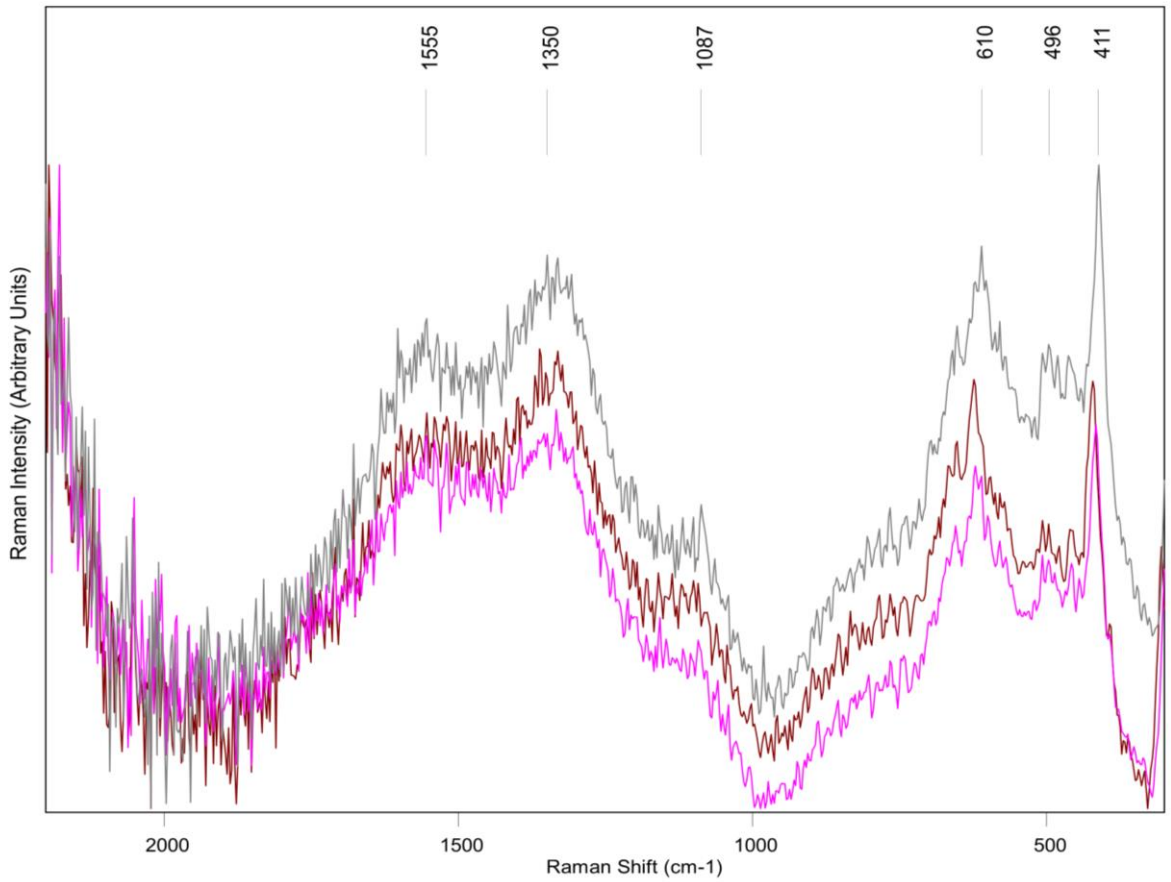

Figure 57 - Raman spectrum Paris 59 (dark red), obtained with BRAVO displaying shifted

Signals of carbon are detected with the 1064 nm laser of B&WTEK and with the BRAVO. The strong reduction of fluorescence in the 1064 nm laser enhances the carbon signal. Two broad bands (D and G bands) are identified, however the D band is shifted towards lower wavenumbers. The wavenumbers of the two bands (D and G) identified with the BRAVO match amorphous carbon in literature (Ferrari and Robertson, 2000).

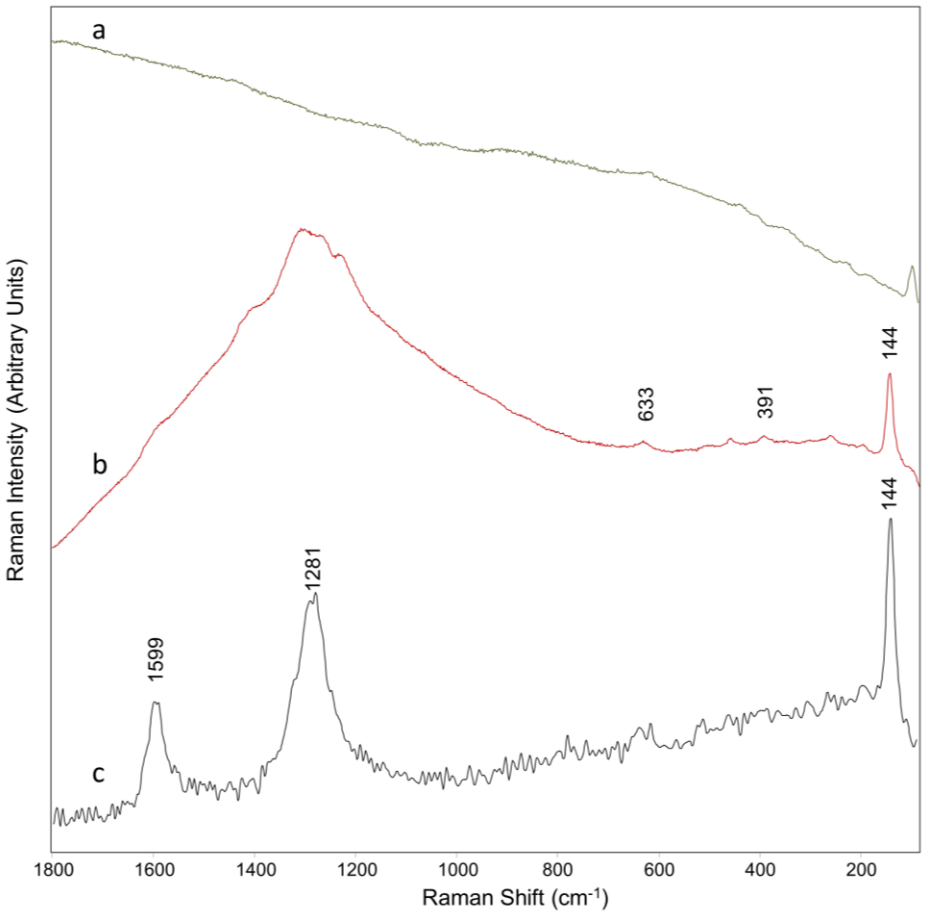

Figure 58 - Raman spectra Paris 78 (black): a (532 nm), b (785 nm), c (1064 nm) obtained between 85 and 1800 cm^{-1}

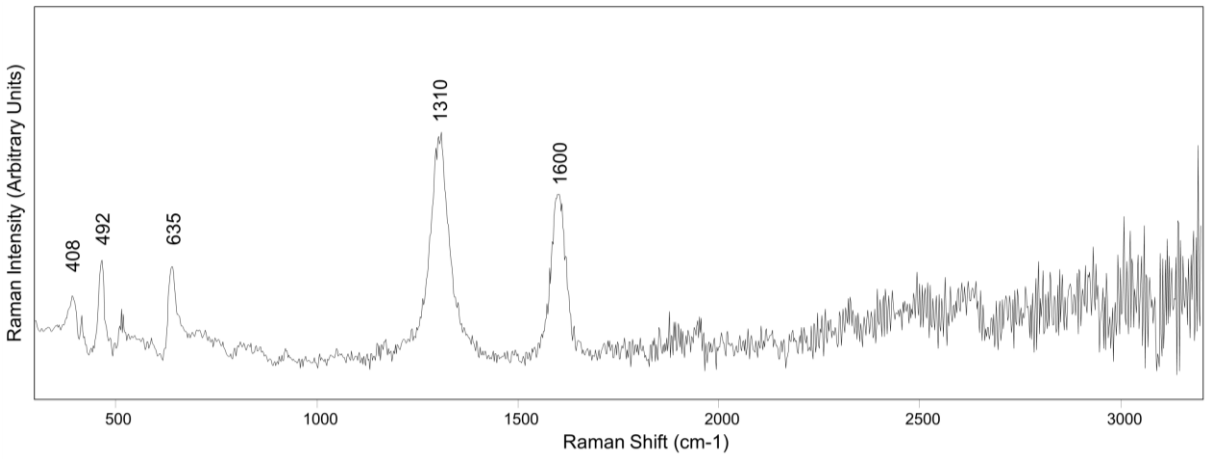

Figure 59 - Raman spectrum Paris 78 (black) obtained with BRAVO.

Having discussed different parameters and some of the differences in spectroscopic results of the different instruments and lasers.

The execution of the *in situ* measurements resulted in an additional challenge for the study. The site is open to the public so there was a certain level of accessibility. Reaching the study room was no problem, but the level of the mosaic was situated a few meters below the current stratigraphic level. All the instruments had to be carried down and up a few meters every day. Consequently, the set-up of the instruments required the necessary time and effort. Practical limitations were especially present when operating the digital microscope. Given the weight and fragility of the equipment, the instrument was only brought on to the site for one day. Furthermore, the hXRF measurements were very time consuming. Given the radiation of the X-rays, a minimum distance had to be kept between the researchers and the machine to maintain safety. Consequently, this further limited the mobility of the Raman measurements on the mosaic. The B&WTEK and ENWAVE spectrometer were user friendly due to their fiber optics probe and probe head. Since the tesserae had to be measured on the field, this allowed for more mobility The BRAVO however, did not have this feature, so the spectrometer had to be hand positioned on the tesserae and be kept in place for the duration of the spectrum acquisition. In some cases the acquisition time increased up to several minutes and to keep the instrument correctly positioned was a challenge (Fig. 60).

Figure 60 - Positioning BRAVO spectrometer in the field

5 Conclusion

The aim of this thesis was to study the mosaic tesserae from the *Mosaico de los Amores* with non-destructive analysis. The mineralogical and elemental composition of the tesserae was obtained through a multi-analytical approach. In order to understand the composition and the conservation state of the mosaic tesserae, this complimentary approach was necessary. The non-destructive *in situ* analyses of the tesserae aims to better understand Roman mosaic composition and production technology. Another objective of this thesis project was to compare different non-destructive mobile instrumentations, focusing on the Raman spectrometers employed in this study. This thesis was the ideal opportunity to compare the results and effectiveness of different spectrometers and lasers for *in situ* measurements of mosaic tesserae. Combining the results from Raman spectroscopy and the hXRF is not evident and caution is recommended. The two techniques are not readily comparable since have different penetration depths. Raman spectroscopy delivers information from the top layer of the artefact, whereas X-rays can penetrate deeper into the sample and will provide information of not only the surface layer but also of the bulk of the sample.

The study of the *Mosaico de los Amores* revealed two major material groups: stone tesserae and glass tesserae. The stone tesserae were identified via different Raman lasers because of the presence of calcite and/or dolomite. The hXRF confirms higher calcium contents, typical of calcite and/or dolomite. It is possible that these stone tesserae were cut from carbonaceous rocks quarried from nearby the site. The geological context sketched in chapter 2 showed the presence of calcitic and dolomitic rock formations surrounding the site. The rocks were used to produce stone tesserae of different hues, ranging from tones of white, beige and nude, to red, dark red, grey and black. Stone tesserae are present in similar colours in both mythological scenes studied. In the dark red stone tesserae, haemetatite was identified by Raman spectroscopy and the results were confirmed by the high presence of Fe in the hXRF data. The haematite signals are shifted when studied with different lasers and the intensity of the signals depends on the laser wavelength used. The red laser (785 nm) as well as the BRAVO spectrometer proved to be the best lasers to identify clear haematite signals.

To produce brighter and more vibrant colours than the stone tesserae, glass tesserae were introduced in the mosaics. These colours comprise different hues of green, yellow, blue, red, orange and black. The hXRF data provided preliminary elemental information concerning the chemical composition of the glass. No absolute values are obtained because only hXRF was performed, and therefore no strict attribution to colorants can be made. However, the combination of certain elements and their relative abundance give a hint as to which elements were present in the glasses.

Roman glasses are typically soda-lime type glasses, which are extremely chemically stable. No substantial amounts of K or Mg were found in the elemental dataset, which are related to chemically less stable potash glasses. Therefore, we can assume the glass tesserae of the *Mosaico de los Amores* are soda-lime type glasses. However, since this study was performed *in situ* and had a non-destructive protocol, the results are not decisive to group the glasses as soda-lime glasses with 100% certainty. Follow up research is necessary in which the elemental composition can be obtained in absolute values.

In most glasses, the elemental information corresponds to the profile of Roman glass tesserae established in the literature. Higher amounts of Ca, in combination with the presence of Sb, suggest the use of calcium antimonite ($Ca_2Sb_2O_7$ or $CaSb_2O_6$) as an opacifier. Transition metals such as Cu, Fe and Co are responsible for producing different colours and hues such as green and blue tesserae. The red and orange colours are most likely obtained by the presence of Cu nanoparticles. A high Pb and Sn content in the yellow glasses indicate the possible use of Naples Yellow ($Pb_2Sb_2O_7$) as a colorant. The Raman analysis of the glasses did not yield suitable results. Nevertheless, it was possible to identify some mineral phases such as calcium antimonite ($Ca_2Sb_2O_7$ or $CaSb_2O_6$), anatase (TiO_2), and quartz (SiO_2). Different black glasses yielded exciting results in the Raman spectra. It was possible to obtain good Raman signals of amorphous carbon and a band that can be attributed to manganese oxide (γ-Mn_2O_3). The latter is known to be a colorant for producing black glasses.

Overall, this research shows very promising results. The combination of both techniques (hXRF and Raman) allows for a complimentary aspect of the study. Where the Raman data on the glass tesserae showed limited results, the XRF data could provide addition information showing the successful use of a combined technical approach in archaeometric

studies. By using different Raman spectrometers and different lasers, the best possible Raman data were obtained. Future archaeometric studies on these types of materials can utilize the information obtained with the comparison of the Raman spectrometers.

6 Bibliography

Abd-allah, R., 2010. Chemical characterisation and manufacturing technology of late Roman to early Byzantine glass from Beit Ras / Capitolias , Northern Jordan, *Journal of Archaeological Science* 37, 1866–1874.

Arletti, R., Quartieri, S., Vezzalini, G., 2006. Glass mosaic tesserae from Pompeii: An archeometrical investigation, *Periodico di Mineralogia* 75, 25–38.

Barber, D.J., Freestone, I., K.M., M., 2009. Ancient Copper Red Glasses : investigation and analysis by microbeam techniques, in: Shortland, A.J., Freestone, I.C., Rehren, T. (Eds.), *From Mine to Microscope: Advances in the Study of Ancient Technology*. Oxbow Books, 115–127.

Barca, D., Basso, E., Bersani, D., Galli, G., Invernizzi, C., La Russa, M.F., Lottici, P.P., Malagodi, M., Ruffolo, S.A., 2016. Vitreous tesserae from the calidarium mosaics of the Villa dei Quintili, Rome. Chemical composition and production technology, *Microchemical Journal* 124, 726–735.

Basso, E., Invernizzi, C., Malagodi, M., La Russa, M.F., Bersani, D., Lottici, P.P., 2014. Characterization of colorants and opacifiers in roman glass mosaic tesserae through spectroscopic and spectrometric techniques, *Journal of Raman Spectroscopy* 45, 238–245.

Bersani, D., Conti, C., Matousek, P., Pozzi, F., Vandenabeele, P., 2016. Methodological evolutions of Raman spectroscopy in art and archaeology, *Analytical Methods* 8, 8395–8409.

Blázquez, J.M., García-Gelabert, M.P., 2000. Secuencia histórica de Castulo (Linares, Jaén) 396, 391–396.

Blázquez Martínez, J.M., 2014. Mitos del mosaico de Cástulo, *Siete Esquinas* V, 109–112.

Blázquez Martínez, J.M., 2000. La ciudad de Castulo*,* 119–156.

Boschetti, C., Henderson, J., Evans, J., 2017. Mosaic tesserae from Italy and the production of Mediterranean coloured glass (4th century BCE–4th century CE). Part II: Isotopic provenance, *Journal of Archaeological Science*: *Reports* 11, 647–657.

Boschetti, C., Leonelli, C., Macchiarola, M., Veronesi, P., Corradi, A., Sada, C., 2008. Early evidences of vitreous materials in Roman mosaics from Italy: An archaeological and archaeometric integrated study, *Journal of Cultural Heritage* 9, e21–e26.

Brems, D., Degryse, P., Hasendoncks, F., Gimeno, D., Silvestri, A., Vassilieva, E., Luypaers, S., Honings, J., 2012. Western Mediterranean sand deposits as a raw material for Roman glass production, *Journal of Archaeological Science* 39, 2897–2907.

Buciuman, F., Patcas, F., Craciun, R., Zahn, D.R.T., 1999. Vibrational spectroscopy of bulk and supported manganese oxides, *Physical Chemistry Chemical Physics* 1, 185–190.

Buzgar, N., Apopei, A.I., Diaconu, V., Buzatu, A., 2013. The composition and source of the raw material of two stone axes of Late Bronze Age from Neamț County (Romania)-A Raman study.

Seria Geologie 59, 5–22.

Caggiani, M.C., Acquafredda, P., Colomban, P., Mangone, A., 2014. The source of blue colour of archaeological glass and glazes: The Raman spectroscopy/SEM-EDS answers, *Journal of Raman Spectroscopy* 45, 1251–1259.

Caggiani, M.C., Colomban, P., Valotteau, C., Mangone, A., Cambon, P., 2013. Mobile Raman spectroscopy analysis of ancient enamelled glass masterpieces, *Analytical Methods* 5, 4345.

Caggiani, M.C., Cosentino, A., Mangone, A., 2016. Pigments Checker version 3.0, a handy set for conservation scientists: A free online Raman spectra database, *Microchemical Journal* 129, 123–132.

Caggiani, M.C., Mangone, A., Mastrorocco, F., Taccogna, C., Laviano, R., Giannossa, L.C., 2017. The Tetris game of scientific investigation. Increase the score embedding analytical techniques. Raw materials and production technology of Roman glasses from Pompeii, *Microchemical Journal* 131, 21–30.

Calligaro, T., 2007. PIXE in the study of archaeological and historical glass. *X-Ray Spectrometry.* 36, 27–34.

Capedri, S., Venturelli, G., De Maria, S., Uguzzoni, M.P.M., Pancotti, G., 2001. Characterisation and provenance of stones used in the mosaics of the domus dei Coiedii at Roman Suasa (Ancona, Italy). *Journal of Cultural Heritage.* 2, 7–22.

Castro López, M., 2014. Avatares constructivos de la sala del mosaico de los Amores 127–128.

Ceglia, A., Meulebroeck, W., Cosyns, P., Nys, K., Terryn, H., Thienpont, H., 2013. Colour and Chemistry of the glass finds in the Roman villa of Treignes, Belgium, *Procedia Chem*istry 8, 55–64.

Coccato, A., Costa, M., Rousaki, A., Clist, B., Karklins, K., Bostoen, K., Manhita, A., Cardoso, A., Dias, B., Candeias, A., 2017. Micro-Raman spectroscopy and complementary techniques (hXRF ,VP-SEM-EDS ,μ-FTIR and Py-GC/MS) applied to the study of beads from the Kongo Kingdom (Democratic Republic of the Congo), *Journal of Raman Spectroscopy* 48, 1468–1478.

Colomban, P., Schreiber, H.D., 2005. Raman signature modification induced by copper nanoparticles in silicate glass. *Journal of Raman Spectroscopy* 36, 884–890.

Colomban, P., Slodczyk, A., 2009. Raman intensity: An important tool to study the structure and phase transitions of amorphous/crystalline materials, *Optical Materials* 31, 1759–1763.

Colomban, P., Tournie, A., Bellot-Gurlet, L., 2006. Raman identification of glassy silicates used in ceramics, glass and jewellery: A tentative differentiation guide, *Journal of Raman Spectroscopy* 37, 841–852.

Colomban, P., Tournié, A., Meynard, P., 2012. On-site Raman and XRF analysis of Japanese / Chinese bronze / brass patina – the search for specific Raman signatures, *Journal of Raman Spectroscopy*

43, 799–808.

Cosano, D., Mateos, L.D., Jiménez-sanchidrián, C., Ruiz, J.R., 2017. Identification by Raman microspectroscopy of pigments in seated statues found in the Torreparedones Roman archaeological site (Baena, Spain), *Microchemical Journal* 130, 191–197.

de Faria, D.L.A., Venâncio Silva, S., de Oliveira, M.T., 1997. Raman microspectroscopy of some iron oxides and oxyhydroxides, *Journal of Raman Spectroscopy* 28, 873–878.

Del Castillo, H. C., and D. Strivay, 2012, X-ray methods, in *Analytical archaeometry - Selected topics*, 59-113, H. G. M. Edwards, and P. Vandenabeele, eds., The royal society of chemistry, Cambridge.

Edwards, H.G.M., Villar, S.E.J., Jehlicka, J., Munshi, T., 2005. FT-Raman spectroscopic study of calcium-rich and magnesium-rich carbonate minerals. S*pectrochimica Acta Part A Molecular and Biomolecular Spectroscopy* 61, 2273–2280.

Fernàndez, M., Berástegui, X., Puig, C., García-Castellanos, D., Jurado, M.J., Torné, M., Banks, C., 1998. Geophysical and geological constraints on the evolution of the Guadalquivir foreland basin, *Geological Society London Special Publications* 134, 29–48.

Ferrari, A.C., Robertson, J., 2000. Interpretation of Raman spectra of disordered and amorphous carbon, *Physical Review. B, Condensed matter* 61, 95–107.

Freestone, I., 1987. Composition and Microstructure of Early Opaque Red Glass, *Early Vitreous Materials*, 173–191.

Galli, S., Mastelloni, M., Ponterio, R., Sabatino, G., Triscari, M., 2004. Raman and scanning electron microscopy and energy- dispersive x-ray techniques for the characterization of colouring and opaquening agents in Roman mosaic glass tesserae, *Journal of Raman Spectroscopy* 35, 622–627.

Gallo, F., Silvestri, A., Molin, G., Roman, E., 2013. Glass from the Archaeological Museum of Adria (North-East Italy): new insights into Early Roman production technologies. *Journal of Archaeological Science* 40, 2589–2605.

Ganio, M., Boyen, S., Fenn, T., Scott, R., Vanhoutte, S., 2012. Roman glass across the Empire : an elemental and isotopic characterization, *Journal of Analytical Atomic Spectrometry* 27, 743–753.

García-Gelabert Pérez, M.P., Blázquez Martínez, J.M., 1994. La importancia de Castulo (Linares) en la Alta Andalucía. *Actas del II Congr. Hist. Andalucía. Córdoba, 1991,* 331–345.

Gedzevičiute, V., Welter, N., Schüssler, U., Weiss, C., 2009. Chemical composition and colouring agents of Roman mosaic and millefiori glass, studied by electron microprobe analysis and Raman microspectroscopy, *Archaeological Anthropological Science*s 1, 15–29.

Gliozzo, E., Santagostino Barbone, A., D'acapito, F., Turchiano, M., Turbanti Memmi, I., Volpe, G., 2010. The Sectilia Panels Of faragola (Ascoli Satriano, Southern Italy): A multi-analytical study of

the green, marbled (Green and Yellow), blue and blackish glass slabs, *Archaeometry* 52, 389–415.

Harris, L.M., Hutchinson, I.M., Ignley, R., Marshall, C.P., Marshall, A.O., Edwards, H.G.M., 2015. Selection of Portable Spectrometers for Planetary Exploration: A Comparison of 532nm and 785nm Raman Spectroscopy of Reduced Carbon in Archean Cherts, *Astrobiology* 15, 420–429.

Hernanz, A., Bratu, I., Marutoiu, O.F., Marutoiu, C., Gavira-Vallejo, J.M., Edwards, H.G.M., 2008. Micro-Raman spectroscopic investigation of external wall paintings from St. Dumitru's Church, Suceava, Romania, *Analytical and Bioanalytical Chemistry* 392, 263–268.

Izzo, F., Arizzi, A., Cappelletti, P., Cultrone, G., De Bonis, A., Germinario, C., Graziano, S.F., Grifa, C., Guarino, V., Mercurio, M., Morra, V., Langella, A., 2016. The art of building in the Roman period (89 B.C. - 79 A.D.): Mortars, plasters and mosaic floors from ancient Stabiae (Naples, Italy), *Construction Building Materials* 117, 129–143.

Jehlička, J., Culka, A., Košek, F., 2017. Obtaining Raman spectra of minerals and carbonaceous matter using a portable sequentially shifted excitation Raman spectrometer – a few examples, *Journal of Raman Spectroscopy* 48, 1583–1589.

Jiménez-Espinosa, R., Jiménez-Millán, J., 2003. Calcrete development in mediterranean colluvial carbonate systems from SE Spain, *Journal of Arid Environments* 53, 479–489.

Jiménez-Espinosa, R., Jiménez-Millán, J., García-Tortosa, F.J., 2016. Upper-Pleistocene terrace deposits in Mediterranean climate: Geomorphological and source-rock control on mineral and geochemical signatures (Betic Cordillera, SE Spain), *Journal of Iberian Geology* 42, 187–200.

Keay, S., 2003. Recent Archaeological Work in Roman Iberia (1990-2002), *Journal of Roman Studies* 93, 146–211.

Košařová, V., Hradil, D., Němec, I., Bezdička, P., Kanický, V., 2013. Microanalysis of clay-based pigments in painted artworks by the means of Raman spectroscopy, *Journal of Raman Spectroscopy* 44, 1570–1577.

Lauwers, D., Hutado, A.G., Tanevska, V., Moens, L., Bersani, D., Vandenabeele, P., 2014. Characterisation of a portable Raman spectrometer for in situ analysis of art objects, S*pectrochimica Acta Part A Molecular and Biomolecular Spectroscopy* 118, 294–301.

Licenziati, F., Calligaro, T., 2016. Study of mosaic glass tesserae from Delos, Greece using a combination of portable μ-Raman and X-ray fluorescence spectrometry, *Journal of Archaeological Science Reports* 7, 640–648.

Lima, A., Medici, T., Pires, A., Matos, D., Verità, M., 2012. Chemical analysis of 17th century Millefiori glasses excavated in the Monastery of Sta . Clara-a-Velha , Portugal : Comparison with Venetian and façon-de-Venise production, *Journal of Archaeological Science* 39, 1238–1248.

López Martínez, T., 2015. Las pinturas murales del conjunto arqueológico de Cástulo. Problemática

de conservación y metodología de intervención, *Arqueologiq y Territorio* 12, 165–175.

López Martínez, T., López Cruz, O., García Bueno, A., Calero-Castillo, A.I., Medina Flórez, V., 2016. Las pinturas murales de Castvlo. Primeras aportaciones a la caracterización de materiales y técnicas de ejecución, *Lvcentvm* 155–170.

Lopéz Monteagudo, G., 2014. El Mosaico De Los Amores De Castulo.

Melcher, M., Schreiner, M., 2006. Leaching studies on naturally weathered potash-lime–silica glasses, *Journal of Non-Crystalline Solids* 352, 368–379.

Miriello, D., Barca, D., Bloise, A., Ciarallo, A., Crisci, G.M., De Rose, T., Gattuso, C., Gazineo, F., La Russa, M.F., 2010. Characterisation of archaeological mortars from Pompeii (Campania, Italy) and identification of construction phases by compositional data analysis, *Journal of Archaeological Science* 37, 2207–2223.

Miriello, D., Luca, R. De, Bloise, A., Dattola, L., Mantella, G., Gazineo, F., Natale, A. De, Iannelli, M.T., Cuteri, F.A., Crisci, G.M., 2017. Compositional study of mortars and pigments from the B Mosaico della Sala dei Draghi e dei Delfini in the archaeological site of Kaulonía (Southern Calabria , Magna Graecia , Italy), *Archaeological and Anthropological Sciences* 9, 317–336.

Möncke, D., Papageorgiou, M., Winterstein-Beckmann, A., Zacharias, N., 2014. Roman glasses coloured by dissolved transition metal ions: Redox-reactions, optical spectroscopy and ligand field theory, *Journal of Archaeological Science* 46, 23–36.

Morillas, Y.J., 2011. El posible edificio del culto imperial Una reflexión forzosamente penúltima.

Padovani, S., Puzzovio, D., Sada, C., Mazzoldi, P., Borgia, I., Sgamellotti, A., Brunetti, B.G., Cartechini, L., D'Acapito, F., Maurizio, C., Shokoui, F., Oliairy, P., Rahighi, J., Lamehi-Rachti, M., Pantos, E., 2006. XAFS study of copper and silver nanoparticles in glazes of medieval middle-east lustreware (10th-13th century), *Journal of Applied Physics A* 83, 521–528.

Perrone, V., Martín-Algarra, A., Critelli, S., Decandia, F.A., D'Errico, M., Estevez, A., Iannace, A., Lazzarotto, A., Martín-Martín, M., Martín-Rojas, I., Mazzoli, S., Messina, A., Mongelli, G., Vitale, S., Zaghloul, M.N., 2006. 'Verrucano' and 'Pseudoverrucano' in the Central-Western Mediterranean Alpine Chains: palaeogeographical evolution and geodynamic significance, *Geological Society, Londen, Special publications* 262, 1–43.

Pilar San Nicolás, M., 2014. Representaciones de Selene / Luna en la Musivaria Romana 133–144.

Pincé, P., 2018. C*lay in close-up: A spectroscopic and petrographic approach to ceramic production in the Kur River Basin (Fars, Iran)*, phd thesis.

Pincé, P., Vekemans, B., Vandenabeele, P., Haerinck, E., Overlaet, B., 2016. Analysis of pre-Islamic ceramics from the Kur River Basin (Fars, Iran) using handheld X-ray fluorescence spectrometry. S*pectrochimica Acta Part B Atomic Spectroscopy* 123, 150–156.

Polikreti, K., Murphy, J.M.A., Kantarelou, V., Karydas, A.G., 2011. XRF analysis of glass beads from the

Mycenaean palace of Nestor at Pylos, Peloponnesus, Greece: New insight into the LBA glass trade, *Journal of Archaeological Science* 38, 2889–2896.

Pollard A.M., Batt C.M., Stern B., Young S.M.M., 2007. *Analytical chemistry in archaeology*, New York: Cambridge University Press.

Prinsloo, L., Barnard, W., Meiklejohn, I., Hall, K., 2008. Recent Advances in linear and nonlinear Raman spectroscopy, *Journal of Raman Spectroscopy* 38, 1538–1553.

Ricciardi, P., Colomban, P., Tournié, A., Macchiarola, M., Ayed, N., 2009a. A non-invasive study of Roman Age mosaic glass tesserae by means of Raman spectroscopy, *Journal of Archaeological Science* 36, 2551–2559.

Ricciardi, P., Colomban, P., Tournie, A., Milande, V., 2009b. Nondestructive on-site identification of ancient glasses: Genuine artefacts, embellished pieces or forgeries? *Journal of Raman Spectroscopy* 40, 604–617.

Rickard, T.A., 1928. The Mining of the Romans in Spain, *Journal of Roman Studies* 18, 129–143.

Rodney, N.B., 1967. "The judgment of Paris." *Music Lett*. 48, 101–102.

Roldán, J.M., Blázquez, J.M., del Castillo, A., 1999. El Imperio romano : siglos I-III. *Hist. Roma* II, 562.

Rousaki, A., Bellelli, C., Carballido Calatayud, M., Aldazabal, V., Custo, G., Moens, L., Vandenabeele, P., Vázquez, C., 2015. Micro-Raman analysis of pigments from hunter-gatherer archaeological sites of North Patagonia (Argentina), *Journal of Raman Spectroscopy* 46, 1016–1024.

Rousaki, A., Vargas, E., Vázquez, C., Aldazábal, V., Bellelli, C., Carballido Calatayud, M., Hajduk, A., Palacios, O., Moens, L., Vandenabeele, P., 2018. On-field Raman spectroscopy of Patagonian prehistoric rock art: Pigments, alteration products and substrata, *Trends in Analytical Chemistry* 105, 338–351.

Santagostino Barbone, A., Gliozzo, E., D'acapito, F., Turchiano, M., Turbanti Memmi, I., Volpe, G., 2008. The Sectilia Panels Of faragola (Ascoli Satriano, Southern Italy): A multi-analytical study of the green, marbled (Green and Yellow), blue and blackish glass slabs, *Archaeometry* 50, 451–473.

Scholze, F., 2006. X-Ray detectors and XRF detection channels, in *Handbook of practical X-ray fluoresence analysis,* 199-308, B. Beckhoff, B. KanngieSer, N. Lqnghoff, R. Wedell, and H. Wolff, eds., Springer. Berlin.

Shackley M.S., 2011. An Introduction to X-Ray Fluorescence (XRF) Analysis in Archaeology, in: Shackley M.S., (ed.), *X-Ray Fluorescence Spectrometry (XRF) in Geoarchaeology*, New York: Springer, 7-44.

Silvestri, A., Tonietto, S., Molin, G., Guerriero, P., 2014. The palaeo-Christian glass mosaic of St. Prosdocimus (Padova, Italy): Archaeometric characterisation of tesserae with copper- or tin-based opacifiers, *Journal of Archaeological Science* 42, 51–67.

Tanaka, R., Yuge, K., Kawai, J., Alawadhi, H., 2017. Artificial peaks in energy dispersive X-ray spectra: sum peaks, escape peaks, and diffraction peaks. *X-Ray Spectrometry* 46, 5–11.

Tite, M., Pradell, T., Shortland, A., 2008. Discovery, production and use of tin-based opacifiers in glasses, enamels and glazes from the Late Iron Age onwards: A reassessment, *Archaeometry* 50, 67–84.

Vagnini, M., Gabrieli, F., Daveri, A., Sali, D., 2017. Handheld new technology Raman and portable FT-IR spectrometers as complementary tools for the in situ identification of organic materials in modern art, S*pectrochimica Acta Part A Molecular and Biomolecular Spectroscopy* 176, 174–182.

van der Werf, I., Mangone, A., Giannossa, L.C., Traini, A., Laviano, R., Coralini, A., Sabbatini, L., 2009. Archaeometric investigation of Roman tesserae from Herculaneum (Italy) by the combined use of complementary micro-destructive analytical techniques, *Journal of Archaeological Science* 36, 2625–2634.

Van Espen, P., Janssens, K., Nobels, J., 1986. AXIL-PC, software for the analysis of comlex X-Ray spectra, *Chemometrics and Intelligent Laboratory Systems* 1, 109–114.

Van Pevenage, J., Lauwers, D., Herremans, D., Verhaeven, E., Vekemans, B., De Clercq, W., Vincze, L., Moens, L., Vandenabeele, P., 2014. A combined spectroscopic study on Chinese porcelain containing ruan-cai colours, *Analytical Methods* 6, 387–394.

Vandenabeele, P., 2004. Raman spectroscopy in art and archaeology, *Journal of Raman Spectroscopy* 35, 607–609.

Vandenabeele, P., Edwards, H.G.M., Jehlička, J., 2014. The role of mobile instrumentation in novel applications of Raman spectroscopy: Archaeometry, geosciences, and forensics, *Chemical Society Reviews* 43, 2628–2649.

Vekemans, B., Janssens, K., Vincze, L., Adams, F., Vanespen, P., 1994. Analysis of X-ray spectra by iterative least-squares - New developments, *X-ray Spectrometry* 23, 278–285.

Veneranda, M., Aramendia, J., Gomez, O., Fdez-Ortiz de Vallejuelo, S., Garcia, L., Garcia-Camino, I., Castro, K., Azkarate, A., Madariaga, J.M., 2017. Characterization of archaeometallurgical artefacts by means of portable Raman systems: corrosion mechanisms influenced by marine aerosol, *Journal of Raman Spectroscopy* 48, 258–266.

Verità, M., 2000. Technology and deterioration of vitreous mosaic tesserae Technology and deterioration of vitreous filosaic tesserae, *Studies in Conservation* 45, 65-76.

Walcot, P., 1977. The Judgement of Paris, *Greece Rome* 24, 31–39.

Woisetschläger, G., Dutz, M., Paul, S., Schreiner, M., 2000. Weathering phenomena on naturally weathered potash-lime-silica-glass with medieval composition studied by secondary electron microscopy and energy dispersive microanalysis, *Mikrochimica Acta* 135, 121–130.

Appendix I: hXRF data Paris 40kV

paris	Al-Ka	Si-Ka	S-Ka	Cl-Ka	Ar-Ka	K-Ka	Ca-Ka	Ti-Ka	V-Ka	Cr-Ka	Mn-Ka	Fe-Ka	Co-Ka	Ni-Ka	Cu-Ka	Zn-Ka	As-Ka	Br-Ka	Rb-Ka	Sr-Ka	Y-Ka	Zr-Ka	Nb-Ka	Mo-Ka	Cd-La	Sn-La	Sb-La	Ba-La	Hg-La	Pb-La
1	567	1006	.	1329	936	1148	11233	165	.	.	11797	33984	15882	775	44317	1206	.	.	.	25716	.	2085	.	.	.	.	5301	.	.	254052
2	592	995	.	1242	927	1213	11016	317	.	263	2617	36397	10896	539	42319	1770	.	.	.	23224	.	.	.	.	.	.	5850	.	.	308823
3	615	1610	.	1188	851	878	11651	211	.	.	2327	27651	5594	398	14144	2378	.	.	.	15670	.	699	.	.	.	.	4533	.	1089	546782
5	.	217	.	740	1241	868	204837	71	.	.	49	1526	.	122	57	722	.	.	56	8795	.	.	.	.	.	.	.	.	.	357
6	853	2248	.	1819	1478	1712	12290	382	.	.	3920	19576	.	475	227998	7022	.	649	390	25570	.	2952	.	.	.	492	5377	.	.	50069
7	425	823	.	1559	1196	1424	14934	510	.	.	2547	26065	267	337	286017	3866	1818	676	553	26626	.	3579	.	.	.	240	2809	.	.	40969
8	268	646	.	1247	1105	1705	12737	387	.	.	2122	21872	251	382	259718	4417	1896	697	563	26326	.	3650	.	.	.	.	3196	.	.	43557
9	658	1206	598	1619	1193	1610	11867	470	.	.	8161	24007	410	264	3856	1691	1399	413	1277	36629	.	5727	.	.	.	.	2215	.	.	11129
10	469	910	587	1426	1266	1857	11263	478	.	.	7525	23590	214	231	16615	2953	1648	407	1074	35631	.	6441	.	.	.	.	1834	.	.	11477
11	370	877	787	1585	1315	1825	10086	389	.	.	8648	22350	186	250	20507	2228	1631	492	1377	38141	.	5932	.	.	.	.	1801	.	.	12357
12	157	1214	.	988	954	1656	10524	348	.	.	9976	21042	861	224	2988	2165	.	623	806	37146	.	5382	.	.	.	.	1374	.	.	77289
13	176	781	365	1086	1118	1177	13579	311	.	.	4625	103349	1162	394	137209	1797	992	320	641	28773	.	5585	.	.	.	.	758	.	.	10255
14	61	365	741	896	1294	990	93941	112	.	.	1008	26448	224	180	211	903	70	122	290	8762	.	356	.	.	.	.	999	.	.	300
15	.	866	.	612	664	2095	8799	693	.	82	7529	82112	.	224	114295	5279	.	1059	514	31665	.	4930	257	.	.	.	413	.	.	246285
18	64	84	76	84	489	887	98603	281	95	253	1171	729960	.	97	312	1324	2484	.	239	13591	292	1606	.	2308	.	.	.	63	.	1341
19	45	156	.	82	603	1043	88695	207	.	.	1007	758162	.	100	300	1547	2154	.	292	13023	190	295	.	2359	.	.	.	180	.	1483
21	77	226	.	736	1197	1558	155523	250	.	.	644	13482	.	163	235	1619	254	.	475	7468	552	779	.	.	.	.	.	.	.	686
22	119	400	.	637	1190	1679	175399	180	.	.	579	20117	.	212	247	1196	.	.	709	8613	852	1178	.	.	.	.	.	.	.	2000
24	249	584	.	906	414	1413	6188	572	115	150	760	30317	708	.	1980	1747	.	.	.	2028	.	.	.	.	291	.	.	.	6146	2,50E+06
27	169	778	.	1645	720	1262	9116	760	416	303	1674	42262	1221	.	2624	2528	.	.	.	5545	.	.	.	.	.	.	255	.	5017	2,15E+06
28	72	734	.	823	665	879	10977	257	.	.	7944	17292	126	115	118310	1438	.	1398	.	28749	.	2591	.	.	.	223	869	.	.	346250
29	172	929	.	1275	1176	1299	14906	445	.	.	5766	25779	288	300	83374	2236	.	455	683	38349	481	4333	.	.	.	313	566	.	.	5901
30	222	994	.	931	810	1059	12920	350	.	.	7238	20026	147	141	114575	2438	.	1470	135	27914	367	2411	.	.	.	207	893	.	.	342054
31	238	991	.	939	789	1336	12096	489	.	.	10810	32708	436	177	195155	2670	.	1028	656	27836	403	3986	.	.	.	404	1103	.	.	282296
32	191	830	.	872	687	906	10884	293	.	.	4746	19500	156	99	113221	1406	.	2148	.	23551	.	1793	.	.	.	438	1455	.	.	633237
33	36	262	.	992	1239	877	92230	134	.	.	279	6787	.	193	174	1056	.	101	.	7120	.	.	.	.	.	.	.	.	.	336
34	88	307	.	733	1291	1168	166343	144	.	.	143	8941	.	167	160	1212	.	55	111	15839	264	.	.	.	.	.	.	.	.	579
35	131	773	.	990	802	1170	11813	237	.	.	3349	17072	171	176	661	1177	.	678	725	28445	.	3499	.	.	.	.	1114	.	.	174372
36	283	776	.	1196	733	1636	16056	1026	.	.	2305	51736	.	219	329944	18702	.	2446	.	8692	.	.	.	.	.	1025	517	.	2788	1,51E+06
37	204	578	.	1107	1088	1934	14928	804	.	.	9053	44300	504	276	94639	3540	.	651	831	38030	.	6787	.	.	.	347	847	.	.	19014
38	.	329	.	88	126	1701	17368	1088	196	140	13436	63428	544	120	100756	5632	.	1905	587	33273	.	8129	.	.	.	.	107	.	.	210238
39	87	306	504	681	1141	1245	134012	224	.	.	893	18142	.	199	304	1533	114	.	486	20437	869	.	.	.	.	.	.	.	.	1109
40	159	331	.	704	1222	1305	195609	94	.	.	248	9618	.	128	129	941	178	.	273	6268	601	.	.	.	.	.	.	.	.	160
41	.	298	.	969	1271	1190	93575	270	.	.	990	26752	.	151	221	1272	.	167	454	9125	179	.	.	.	.	.	.	.	.	577
42	239	324	.	459	965	350	188785	88	.	.	143	4928	.	165	174	1081	.	62	54	15901	293	.	.	.	697	.	.	.	.	311
43	369	800	.	786	1115	4433	5768	3426	335	180	1258	142563	1013	200	255	2051	.	.	15215	8654	1929	10137	1512	.	.	.	.	.	.	707
44	.	228	.	644	1229	1355	179538	119	.	.	181	9836	.	126	179	1307	62	.	539	16005	444	.	.	.	.	.	.	.	.	292
45	124	70	.	165	659	443	119342	129	.	.	6168	860235	.	83	178	1976	1063	.	.	7482	484	.	.	.	.	.	.	.	.	2728

46	266	811	.	1747	761	573	4753	487	.	.	846	26623	.	97	7150	3335	.	.	.	2090	.	.	.	.	662	.	.	.	.	2,33E+06
47	369	911	468	1443	1147	1426	12717	385	.	.	4852	18601	1404	258	5879	1828	358	275	744	36737	.	.	3988	.	.	.	.	1705	.	.	44074
48	403	981	.	1287	1097	1251	10405	422	.	.	2681	27923	266	392	288777	3447	1816	426	557	25401	.	.	3530	.	.	.	181	3746	.	.	43378
49	212	806	.	1215	647	846	3524	706	.	.	556	22071	217	79	5507	1469	.	.	.	2302	.	.	.	.	616	.	.	82	.	6305	2,44E+06
50	135	678	.	779	464	1017	9220	329	.	.	1895	17556	.	178	3196	1750	.	.	.	5893	.	.	.	.	.	100	1688	.	4010	1,48E+06	
51	68	520	.	876	505	688	10364	256	.	40	4981	23907	.	284	3817	2273	.	.	.	8160	.	.	.	.	.	259	922	.	4366	1,53E+06	
52	51	314	400	784	1178	1032	89252	147	.	.	1820	16683	.	219	1017	1363	.	.	342	7960	286	587	.	.	.	.	.	.	.	4284	
53	147	632	.	919	480	937	8521	532	71	67	7428	64439	.	257	2246	2713	.	.	.	8215	.	.	.	.	.	219	1265	.	4357	1,59E+06	
54	152	367	.	686	1260	1632	171552	217	.	.	608	13940	.	148	477	1356	.	.	599	8978	931	.	.	.	.	.	.	.	.	993	
55	240	749	.	1393	928	1159	8298	569	64	.	2893	88330	.	161	357015	4809	.	2440	.	5628	.	261	.	.	.	569	521	.	2569	1,58E+06	
56	231	388	254	940	1353	938	96369	113	.	.	523	11769	.	177	167	983	.	65	345	8374	.	.	.	.	.	.	.	.	.	360	
57	238	772	.	1365	765	1476	12352	836	.	.	2663	59790	.	172	301607	18181	.	3130	.	9443	.	.	.	.	.	686	641	.	2776	1,70E+06	
58	138	119	567	749	1272	1243	174549	227	.	.	429	21287	.	139	269	1779	.	.	438	42621	217	.	.	.	.	.	.	.	.	1319	
59	122	149	150	134	588	718	65876	520	.	586	9079	1,48E+06	.	97	747	1849	267	112	.	5497	194	.	.	.	.	.	.	.	.	2308	
60	91	59	.	116	544	557	85720	273	.	496	7374	1,20E+06	.	128	276	1520	216	133	26	5402	294	.	.	.	.	.	.	.	.	2608	
61	129	695	.	870	528	935	15564	333	46	.	4307	25830	.	232	3760	2235	.	.	.	8272	.	.	.	.	.	105	1068	.	3953	1,43E+06	
62	80	667	.	396	393	1174	15498	548	95	102	3671	32640	.	217	2168	2955	.	.	.	14446	.	1088	.	.	.	.	821	.	2555	942738	
63	64	321	265	710	1295	1242	157149	221	.	.	163	14494	.	174	198	1097	.	71	273	3064	290	687	.	.	.	.	.	.	.	572	
64	201	779	.	838	675	1032	11819	332	.	.	4283	19968	236	188	100442	2461	.	2214	.	22106	.	1637	.	.	.	259	1188	.	.	578550	
65	267	741	.	1075	814	1512	12345	520	.	.	10625	29631	248	185238	27719	510	.	44	2154	38	342	96	.	.	.	10	169	.	.	100	
66	56	858	.	845	710	1017	13201	309	49	.	7097	18788	100	110	105774	2064	.	1410	.	27843	.	2468	.	.	.	164	787	.	.	330114	
67	189	543	.	989	1016	2252	30338	1200	.	.	1862	55529	3435	401	15596	7219	.	528	1303	17939	.	8630	.	.	.	.	892	.	.	13778	
68	458	1052	535	1641	1303	1890	13777	531	.	.	8653	25827	230	230	20869	2985	1498	826	1289	38401	.	6251	.	.	.	.	1898	.	.	13862	
69	678	2091	.	1703	1454	1387	13172	305	.	.	11434	42315	10351	564	22764	1152	1176	306	481	34977	.	2357	.	.	.	.	4159	.	.	51274	
70	196	584	.	905	684	1883	12065	1039	320	209	2055	57851	.	245	368823	21334	.	2660	.	9670	.	.	.	745	.	1103	594	.	2105	1,25E+06	
71	172	469	323	943	1323	879	94343	60	.	.	1288	10081	.	159	177	679	.	71	66	7170	164	.	.	.	.	.	.	.	.	242	
72	169	333	140	854	1283	860	95374	35	.	.	2761	7646	.	206	131	644	.	154	102	5753	.	.	.	.	.	.	.	.	.	203	
73	325	1255	.	1147	870	1058	12199	120	.	.	18128	46666	10016	700	25478	1119	.	632	237	35000	.	1778	.	.	.	.	3347	.	.	212585	
74	186	388	.	807	1206	1265	133348	167	.	.	794	26515	.	210	211	1469	.	77	483	18728	761	.	.	.	.	.	.	.	.	782	
75	22	236	.	686	1216	803	214749	80	.	.	98	3030	.	124	372	963	.	.	92	4570	.	136	.	.	.	.	.	.	.	776	
76	71	272	481	715	1211	1471	174751	158	.	.	114	15746	.	175	147	1496	.	68	478	2445	444	967	.	.	.	.	.	.	.	475	
77	254	1011	.	1865	571	658	8680	634	.	.	801	34043	459	179	3749	3431	.	.	.	2895	.	.	.	.	654	.	.	.	6381	2,31E+06	
78	.	954	.	804	1003	4721	3658	3618	.	258	1452	164029	1136	306	276	1882	.	.	15772	9231	1472	10010	1205	.	.	.	.	.	.	543	
79	.	764	.	888	1090	4755	4386	3520	.	246	1347	155124	1077	228	835	1617	.	.	15646	10302	1734	9767	1385	.	.	.	.	.	.	1824	
80	.	693	.	750	1056	4733	5090	3480	.	281	1607	183213	.	316	276	1979	.	.	15862	8845	1431	9888	1459	.	.	.	.	.	.	967	
81	200	546	.	1826	697	693	7790	591	.	.	726	27222	172	85	1847	2007	.	.	.	1921	.	.	.	.	648	.	.	.	6193	2,23E+06	
82	263	655	.	1488	525	755	7942	617	.	.	768	28053	339	154	2010	1798	.	.	.	2000	.	.	.	.	655	.	.	.	6176	2,23E+06	
83	165	563	.	451	454	1495	9852	416	.	.	4022	45140	270	39	102878	3506	.	4380	.	11161	.	.	.	.	.	59	1112	.	.	1,14E+06	
84	124	839	.	923	751	1165	13061	424	.	.	7929	19989	169	156	114959	2625	.	1630	102	29428	.	2891	.	.	.	125	1007	.	.	336749	
85	230	950	.	853	708	998	11325	306	.	.	7555	17988	182	179	115460	2462	.	1518	.	28784	.	2499	.	.	.	214	832	.	.	341552	
88	134	169	150	205	453	767	82028	314	.	318	7309	1,06E+06	.	130	286	2156	339	149	202	6969	319	570	.	.	.	.	.	.	.	1943	
89	85	257	186	768	1177	1334	187607	151	.	.	210	8249	.	186	204	1574	.	.	272	6163	639	.	.	.	.	.	.	.	.	373	
90	132	250	158	670	1215	1454	169173	197	.	.	166	14285	.	160	234	1432	243	30	401	2781	275	980	.	.	.	.	.	.	.	377	
91	541	1062	675	1661	1326	1684	14396	504	.	.	8780	22479	246	248	19944	2058	.	638	1139	36501	.	5098	.	.	.	.	2521	.	.	15571	
92	138	852	.	977	667	1050	13040	336	.	.	4148	22390	173	107	90748	2424	.	2050	.	22038	.	2139	.	.	.	346	1400	.	.	548600	
93	134	491	.	551	905	8637	29108	2977	374	99	2888	213246	1412	157	1235	2597	.	.	13630	121013	2142	30967	2317	.	.	.	.	671	.	3100	
94	422	604	.	635	1016	8943	30281	2627	.	90	2200	171021	.	169	626	2754	.	.	23580	78603	1234	22922	957	.	.	.	.	.	.	1319	
95	112	460	.	537	846	6009	16419	3790	.	145	1714	198563	.	180	607	3009	.	.	27188	105472	681	25898	1848	.	.	.	.	.	.	4451	

Appendix II: hXRF data Paris 10 kV

paris	F-Ka	Mg-Ka	Al-Ka	Si-Ka	P-Ka	S-Ka	Cl-Ka	Ar-Ka	K-Ka	Ca-Ka	Ti-Ka	V-Ka	Cr-Ka	Mn-Ka	Fe-Ka	Co-Ka	Ni-Ka	Cu-Ka	Zn-Ka	Rh-La	Cd-La	Sn-La	Sb-La	Ba-La
1	.	321	7179	298250	.	.	35862	42137	74338	560661	3042	.	.	96468	178000	46975	.	20765	.	81555	.	.	102969	.
2	.	494	7384	279420	.	.	43923	41409	79246	553628	6908	.	7378	23234	199990	31900	473	19916	.	81337	.	.	121418	.
3	.	358	6113	304518	.	.	42983	41336	59396	577506	4784	.	.	18435	146194	16245	.	6476	.	82738	.	.	82082	.
5	.	472	2825	20460	.	.	11589	63162	16732	6,14E+06	2971	.	.	5246	15560	.	.	.	.	100293	.	.	.	.
6	.	416	7424	295763	.	11449	34910	40856	87301	653611	7125	.	.	31965	99028	1526	.	108998	.	84869	.	10205	102209	.
7	.	449	7031	249372	.	23223	42590	42841	74674	810111	12716	.	.	22757	127879	2551	.	123485	.	83308	.	.	56399	.
8	.	485	8011	270287	.	7859	26775	43650	97327	708867	11830	.	.	16031	121204	2147	.	108707	.	83205	.	.	64936	.
9	.	369	7879	297554	.	5829	46029	45842	86506	605133	15153	.	.	74004	133260	2760	.	2595	.	81353	.	.	45703	.
10	.	382	7446	288010	.	5207	33905	45324	95037	571968	13340	.	.	61557	124539	2082	.	9889	.	82241	.	.	36452	.
11	.	518	8191	343546	.	5704	42113	41582	93830	523700	11941	.	.	74039	121491	1725	.	12799	.	79535	.	.	39896	.
12	.	296	8231	302064	.	6582	44895	44568	106397	542121	12650	.	.	84672	120114	3421	.	2331	.	81916	.	.	29288	.
13	.	534	6344	320357	.	6992	54693	43602	56005	642521	14121	.	.	46473	545818	.	.	68137	2287	79804	.	.	12749	.
14	.	1432	2725	30626	.	3169	10142	59148	28540	3,94E+06	7176	.	.	11890	138643	.	.	.	.	76134	.	.	.	.
15	.	290	7470	242418	.	2401	29024	43427	129654	422960	23947	.	.	58137	448332	.	.	50215	2560	81882	.	.	9728	.
18	.	385	4147	56570	.	9804	18894	41992	38465	3,18E+06	19714	.	5803	16661	2,55E+06	.	.	.	.	105919	.	.	.	.
19	.	480	4406	69418	.	.	17032	43093	47105	2,88E+06	22548	.	.	16237	2,58E+06	.	.	.	479	104088	.	.	.	.
21	.	434	3268	44431	.	11203	10408	60311	50518	5,13E+06	7718	.	.	8977	83389	.	.	.	2393	91328	.	.	.	.
22	.	428	4984	49188	.	10134	12380	61180	55588	5,45E+06	7775	.	.	8726	92070	.	.	.	2556	95988	.	.	.	.
24	.	254	9823	221780	18029	.	28159	46174	103278	318478	18943	.	.	8159	153952	2959	.	.	.	80547	2446	.	.	.
27	.	237	6189	142447	.	.	27635	46798	62487	366168	17094	.	.	11539	173925	3520	.	.	.	85459	.	.	.	.
28	.	450	7006	330136	.	3423	64093	43606	56459	571790	12056	.	.	71040	94004	1602	.	59003	.	82095	.	693	16877	.
29	.	334	7485	344479	.	6355	62768	45469	63402	768033	15361	.	.	51200	137017	2085	.	42888	.	83149	.	425	13704	.
30	.	366	7134	306477	.	3110	55379	42362	61976	669586	13351	.	.	66868	114658	2513	.	53268	.	81759	.	378	15105	.
31	.	282	6619	280790	.	2374	52224	44962	84095	627257	16249	.	.	89893	167423	2424	.	95627	.	82695	.	5929	22324	.
32	.	427	6027	320925	.	252	52964	42630	53143	564270	11200	.	.	43103	101330	2630	.	50465	.	81587	.	6711	27452	.
33	.	1278	3636	48487	.	.	15445	56770	28544	3,80E+06	4782	.	.	5168	39079	.	.	.	.	76403	.	.	.	.
34	.	574	5571	54254	.	7412	15734	60213	42343	5,23E+06	6568	.	.	5559	63624	.	.	.	2091	90510	.	.	.	.
35	.	454	7593	329346	.	3379	46827	43934	65829	629395	12529	.	.	33509	97810	2178	.	.	.	80445	.	.	24347	.
36	.	344	7014	186240	.	.	32125	44755	80695	647952	26252	.	.	19521	223176	.	.	125724	.	92181	.	21236	5033	.
37	.	472	7669	241491	.	31267	38430	43164	100306	726541	26871	.	.	86418	243625	4930	.	43012	.	83263	.	3945	14634	.
38	.	.	3524	227520	.	.	34738	42459	126053	884241	38671	.	.	113782	339997	6465	.	38327	.	85949	.	.	7226	.
39	.	396	3993	91724	.	10991	9488	57657	43257	4,77E+06	7376	.	.	11241	107152	.	.	.	2892	90377	.	.	.	.
40	.	369	3378	22229	.	672	10865	61437	34787	6,01E+06	4406	.	.	5648	57843	.	.	.	2770	85823	.	.	.	.
41	.	1103	3897	41378	.	7777	10913	57015	38210	3,80E+06	8593	.	.	11217	138187	.	.	.	.	77798	.	.	.	.
42	.	468	2814	23116	.	7903	14440	60666	8782	5,85E+06	3296	.	1986	7301	34872	.	.	.	1578	91951	11914	.	.	.
43	.	285	21842	228501	4649	.	6351	43527	276204	198802	96167	.	6434	9933	727320	10566	.	.	.	89301	.	.	.	.
44	.	276	3323	33250	.	4479	9086	61003	28774	5,64E+06	4046	.	.	5741	60766	.	.	.	2478	96369	10722	.	.	.
45	.	459	3971	44522	.	12613	19804	42652	20307	3,51E+06	15310	.	9141	54365	2,66E+06	.	.	.	.	98668	.	.	.	.

46	.	223	6626	156402	.	.	16631	47721	61968	197354	14191	.	.	8676	119698	.	.	2205	.	85388	.	.	.	.
47	.	.	5518	293831	.	4878	33931	46112	69794	644175	12564	.	.	47866	98482	5492	.	1591	.	83097	.	.	41309	.
48	.	356	6279	277242	.	7965	29237	42728	60941	564652	9867	.	.	21790	115385	1484	.	133266	.	84747	.	.	75266	.
49	.	354	8054	211249	.	.	15006	47983	80870	139000	14424	.	2144	5607	104174	1816	.	1733	.	82240	.	.	.	.
50	772	387	6103	213593	.	.	22841	43566	56769	394261	8885	.	.	16979	86041	.	.	578	.	79694	.	4724	27125	.
51	.	244	5272	235158	.	.	27492	44221	46212	443385	9166	2184	.	39948	116688	.	.	968	.	81659	.	6343	17346	.
52	.	1292	2895	31279	.	2593	7425	55082	23620	3,66E+06	4204	.	.	19979	86110	.	.	.	.	78036	8976	1027	27019	.
53	.	345	5747	202722	.	.	33906	44351	55180	387395	16902	.	.	55574	297446	.	.	.	.	86504	.	3594	22030	.
54	.	475	4332	40510	.	8053	9887	63203	50624	5,53E+06	7492	.	.	9269	76685	.	.	.	2822	95157	.	.	.	.
55	.	253	4937	161921	.	.	25567	44124	52880	368821	14652	3851	.	24609	375623	.	.	132480	.	91918	.	7500	4456	.
56	.	1638	2719	27318	.	1562	9731	59576	27365	4,00E+06	6886	.	.	8079	63176	.	.	.	.	75871	.	.	.	.
57	.	396	6197	183409	.	.	33591	40735	67863	483225	21822	3960	.	22943	254792	.	.	120216	.	94695	.	16245	3371	.
58	.	466	3727	41306	.	2956	10322	62585	33248	5,45E+06	5656	.	.	7839	116094	.	.	.	2744	96464	.	.	.	.
59	.	448	5016	71448	.	42754	26758	37706	34785	2,02E+06	23419	.	9057	67739	3,90E+06	.	.	748	.	101852	.	.	.	.
60	.	486	4563	60213	.	20724	29337	39126	26471	2,74E+06	18078	.	6909	56152	3,23E+06	.	.	.	.	104493	.	.	.	.
61	.	322	5132	200014	.	.	40586	45913	50664	674112	9106	.	.	33309	117094	.	.	621	.	82666	.	5512	17544	.
62	.	448	6637	192748	.	31150	31574	43755	72949	752681	18045	.	.	28527	159228	.	.	.	.	80858	.	1402	18903	.
63	.	762	3974	28459	.	2117	12893	56121	38596	5,36E+06	7683	.	.	4594	79255	.	.	.	1972	90273	.	.	.	.
64	.	452	6230	275584	.	5823	49262	43325	62128	625126	12570	.	.	39616	102431	2912	.	46948	.	84078	.	6444	22448	.
65	.	445	6542	277497	.	6131	63094	43586	83753	651066	16171	.	.	92766	156329	2673	.	90791	.	84870	.	5344	21418	.
66	.	327	5626	238163	.	7808	56231	47404	55947	671216	12805	.	.	61014	97327	1156	.	52768	.	83434	.	.	17711	.
67	.	434	7636	117109	.	20728	20322	50165	122788	1,47E+06	32993	.	.	16940	308307	12612	.	4889	.	85733	.	.	16309	.
68	.	416	8411	312587	.	13442	66685	40234	99102	707235	14258	.	.	74568	140045	2423	.	11767	.	84855	.	.	38364	.
69	.	304	5911	316162	.	8786	50050	40650	64163	684264	7840	.	.	107901	226112	33888	.	10220	.	82388	.	.	87560	.
70	.	419	6076	163376	.	.	53116	46324	101125	481127	26940	.	7197	17599	276448	.	.	146271	.	87929	.	31448	6119	.
71	.	1527	2020	17377	.	2371	11742	59909	17129	3,94E+06	4237	.	.	15751	49369	.	.	.	.	79110	.	.	.	.
72	.	1751	2090	16724	.	.	13024	59160	15964	4,00E+06	2820	.	.	29190	42371	.	.	.	.	79109	.	.	.	.
73	.	465	5890	283068	.	4761	45044	39503	56148	640881	4630	.	.	157812	247899	30712	.	12690	.	81154	.	.	68739	.
74	.	423	3888	86721	.	8019	12373	58133	41792	4,78E+06	5524	.	.	11141	148094	.	.	.	2759	93234	.	.	.	.
75	.	378	3172	22867	.	5467	13928	64399	17848	6,20E+06	3189	.	1653	6056	22733	7080	.	.	1923	95513	.	.	.	.
76	.	455	4072	33463	.	4105	14367	68042	47722	5,57E+06	7441	.	.	4504	89948	.	.	.	3052	90368	.	.	.	.
77	.	226	6144	136517	.	.	28695	45508	53442	312938	15941	.	.	8781	139143	3355	.	707	.	85366	3152	.	.	.
78	.	251	25106	253290	5255	1644	11406	40380	300908	127958	112220	.	15049	16509	845978	14889	.	.	.	99945	.	.	.	.
79	.	339	25700	259497	3579	1883	8031	40253	303564	142178	101391	.	7484	10408	779630	11494	.	.	1979	92145	.	.	.	.
80	.	292	26155	252294	3329	2538	9681	40301	308347	211774	111258	.	14732	20299	945495	.	.	.	.	92861	.	.	.	.
81	.	300	6377	134564	.	.	28603	47513	65821	327366	15230	.	.	8208	121332	2268	.	.	.	86040	.	.	.	.
82	.	318	6916	138405	.	.	28905	46835	67522	333077	16041	.	.	8893	123174	2846	.	.	.	86474	.	.	.	.
83	.	433	7647	270312	.	4218	53842	43333	94580	525723	15187	.	.	31156	239055	3998	.	39433	.	84807	.	3795	21003	.
84	.	307	7334	278214	.	5608	70512	44759	69478	728764	13777	.	.	65687	111241	1451	.	57078	.	86628	.	2437	16122	.
85	.	339	5577	248641	.	5457	60450	45039	56657	618496	14536	.	.	70599	99083	2414	.	54462	.	82068	.	.	18553	.
88	.	358	5528	87861	.	10327	26244	40862	44018	2,51E+06	21068	.	7797	58724	3,08E+06	.	.	.	.	101025	.	.	.	.
89	.	582	4064	37447	.	4673	14992	76730	38203	5,73E+06	6922	.	.	7306	50748	.	.	.	2229	103016	.	.	.	.
90	.	537	4057	43636	.	6222	13671	59613	45465	5,40E+06	11825	.	.	12959	94057	.	.	.	.	92291	.	.	.	.
91	.	437	7612	290177	.	9171	58581	43128	84242	732657	15543	.	.	75390	126924	2302	.	11113	.	82438	.	.	48209	.
92	.	415	6577	280056	.	5918	44917	42878	65227	695394	13876	.	.	40446	122774	3334	.	41817	.	82051	.	.	25347	.
93	.	420	1546	175677	.	5674	11786	34873	505483	1,29E+06	77542	.	8165	27313	948081	14566	.	.	.	106772	.	.	.	15324
94	.	421	16238	148850	.	5447	6955	45967	515122	1,53E+06	65245	.	.	17261	714951	.	.	1771	.	94041	.	.	.	.
95	.	355	19566	184824	.	2034	13346	42548	367276	806002	73199	.	7466	17045	849010	.	.	.	.	85979	.	.	.	17320

Appendix III: hXRF data Spring 40 kV

Spring	Al-Ka	Si-Ka	P-Ka	S-Ka	Cl-Ka	Ar-Ka	K-Ka	Ca-Ka	Ti-Ka	V-Ka	Cr-Ka	Mn-Ka	Fe-Ka	Co-Ka	Ni-Ka	Cu-Ka	Zn-Ka	Ga-Ka	As-Ka	Br-Ka	Rb-Ka	Sr-Ka	Y-Ka	Zr-Ka	Nb-Ka	Mo-Ka	Sn-La	Sb-La	Ba-La	Hg-La	Pb-La
1	281	666	.	.	1450	888	1041	8752	452	.	.	3724	84596	957	365	497300	10726	.	.	2630	.	4448	.	.	.	.	406	634	.	2414	1,43E+06
2	154	659	.	.	1341	871	1247	11063	463	.	.	3986	98768	965	177	567859	15102	.	.	2354	.	6968	.	.	.	.	675	594	.	1577	1,17E+06
3	47	573	.	.	371	412	1560	10434	578	.	135	9914	107462	.	165	114646	3657	.	.	.	774	27957	.	4058	.	.	178	151	.	.	296153
4	143	303	.	.	251	246	1101	11115	1366	505	104	54842	87324	3718	.	157153	5086	.	.	1289	.	28113	.	6531	.	.	.	129	.	252	270648
5	269	641	.	.	632	596	1402	8169	585	.	.	3647	135676	1462	266	507023	28515	.	.	2042	.	8059	.	.	.	.	1598	535	.	1282	901772
6	179	601	.	.	602	422	1641	9382	1011	.	.	2284	62848	880	374	385637	22108	.	.	2426	.	10088	.	.	.	.	1245	594	.	2521	1,27E+06
7	205	657	.	.	1187	667	921	9927	377	.	.	2632	77832	820	268	334746	3793	.	.	2270	.	4682	.	.	.	.	414	489	.	2635	1,32E+06
8	141	692	.	.	1167	661	1289	8797	687	.	.	2763	48135	714	350	426523	21638	.	.	2435	.	9102	.	.	.	.	779	804	.	2298	1,30E+06
9	316	1255	.	.	1244	1282	1430	12603	379	.	.	5280	21917	259	356	75774	3837	.	.	426	584	37067	.	4230	.	.	239	464	.	.	6346
10	271	368	.	.	808	1274	804	205394	77	.	.	32	1545	.	110	154	811	.	.	.	.	8949	.	.	.	.	.	.	.	.	464
11	123	744	.	.	863	538	711	9934	259	.	64	6769	26569	.	257	1704	1650	.	.	.	.	12786	.	.	.	.	.	1008	.	2952	1,11E+06
12	362	934	.	.	1279	771	716	12075	135	.	.	9848	33500	7745	542	23920	864	.	2254	1391	.	27476	.	859	.	.	.	4032	.	.	448466
13	50	391	.	.	201	330	1765	12811	849	.	.	25665	47880	475	279	157881	2887	.	632	452	.	53757	.	6137	.	.	100	.	.	.	13866
14	14	58	.	.	65	590	845	106276	318	.	247	1219	654726	.	132	371	1951	.	2745	.	307	17683	.	25	.	2432	75	606	.	.	1657
15	143	135	.	137	794	1277	1255	176404	82	.	.	185	12579	118	132	239	1686	.	218	100	566	11109	.	589	.	.	.	1990	.	.	506
17	193	891	.	.	726	538	826	9308	496	.	54	11002	37291	.	294	1988	2758	.	.	.	.	16732	.	.	.	.	.	1148	.	2379	873661
18	142	804	.	.	938	555	888	9877	283	.	.	5100	25069	.	258	3872	2082	.	.	.	.	7558	.	.	.	.	169	1173	.	4479	1,60E+06
19	305	1307	.	.	1386	1342	1269	12042	445	.	.	5363	22877	169	210	79578	1486	.	1177	428	553	37018	.	4350	.	.	344	589	.	.	4442
20	293	749	.	.	1013	1038	1517	11818	611	.	.	12540	29395	259	244	145590	2626	.	.	718	634	33178	810	5047	.	.	369	450	.	.	131314
21	156	756	.	.	715	651	1058	12398	404	.	.	11387	25249	445	211	5577	1226	.	.	1025	766	33110	741	4731	.	.	.	335	.	.	255535
22	.	401	.	228	156	302	1600	10107	850	.	.	24088	48848	502	261	147512	3982	.	444	652	.	51943	.	5876	.	.	102	.	.	.	17739
23	68	335	.	.	617	1148	834	146588	112	.	.	293	11126	.	185	147	1322	.	264	85	158	8619	469	326	.	162	401	1025	.	.	433
24	89	311	.	153	776	1277	898	87376	173	.	.	2907	9572	.	202	197	1346	.	.	284	148	5855	.	.	.	.	.	.	.	.	582
25	178	261	.	602	778	1176	861	173123	113	.	.	53	2903	.	102	101	917	.	.	61	.	4291	.	.	.	.	.	.	.	.	436
26	85	144	.	.	742	1251	855	188951	76	.	.	229	4152	.	77	85	861	.	.	.	.	3828	652	.	.	.	.	.	.	.	483
27	191	244	.	.	786	1294	1491	165646	147	.	.	194	10075	87	167	174	1600	.	.	84	328	8735	630	390	.	.	.	.	.	.	1728
28	22	285	.	162	756	1233	1215	169836	169	.	.	211	8071	.	185	163	1713	.	.	152	106	2085	.	.	.	.	.	.	.	.	1005
29	139	281	.	489	781	1201	847	190007	74	.	.	231	4454	.	112	138	1167	.	.	.	.	6487	941	.	.	.	.	.	.	.	901
30	63	200	.	105	718	1175	930	115368	137	.	.	183	7391	.	233	218	1853	.	.	.	336	10178	.	.	.	.	.	.	.	.	1400
31	184	277	.	.	841	1292	1258	166172	197	.	.	289	10167	.	176	199	2253	.	.	99	144	7742	878	.	.	.	.	.	.	.	1875
32	52	95	.	.	121	457	1117	92524	196	.	.	1534	686229	.	206	319	3829	.	2592	.	296	20681	206	147	.	2720	.	.	625	.	3804
33	25	189	.	.	57	502	7904	24899	2171	397	170	2365	169587	1341	153	1100	2599	83	.	90	23004	81584	1126	19854	1048	.	.	.	436	.	2459
34	150	705	589	475	646	899	9747	19706	2939	436	.	2513	196449	1221	194	774	2435	197	.	.	25048	101461	1304	25034	1068	.	.	.	445	.	1746
35	77	295	.	671	778	1213	1133	167562	170	.	.	144	7699	.	118	301	2310	.	.	112	169	5567	.	.	.	.	.	.	.	.	2576
36	81	158	.	636	708	1218	727	202145	27	.	.	31	1432	.	96	91	760	.	.	.	57	8517	.	.	.	.	.	.	.	.	397
37	337	888	.	.	1208	904	932	12046	166	.	.	18536	46008	10337	621	25463	1046	.	.	.	.	34364	.	1403	.	.	.	3449	.	.	214158
38	459	944	.	564	1619	1360	1744	14475	548	.	.	9430	25426	274	299	20377	2403	.	1410	554	1218	38490	.	6306	.	.	.	2039	.	.	14014
39	139	650	.	.	859	593	786	10040	270	.	.	4516	17676	134	163	104527	1461	.	.	2320	.	21423	.	1319	.	.	206	1456	.	.	590139
40	86	643	.	.	778	716	1342	10911	432	.	.	11329	31500	559	322	192159	2372	.	.	991	214	26699	266	3488	.	.	233	1258	.	.	300791
41	140	820	.	.	912	758	1068	11749	329	.	.	7993	18028	125	215	136869	1408	.	.	1702	.	28955	.	2356	.	.	139	932	.	.	388066
42	335	414	.	150	935	1284	1184	181643	137	.	.	158	5117	.	100	232	1308	.	113	64	85	2936	.	.	.	.	.	.	.	.	1038
43	75	372	.	.	864	1232	1207	184475	163	.	.	109	6498	.	129	128	1302	.	117	130	164	8677	.	.	.	.	.	.	.	.	1144
44	76	213	.	.	726	1210	927	198843	88	.	.	86	2839	.	123	134	1015	.	.	64	76	5192	.	.	.	.	.	.	.	.	609
45	284	299	.	.	719	1278	906	198870	72	.	.	57	1999	.	137	108	696	.	.	.	.	5194	.	.	.	.	.	.	.	.	531
46	140	268	.	761	856	1308	1045	140779	134	.	.	95	5909	.	157	195	1450	.	.	148	217	10447	.	.	.	.	.	.	.	.	754
47	142	365	.	.	785	1254	1253	170708	211	.	.	197	10656	.	130	179	1839	.	.	.	.	2584	.	.	.	.	.	.	.	.	1366
48	62	326	.	.	758	1188	1050	169990	171	.	.	195	5944	.	125	138	1449	.	.	63	63	5309	.	.	.	.	.	.	.	.	1077

Appendix IV: hXRF data Spring 10 kV

Spring	Mg-Ka	Al-Ka	Si-Ka	P-Ka	S-Ka	Cl-Ka	Ar-Ka	K-Ka	Ca-Ka	Ti-Ka	Mn-Ka	Fe-Ka	Co-Ka	Ni-Ka	Cu-Ka	Zn-Ka	Rh-La	Sn-La	Sb-La	Ba-La
1	337	4834	174846	.	.	46771	42479	50428	454740	13318	30548	357561	7207	.	197180	.	98250	6367	6088	.
2	392	5395	194024	.	.	47154	41056	57787	562871	15074	33955	422350	8574	.	223510	.	97506	11052	5167	.
3	394	7159	251569	.	451	37828	46216	106512	484476	24288	80087	558907	.	.	52594	.	87448	6036	4887	.
4	400	5351	182628	.	.	11754	46337	72331	568029	43399	571508	425051	17930	.	82749	.	90576	719	6409	.
5	506	6294	218841	.	.	21658	43343	79772	341384	16113	29627	624030	10101	.	193313	.	88796	44609	4643	.
6	333	7398	238846	5004	.	28055	42799	105604	446151	29959	18941	304101	6286	.	145125	.	87622	34829	7180	.
7	277	4677	145341	3358	.	36424	44389	48067	496734	11808	22564	333134	6639	.	134164	.	92662	6752	4197	.
8	268	5294	202061	4267	.	42829	41798	69778	358774	19202	21860	213443	5339	.	178691	.	97447	17185	10107	.
9	261	6869	259123	.	5526	60014	45989	72254	652669	12477	48661	116820	1107	.	40352	.	82722	.	12974	.
10	437	2538	15591	.	.	19138	68719	13337	6,24E+06	2396	5734	14403	.	.	.	.	95391	.	.	.
11	387	5405	280868	.	.	59138	45631	45229	490529	10032	55429	133146	.	.	.	.	83035	.	15539	.
12	596	5589	326553	.	411	73200	39183	38700	637978	3835	85696	170722	22666	.	10864	.	82934	.	84254	.
13	405	5413	287310	6789	6732	46198	44651	124439	638763	27659	241424	263867	3674	.	78633	.	86038	4754	1727	.
14	314	3497	47053	.	6287	22775	48220	34178	3,50E+06	12817	14989	2,39E+06	.	.	.	.	99171	3938	31613	.
15	435	3640	34683	.	7831	19193	52794	36673	5,67E+06	3095	7327	66776	.	.	.	.	129213	.	31688	.
17	564	5685	287531	.	.	35650	47585	50359	446747	17215	93484	187878	.	.	.	.	81398	.	20233	.
18	345	4738	220179	.	.	52445	47344	49322	439768	7921	37945	121799	.	.	797	.	83402	5225	17700	.
19	304	4750	284896	.	5405	69095	47883	49710	671027	14956	51539	124665	1112	.	43591	.	85470	.	14071	.
20	483	5553	270976	.	3905	59287	46134	83588	594571	18399	115796	155210	2683	.	74540	.	83487	2796	7894	.
21	364	5211	303038	2227	3445	59555	47410	60397	619271	18360	106360	138800	3358	.	1319	.	84043	.	6746	.
22	694	5793	254418	4771	3720	47501	46364	109705	496827	30111	216383	268676	4794	.	70780	.	85354	4024	955	.
23	363	3905	44106	.	8152	27257	64262	32383	4,67E+06	5707	5805	72875	.	.	.	2308	101805	10641	21468	.
24	1151	2962	33467	.	3256	23383	58777	27832	3,55E+06	5916	31259	53238	.	.	.	.	80070	.	.	.
25	434	2533	21945	.	.	12734	63065	15188	5,36E+06	4954	4796	24046	.	.	.	.	105522	.	.	.
26	286	2261	17047	.	1139	15825	62478	12819	5,77E+06	2841	6721	28367	.	1701	.	2476	103312	.	.	.
27	511	3906	36519	.	14340	15583	64686	44302	5,26E+06	3984	5029	62570	.	.	.	2331	97398	.	32754	.
28	319	5408	56404	.	4997	31406	60151	46178	5,00E+06	7829	5424	58875	.	.	.	2372	96858	.	.	.
29	310	2861	17442	.	11573	22740	62438	17133	5,91E+06	3147	6482	32286	.	.	.	2677	97060	.	.	.
30	1151	2512	27945	.	4962	10264	61214	20434	4,49E+06	4060	5660	34442	.	.	.	1519	83957	.	.	.
31	585	5178	51710	.	11249	29344	59547	40189	5,20E+06	7054	7058	59999	.	645	.	2458	94422	.	.	.
32	383	5599	76677	.	8086	23238	47289	59436	3,11E+06	13581	17464	2,37E+06	.	.	.	913	96267	.	.	10227
33	430	16041	148542	.	4351	11959	47160	513126	1,11E+06	57364	18467	717876	9900	.	1084	1470	94853	.	.	9295
34	490	20997	185341	.	1006	8398	38347	602055	932270	73610	19566	826776	9652	.	437	1572	94725	.	.	10066
35	411	3987	48324	.	.	20917	63298	39546	5,19E+06	7615	5361	51595	.	.	.	.	97489	.	.	.
36	474	2693	17552	.	.	18847	60605	12364	5,99E+06	2869	4891	17582	.	.	.	.	104185	.	.	.
37	314	5241	291038	.	.	56819	43289	52147	619960	4302	162235	245827	32448	.	12429	.	83454	.	72504	.
38	393	7721	332150	.	5214	65115	41943	84906	702331	16782	84437	135161	2472	.	11344	.	82924	.	42501	.
39	376	5377	302478	.	475	65625	46544	52621	531531	10121	37229	90183	902	.	51238	.	83873	6149	26000	.
40	402	4799	287596	.	1460	56924	46122	74590	588664	13384	93351	151544	1960	.	97527	.	84498	5219	23720	.
41	313	6962	330066	.	2229	74899	42303	62204	602890	12664	69706	95623	1378	.	65326	.	83743	1116	17340	.
42	354	4665	54026	.	4109	36193	50257	34667	5,56E+06	7644	7588	40537	.	.	.	.	106730	.	.	.
43	401	4118	53902	.	4072	30608	60333	35307	5,54E+06	5723	5273	44803	.	.	.	2572	95209	.	.	.
44	315	2556	17435	.	835	26000	64085	15356	6,02E+06	3065	5048	21065	.	.	.	2541	96058	.	.	.
45	392	2656	18632	.	1757	23094	62909	20713	5,95E+06	3346	4840	18333	.	.	.	2498	96161	.	.	.
46	881	3240	30274	.	.	27973	62445	30990	4,94E+06	4237	3253	28757	.	.	.	.	87232	.	.	.
47	394	5574	62905	.	3276	24479	57899	44140	5,04E+06	6980	5503	65245	.	.	.	3107	89424	.	.	.
48	371	4287	46122	.	2659	32639	58173	31986	5,41E+06	4895	5354	41371	.	.	.	2777	90185	.	.	.